Parnell-Turner, R.E., Briais, A., LeVay, L.J., and the Expedition 395 Scientists
Proceedings of the International Ocean Discovery Program Volume 395
publications.iodp.org

Expedition 395 summary[1]

R.E. Parnell-Turner, A. Briais, L.J. LeVay, Y. Cui, A. Di Chiara, J.P. Dodd, T. Dunkley Jones, D. Dwyer, D.E. Eason, S.A. Friedman, S.R. Hemming, K. Hochmuth, H. Ibrahim, C. Jasper, B.T. Karatsolis, S. Lee, D.E. LeBlanc, M.R. Lindsay, D.D. McNamara, S.E. Modestou, B. Murton, S. OConnell, G.T. Pasquet, P.N. Pearson, S.P. Qian, Y. Rosenthal, S. Satolli, M. Sinnesael, T. Suzuki, T. Thulasi Doss, N.J. White, T. Wu, A. Yang Yang, V. dos Santos Rocha, C. Pearman, and C.Y. Tian[2]

[1] Parnell-Turner, R.E., Briais, A., LeVay, L.J., Cui, Y., Di Chiara, A., Dodd, J.P., Dunkley Jones, T., Dwyer, D., Eason, D.E., Friedman, S.A., Hemming, S.R., Hochmuth, K., Ibrahim, H., Jasper, C., Karatsolis, B.T., Lee, S., LeBlanc, D.E., Lindsay, M.R., McNamara, D.D., Modestou, S.E., Murton, B., OConnell, S., Pasquet, G.T., Pearson, P.N., Qian, S.P., Rosenthal, Y., Satolli, S., Sinnesael, M., Suzuki, T., Thulasi Doss, T., White, N.J., Wu, T., Yang Yang, A., dos Santos Rocha, V., Pearman, C., and Tian, C.Y., 2025. Expedition 395 summary. In Parnell-Turner, R.E., Briais, A., LeVay, L.J., and the Expedition 395 Scientists, Reykjanes Mantle Convection and Climate. Proceedings of the International Ocean Discovery Program, 395: College Station, TX (International Ocean Discovery Program). https://doi.org/10.14379/iodp.proc.395.101.2025
[2] **Expedition 395 Scientists' affiliations.**

Contents

Keywords
International Ocean Discovery Program, IODP, *JOIDES Resolution*, Expedition 395, Expedition 384, Expedition 395C, Reykjanes Mantle Convection and Climate, Earth Connections, Earth in Motion, Site U1554, Site U1555, Site U1562, Site U1563, Site U1564, Site U1602, contourite drifts, mantle plume, hydrothermal alteration, oceanic gateways, climate record, Northern Hemisphere glaciation

Core descriptions

Supplementary material

References (RIS)

MS 395-101
Published 21 January 2025

Funded by NSF OCE1326927, ECORD, and JAMSTEC

Abstract

The intersection between the Mid-Atlantic Ridge and Iceland hotspot provides a natural laboratory where the composition and dynamics of Earth's upper mantle can be observed. Plume-ridge interaction drives variations in the melting regime, which result in a range of crustal types, including a series of V-shaped ridges (VSRs) and V-shaped troughs (VSTs) located south of Iceland. Mantle upwelling beneath Iceland dynamically supports regional bathymetry, and its variations may lead to changes in the height of oceanic gateways, which in turn control the flow of deep water on geologic timescales. Expeditions 384, 395C, and 395 recovered extensive successions of basaltic crust and thick (up to 1.3 km) overlying sediment cover, including successions through a number of contourite drifts of regional significance. Major, trace, and isotope geochemistry of basalts recovered during these expeditions will provide insight into spatial and temporal variations in mantle melting processes. Such analyses will provide data for testing the hypothesis that the Iceland plume thermally pulses on two timescales (5–10 and ~30 Ma), leading to fundamental changes in crustal architecture. This idea will be tested against alternative hypotheses involving propagating rifts and buoyant mantle upwelling. The rapidly accumulated sediments of contourite drifts have the potential to yield exceptional millennial-scale paleoceanographic records, including proxies for current strength, which is thought to be modulated by the dynamic support of the Greenland-Scotland Ridge, an oceanic gateway of global import. The recovered sediments also provide a record of subarctic climate change stretching back to the latest Eocene, including the long-term evolution of the Greenland ice sheet, critical intervals of Miocene and Pliocene warmth, the intensification of Northern Hemisphere glaciation, and Pleistocene millennial-scale variability.

The objectives of Expeditions 395, 395C, and 384 are to explore the relationships between deep Earth processes, ocean circulation, and climate. These objectives were addressed by recovering sediment and basement cores from six sites, completed across three expeditions. Sites U1555 and U1563 are located at a VST/VSR pair nearest to the Reykjanes Ridge, on ~2.8 and 5.2 My old crust, respectively. Sites U1554 and U1562 are located in Björn drift above a VST/VSR pair, on ~12.4 and 14.2 My old crust, respectively. Site U1564 is located in Gardar drift above 32.4 My old oceanic crust that is devoid of V-shaped features. Finally, Site U1602 is located on the eastern Greenland margin above crust that is estimated to be Eocene in age and thus formed during the initial separation of Greenland from Scandinavia. Considered together, the sediments, basalts, and vast array of measurements collected during Expeditions 395, 395C, and 384 will provide a major advance in our understanding of mantle dynamics and the linked nature of Earth's interior, oceans, and climate.

Plain language summary

In the North Atlantic Ocean, hot rocks are thought to rise up beneath Iceland from deep within Earth's interior, forming a giant mantle plume, or hotspot. Interaction between this plume and the nearby mid-ocean ridge has created a pattern of distinctive V-shaped ridges and valleys on the seabed that extends hundreds of kilometers south of Iceland. Some think that this distinctive V-shaped pattern is caused by pulses of more or less intense plume activity, but their precise origin is still not fully understood. Plume activity variations may also have controlled circulation of deep ocean water by changing the water depths above the shallow ridges of ocean floor that link Greenland, Iceland, and Scotland. These ridges are products of volcanism from the plume and act as sills between deeper ocean basins in the Nordic Seas and North Atlantic, thus forming ocean gateways that control the flow of cold, deep water from the Nordic Seas to the Atlantic Ocean. These deep-water currents carry large amounts of sediments that are deposited on the seabed. As a result, these thick piles of sediments contain a detailed proxy record of past marine environments that can be accessed within deep-sea cores. Expeditions 395, 395C, and 384 cored through these sediments at six sites and into the oceanic basement at five sites. Cored samples of sediment and basalt and the fluids and microbes they contain, along with measurements made on the ship and on samples returned from the expedition, will enable scientists to contribute to a better understanding of processes taking place in the mantle, ocean, and climate over the past 32 million years.

1. Introduction

Scientific ocean drilling has transformed our understanding of Earth over the past five decades, from defining our understanding of past climates to the confirmation and refinement of plate tectonic theory. However, the convecting behavior of Earth's mantle and its effects on surface processes such as ocean circulation and climate remains a key scientific problem. Basaltic rocks erupted at mid-ocean ridges (MORs) provide a window into mantle processes. When MORs are located near mantle plumes, interactions between these two systems produce variations in mantle composition and dynamics that are recorded in the erupted basalts and topography and geophysical properties. Although mantle plumes (e.g., beneath Hawaii) are fairly common, intersecting plume-ridge systems are unusual. One such intersecting system is located in the North Atlantic Ocean, where the Iceland mantle plume is strongly influenced by the Mid-Atlantic Ridge, which includes the Reykjanes Ridge southwest of Iceland. Basaltic rocks erupted at the spreading axis record the geochemical signature of the underlying mantle and the melting and extrusion processes, providing a record of the composition and dynamics of the mantle plume and its interaction with the spreading system. The Reykjanes Ridge flanks host a series of V-shaped crustal ridges and troughs, whose origin has been long debated. One of the hypotheses to explain the formation of these ridges is that the Iceland mantle plume has been pulsing at a frequency of several millions of years, causing melt anomalies and driving transient uplift of the surrounding North Atlantic region on geologic timescales. Other hypotheses to explain these ridges do not require pulsing of the Iceland plume.

Basins around the Reykjanes Ridge are blanketed by rapidly accumulating sediments that can record variations in oceanographic conditions as highly resolved as millennial timescales, providing some of the most detailed climate records on Earth (Figure **F1**). Southward-flowing deepwater currents in the North Atlantic Ocean deposit fine-grained sediments called contourite drifts, which accumulate at rates of hundreds of meters per million years. The eastern Reykjanes Ridge flank hosts Björn and Gardar drifts. In contrast, Eirik drift consists of an elongate, mounded contourite deposit that is plastered along the East Greenland margin. Vertical motions caused by variations in the Iceland mantle plume temperature could have altered the depth of the oceanic gateways connecting the Norwegian and Greenland Seas into the North Atlantic Ocean, with implications for deepwater circulation, sediment deposition, and climate. In addition, over time, basaltic crust spreads away from the ridge and interacts with the overlying seawater and sediments, becoming progressively altered because of hydrothermal circulation and associated chemical exchange. The unique juxtaposition of a mantle plume, a spreading ridge, oceanic gateways,

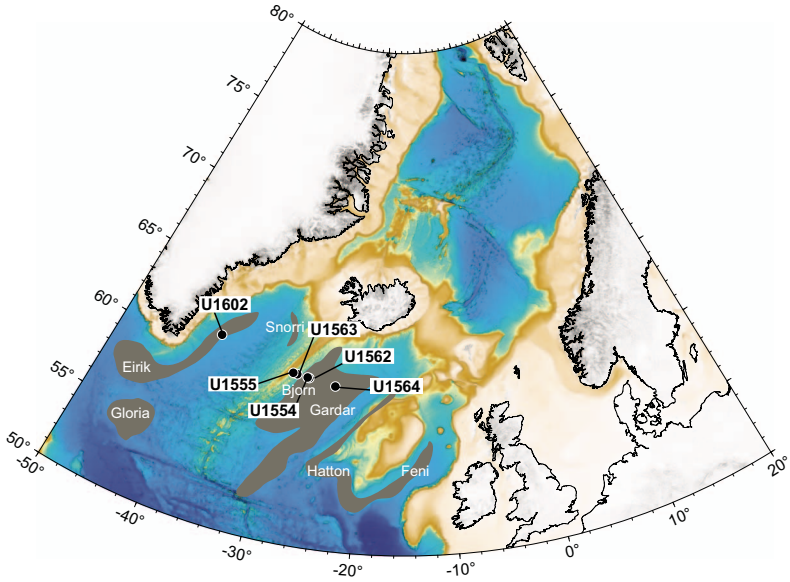

Figure F1. Bathymetry of North Atlantic Ocean. Brown polygons = contourite drifts.

and rapidly accumulating sediment provides an ideal natural laboratory to test multidisciplinary ideas about the interactions between the Earth's deep and surficial domains.

Although the rich scientific potential in this region was demonstrated during Deep Sea Drilling Project (DSDP) Leg 49 and Ocean Drilling Program (ODP) Leg 162 (Luyendyk et al., 1979; Jansen and Raymo, 1996), comprehensive sampling of both the sediment and underlying basaltic crust is still lacking. A transect of holes was drilled during Expeditions 384, 395C, and 395 to address three major objectives: (1) to test the control of the time-dependent behavior of the Iceland mantle plume on crustal accretion at the Reykjanes Ridge; (2) to obtain high-resolution and long-term records of climate and ocean circulation near major North Atlantic oceanic gateways; and (3) to track the accretion, aging, and hydrothermal exchange of oceanic crust over 32 My.

Expedition 395 was originally scheduled for summer 2020; however, because of the COVID-19 pandemic it was postponed twice. Expedition 384 (July–August 2020) operated at Sites U1554 and U1555 and recovered cores in support of Expedition 395 science. In June–August 2021, Expedition 395C was fully dedicated to advancing Expedition 395 operations with *JOIDES Resolution* Science Operator (JRSO) technical staff collecting and processing core at Sites U1554, U1555, and U1562–U1564. In addition, a reentry system and casing was installed at Site U1554 and downhole wireline logging operations were conducted when conditions were favorable. In June–August 2023, Expedition 395 included the science party and collected cores, measurements, and logging data at all previously visited sites (except Sites U1555 and U1563) and the new Site U1602. The cores and data collected during Expeditions 395, 395C, and 384 compose the entirety of the Expedition 395 material. In the following we use "Expedition 395" to refer to the entire three-expedition program, unless otherwise specified.

2. Background

2.1. Geologic setting

As new basaltic oceanic crust is formed, it draws material from the underlying mantle, so rocks recovered from MORs have long been used to assess the thermal and compositional properties of the mantle (e.g., Krause and Schilling, 1969; Hart et al., 1973; Schilling, 1973). Where MORs lie above mantle plumes, such as along Reykjanes and Kolbeinsey Ridges near Iceland, oceanic crustal accretion is thought to be influenced by plume activity (e.g., White, 1997). Close agreement between models of dynamic topography and seismic tomography supports the idea that mantle

upwelling beneath Iceland influences the entire North Atlantic region today (Hartley et al., 2011; Rickers et al., 2013; Schoonman et al., 2017). The set of diachronous V-shaped ridges (VSRs) and V-shaped troughs (VSTs) that straddle the Reykjanes Ridge south of Iceland (Figure **F2**) have been suggested to be a possible sign of time-dependent plume behavior. Vogt (1971) first suggested that the VSRs reflect variations in crustal thickness caused by pulses of hotter asthenosphere advecting horizontally away from the Iceland plume that episodically increase the thickness of crust formed at the axis.

Oceanic crustal accretion is sensitive to small mantle potential temperature perturbations, which can change the thickness of newly formed material by hundreds of meters to kilometers (White et al., 1995). The ratios between incompatible trace elements, such as Nb/Y, are largely insensitive to crustal processes such as fractional crystallization and thus reflect the depth and degree of melting. A southward decrease of Nb/Y on the Reykjanes Ridge correlates with deepening of the axis, a decrease in crustal thickness, and decreasing source enrichment estimated by isotopic indicators such as $^{87}Sr/^{86}Sr$ (Murton et al., 2002; Shorttle and Maclennan, 2011). Along-axis variations in incompatible trace element ratios correlate with patterns in gravity anomaly, bathymetry, and earthquake seismicity (Parnell-Turner et al., 2013; Jones et al., 2014). Compositional variations associated with VSRs cannot be explained by fractional crystallization alone because a corresponding variation in Mg number is absent. Because enrichment in incompatible trace elements is inversely correlated with crustal thickness, mantle temperature variation is thought to play an important role in controlling crustal thickness, in addition to changes in mantle source fusibility (Poore et al., 2011; Parnell-Turner et al., 2017).

Since Vogt's early thermal pulsing hypothesis, the origin of VSRs has been debated (Figure **F3**) (e.g., Parnell-Turner et al., 2014). One alternative idea is that VSRs may be tectonic in origin and have no requirement for melt anomalies originating from temperature variations in the mantle plume itself (Briais and Rabinowicz, 2002; Rabinowicz and Briais, 2002; Hey et al., 2010; Benediktsdóttir et al., 2012). In this hypothesis, a sequence of propagating rifts and southward migrating discontinuities, suggested by the observed asymmetric accretion at the ridge axis, explains the formation of VSRs and VSTs, which are thought to represent ridge segments and pseudofault scarps, respectively (Figure **F3**). A third hypothesis, in which shallow buoyant mantle upwelling instabilities propagate along axis to form the observed crustal structure variations, avoiding the requirement for rapid mantle plume flow (Figure **F3**), has also been suggested (Martinez and Hey, 2017; Martinez et al., 2020).

Crust on the Reykjanes Ridge was last drilled in 1976, during DSDP Leg 49, when basalts were recovered at three sites (Sites 407–409), all located on VSRs. Across these sites, a total basalt thick-

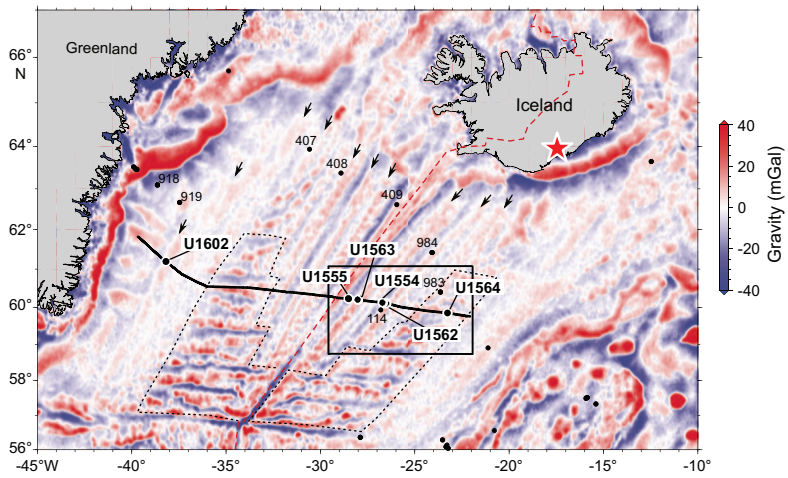

Figure F2. Free-air gravity anomaly filtered to remove wavelengths > 250 km showing Expedition 395 region. Solid black line = Seismic Profile JC50-1, small black circles = DSDP/ODP sites, dashed red line = Mid-Atlantic Ridge, red star = Iceland plume center (Shorttle and Maclennan, 2011), arrows = VSRs, dotted polygons = transition from smooth to segmented ocean floor, black box = location of Figure F4.

ness of 453 m was penetrated (Luyendyk et al., 1979), leading to a series of breakthroughs in our understanding of the nature and scale of mantle heterogeneity and crustal accretion under the influence of a mantle plume (e.g., Wood et al., 1979; Dupré and Allègre, 1980; Fitton et al., 1997). The deepest basement penetration was at Site 409, located 23 km from the ridge axis where 240 m of vesicular basalt was drilled in 2.4 My old crust, with the other Leg 49 sites on older crust (36 and 20 Ma). None of the Leg 49 sites were positioned to recover basalts from a VST and so are unable to unravel the origins of VSRs and VSTs and do not provide detailed stepwise information about the aging of oceanic crust.

The North Atlantic Ocean is separated from the colder, more dense waters of the Arctic Ocean and Norwegian-Greenland Sea by the Greenland-Scotland Ridge (GSR), which represents a critical gateway affecting Cenozoic deepwater circulation patterns and climate. The GSR is generally less than 500 meters below sea level (mbsl) and is only ~1000 mbsl at its deepest point, making the overflow flux sensitive to small variations in the ridge depth. Reconstructions of Neogene mantle plume activity are proposed to correlate with deepwater circulation patterns in the North Atlantic (Wright and Miller, 1996). Inferred times of high mantle plume activity are linked to low Northern Component Water productivity, decreased current strength, and lower sedimentary deposition rates (Wright and Miller, 1996; Poore et al., 2006; Parnell-Turner et al., 2015). Southward-flowing deepwater currents in the North Atlantic Ocean deposit fine-grained sediments called contourite drifts, which accumulate at rates of hundreds of meters per million years. Two contourite drifts, Gardar and Björn, were successfully drilled during Leg 162 (Jansen and Raymo, 1996), providing a record of drift sedimentation back to early Pleistocene and late Pliocene times (~2 and 3 Ma), respectively. A high sedimentation rate combined with near 100% core recovery rates means that these sites contain some of the highest resolution records of ocean circulation and climate to date (Kleiven et al., 2011; Thornalley et al., 2013). These records can be directly compared to atmospheric records from ice cores and provide a unique, high-resolution insight into the Earth's recent climate history (Barker et al., 2019, 2022).

2.2. Site survey data

A detailed geophysical survey of Reykjanes Ridge and its flanks was conducted in June–July 2010 during RRS *James Cook* Cruise JC50, collecting more than ~2400 km of 2D multichannel reflection seismic data (Parnell-Turner et al., 2015, 2017). The survey consisted of two basin-spanning

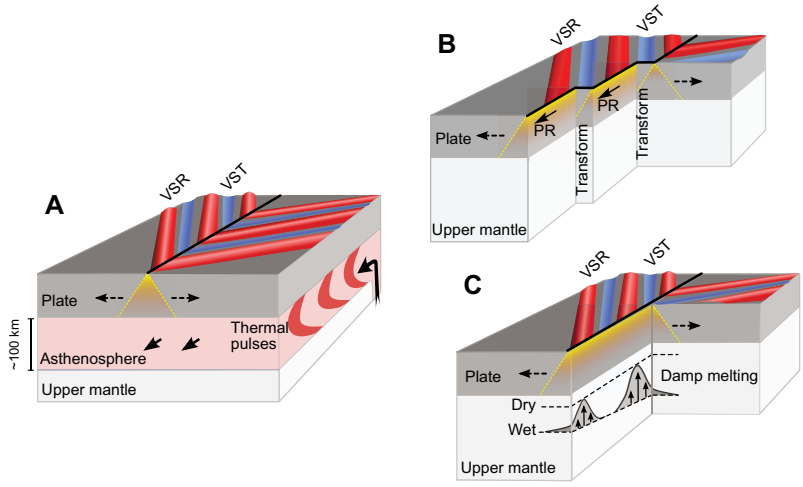

Figure F3. Competing hypotheses for VSR formation (Parnell-Turner et al., 2017). A. Thermal pulsing hypothesis (Vogt, 1971). Dark gray blocks = lithospheric plates, pink block with red patches = asthenospheric channel containing thermal pulses, light gray block = upper mantle, solid arrows = propagation direction of thermal pulses, dashed arrows = plate spreading direction, yellow shading = melting region, red/blue ribs = VSRs/VSTs, black line = MOR. B. Propagating rift hypothesis (Hey et al., 2010). Solid arrows = propagating rift direction. VSRs are regarded as ridge segments with thicker crust and VSTs are regarded as pseudofaults that propagate along axis generating thinner crust. C. Buoyant mantle upwelling hypothesis (Martinez and Hey, 2017). Gray blobs = buoyant upwelling cells that generate damp melting and thicker crust in absence of thermal anomaly, vertical arrows = vertical upwelling in a given cell, dashed lines = dry/wet solidi.

regional seismic reflection profiles, oriented parallel to plate-spreading flowlines, and a series of 19 shorter perpendicular crossing lines. These multichannel data are of sufficient quality to identify the sediment/basement interface, as well as potential drilling hazards such as faults, gas accumulations, and stratigraphic discontinuities. Based on seismic reflection profiles, primary and alternate sites were positioned on thick sediment or in localized sediment ponds so that holes could easily be established. Sites were located as close to crossing seismic profiles as possible while avoiding sedimentary disturbances, faults, and basement discontinuities. Sediment thicknesses were estimated using interval sediment velocities from ODP Leg 162 where possible and from stacking velocities for deeper levels.

3. Scientific objectives

3.1. Objective 1: crustal accretion and mantle plume behavior

Expedition 395 aimed to use the composition of basaltic samples to understand crustal formation south of Iceland at two temporal scales. First, on ~5–10 My timescales, we sought to test three alternative hypotheses for the formation of VSRs: (1) thermal pulsing, (2) propagating rifts, and (3) buoyant mantle upwelling. Drilling allowed us to test these hypotheses, which predict differing depths, temperatures, and degrees of melting between VSRs and VSTs recorded in basalt composition. Dredged samples are restricted to the ridge axis because deep-sea corals and sediments cover off-axis areas (Murton et al., 2002; Jones et al., 2014). Hence, off-axis VSRs and VSTs can only be sampled by drilling. Second, we aimed to test the controls on crustal architecture over longer, ~30–40 My timescales. Oceanic crust south of Iceland can be divided into two distinct structural types—smooth and segmented—using gravity, magnetic and bathymetric data sets (e.g., White, 1997). Smooth oceanic crust contains VSRs and VSTs but also exhibits seafloor magnetic anomalies that are largely unbroken by fracture zone offsets, similar to those more typical at fast-spreading ridges. Segmented oceanic crust exhibits traces of ridge axis discontinuities that are more typical of slow-spreading ridges; hence, the seafloor here represents a microcosm of global variability in ocean crustal structure. The location of the boundary between smooth and segmented crustal styles has shifted through time (Jones et al., 2002). This transition has been proposed to reflect changes in melt supply to the ridge and may record expansion and contraction of the Iceland plume over ~35 My. Segmented oceanic crust usually forms above cooler asthenosphere or at slow-spreading ridges, whereas smooth crust usually forms above relatively hot asthenosphere close to plume heads or at intermediate- to fast-spreading ridges. Therefore, in the North Atlantic Ocean, small changes in melt flux, temperature, and/or spreading behavior may drive regime changes in crustal architecture. Our objective of understanding how crustal formation responds to mantle temperature, degree of melting, and plume activity can be achieved by comparing the geochemistry of basalts from smooth and segmented crustal domains.

3.1.1. Basalt geochemistry

The accretion of oceanic crust is sensitive to small mantle potential temperature perturbations, which can change the thickness of newly formed material by hundreds of meters to kilometers (White et al., 1995). Certain basalt trace element ratios such as Nb/Y are largely insensitive to crustal processes such as fractional crystallization, instead reflecting mantle melting processes and source composition. A southward decrease of Nb/Y between 63°N and 61°N on Reykjanes Ridge correlates with deepening of the axis, a decrease in crustal thickness, and decreasing source enrichment estimated by isotopic indicators such as $^{87}Sr/^{86}Sr$ and $^{143}Nd/^{144}Nd$ (Murton et al., 2002; Jones et al., 2014).

Leg 49 yielded major advances in understanding mantle heterogeneity (e.g., Wood et al., 1979), plume structure (e.g., Fitton et al., 1997), and melting processes (e.g., Kempton et al., 2000). However, the location of these sites precludes their use to fully address the temporal and spatial variability of plume dynamics. Expedition 395 sites, located along a spreading-parallel flowline, minimize the issue of variable distance from the plume. Incompatible trace element concentrations and ratios (e.g., Nb/Y and La/Sm) will be used to constrain mantle melting models, building upon previous work on samples from the ridge axis. Major and trace element concentrations will be used to constrain differences in the depth and extent of melting, as well as mantle source

composition, between VSR/VST pairs and segmented crust unaffected by VSRs. Indirect reconstruction of axial depth is possible using volatile elements such as carbon, water, and sulfur, which de-gas when erupted at the seafloor. For example, advances in understanding the CO_2 concentration in ridge basalts enable quantification of eruption pressure (Le Voyer et al., 2017). Recovery of basaltic glass during Expedition 395 will enable electron and ion-probe analyses to measure volatile elements and therefore estimate eruption pressures and test the plume pulsing hypothesis.

Objective 1 of Expedition 395 addresses 2050 Science Framework Strategic Objective 2: Ocean Life Cycle of Tectonic Plates, which concerns the formation, aging and eventual destruction of oceanic plates. The coincidence of the Reykjanes Ridge with the Iceland plume provides an opportunity to observe the composition and behavior of Earth's interior, as recorded by oceanic crust. Major, rare earth, and trace element concentrations of basalts recovered from Expedition 395 sites will be used to constrain mantle melting models to investigate how crust forms on slow-spreading ridges.

Crustal architecture south of Iceland is dominated by two main features: the diachronous VSRs that straddle the Reykjanes Ridge flanks and the transition from smooth to segmented oceanic crust that took place at ~35 Ma. By using similar basalt geochemistry and isotopic systematics, we will investigate the corresponding changes in mantle melting and composition associated with these changes in crustal formation (Figure **F4**). In addition, the transect of sites is situated on crust of progressively increasing age and varying sedimentary cover. Basalts from Expedition 395 sites exhibit varying degrees of alteration along the transect, recording the progressive aging of the oceanic crust as it interacts with seawater, sediment, and possibly microbial life over millions of years, as explained below as part of Objective 3.

3.2. Objective 2: oceanic circulation, gateways, and sedimentation

Cores and data from Expedition 395 sites allow us to quantify variations in oceanic circulation in the North Atlantic Ocean since Oligocene times. Deep water flow in the North Atlantic is dominated by two oceanic gateways, the Iceland-Faroe Ridge and the Denmark Strait, that control the southward flow of water from the Norwegian Sea and exert a major influence on global ocean circulation (Figure **F5**).

The rate of accumulation of contourite drift sediments in the North Atlantic Ocean is primarily controlled by deep water flow along bathymetric rises; hence, the strength and pathways of deep-water currents are recorded by these drift sediments (e.g., Wright and Miller, 1996). The accumulation of these deposits provides an indirect proxy for temporal variations in deep water flow. Additionally, short-term climatic effects relating to the location of oceanic fronts during both glacial–interglacial and (shorter) stadial–interstadial cycles may play a role in circulation patterns

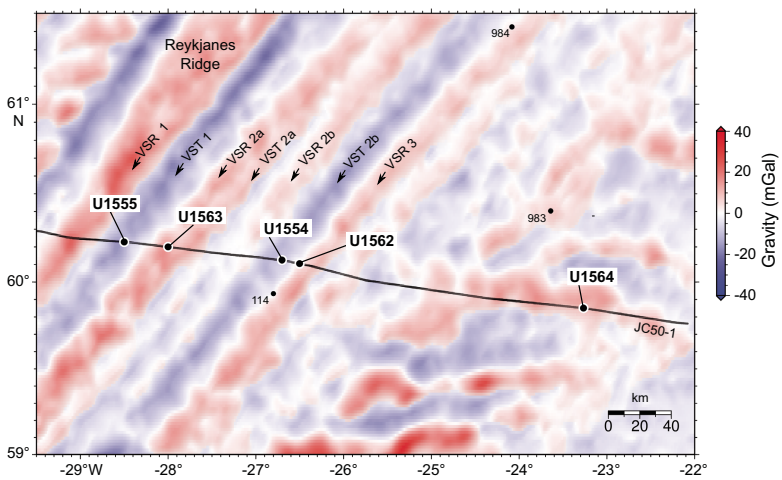

Figure F4. Free-air gravity anomaly filtered to remove wavelengths > 250 km showing numbered VSRs and VSTs. Small black circles = ODP sites.

on shorter timescales (thousands of years). It has been suggested that uplift and subsidence of the Iceland-Faroe Ridge and Denmark Strait are influenced by mantle upwelling beneath Iceland and that there may therefore be an indirect connection between ocean circulation and mantle plume behavior (e.g., Parnell-Turner et al., 2015; Poore et al., 2011). Age-depth relationships at the six Expedition 395 sites will allow us to test the proposed correlation between mantle plume activity and ocean circulation by using sediment accumulation rates as a first-order proxy for deep water current strength. The oldest previously drilled sediments in the Iceland Basin are from ~3 Ma (Jansen and Raymo, 1996), and Expedition 395 extends that record back to ~32 Ma, allowing us to investigate the relationships between mantle convection, oceanic gateway configuration, and climate over long timescales.

High sedimentation rates of contourite drift deposits in the North Atlantic Ocean (12–16 cm/ky) have led to paleomagnetic and isotopic records that are among the most detailed available (Channell et al., 2002). Existing boreholes provide high-resolution climate records back to 1.7 Ma (Site 983), and Expedition 395 extends the high-resolution climate record further into late Pliocene times. Coring the full depth of both Gardar drift at Site U1564 and Björn drift at Sites U1554 and U1562, with further coring into predrift Oligocene–Miocene sediments, provides unique long-term constraints on sedimentation rates and ocean circulation over tens of millions of years. Work on Leg 162 sites demonstrates the utility of sediments for millennial-scale reconstructions of surface and deepwater properties (Barker et al., 2015, 2019, 2022; Raymo et al., 1998). Planktonic foraminifer assemblages give a first-order constraint on sea-surface temperatures and the latitudinal migration of the polar front, which fluctuates in line with millennial-scale temperature recorded by Greenland ice cores over the past ~100 ky (Bond et al., 1993). Similar relationships can be derived for intervals beyond the reach of Greenland ice cores, documented by the strong correlations between regional climate and %*Neogloboquadrina pachyderma* (e.g., ODP Site 983). Ice-rafted debris (IRD) is a useful tracer for iceberg fluxes, which are likely associated with the cooling/freshening of the surface ocean and changes in surface water buoyancy, with consequences for deepwater production rates (Menviel et al., 2014). Intensive ice rafting has occurred in the North Atlantic since northern hemisphere glaciation intensification at around 2.7 Ma (Bailey et al., 2013), and its occurrence at Site 983 has been used to document millennial-scale variability over the past 1.2 My. Sediments on Björn and Gardar drifts experienced changes in accumulation rate due to variations in deepwater overflow of proto-North Atlantic Deep Water. Variations in the vigor of these overflows can be detected with the sortable silt proxy for bottom water current speed (McCave et al., 2017), an approach that has documented overflow changes on submillennial timescales at Sites 983 and 984 (Kleiven et al., 2011; Thornalley et al., 2013). These proxies, in combination with foraminifer paired oxygen isotope Mg/Ca paleothermometry (for temperature/salinity) and carbon isotopes (deep ocean mixing) give the potential to reconstruct submillennial-scale variations in ocean properties throughout the interval of drift deposition.

Expedition 395 addresses 2050 Scientific Framework Strategic Objective 3: Earth's Climate System and Strategic Objective 4: Feedbacks in the Earth System. Subsidence and uplift of the Denmark

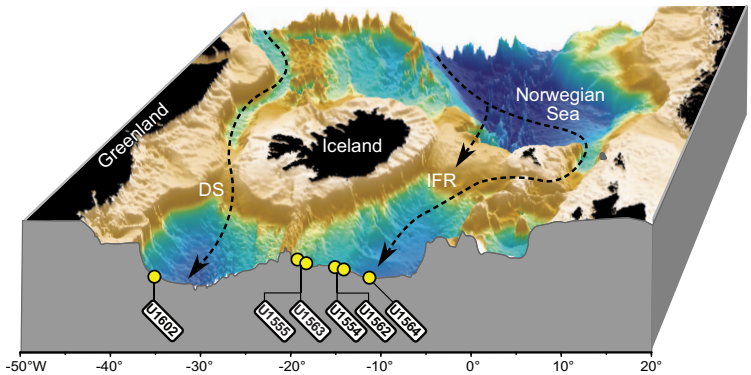

Figure F5. 3D perspective view, Expedition 395 sites. Dotted lines = overflow of deep water from Norwegian Sea, via Denmark Strait (DS) and Iceland-Faroe Ridge (IFR).

Strait and Iceland-Faroe Ridge may have controlled the deepwater exchange between the Arctic Ocean, Nordic Seas, and Atlantic Ocean. Under this hypothesis, the tectonic evolution of these oceanic gateways and sills modifies large-scale ocean circulation, which is a component of multiple climate and biogeochemical feedback loops. Thus, the histories of these gateways and their associated deep water flow are central to our understanding of Northern Hemisphere climate and its interaction with global thermohaline circulation. Sediments at Expedition 395 drilling sites were accumulated at high rates (>10 cm/ky) and therefore provide a millennial-scale paleoclimate record since drift initiation. This extended record spans the critical future climate analogs of the mid-Pliocene, when global mean surface temperatures were 2°–3°C warmer than today. We will be able to test the sensitivity of ocean circulation to changes in gateway conditions, which will inform boundary conditions for climate models targeting these future analog warm climate states. Finally, the record of crustal alteration across the five crustal sites will enable us to examine the styles and process of crustal weathering that likely plays a role in modulating CO_2 sequestration on long timescales.

3.3. Objective 3: time-dependent hydrothermal alteration of oceanic crust

Sites cored during Expedition 395 address the nature, extent, timing, and duration of hydrothermal alteration of oceanic crust formed at the Reykjanes Ridge. Hydrothermal circulation along MORs and across their flanks is responsible for one-third of the heat loss through the ocean crust (Sclater et al., 1980; Bodine et al., 1981). It influences tectonic, magmatic, and microbial processes on a global scale and is a fundamental component of global biogeochemical cycles (Coggon and Teagle, 2011). There is also growing evidence that the long-term carbon cycle is influenced by the reaction of seawater with the oceanic crust in low-temperature, off-axis hydrothermal systems, perhaps representing an important mechanism for carbon drawdown (e.g., Gillis and Coogan, 2011). The relative contribution of this process remains controversial; ultimately, quantifying the degree of low-temperature off-axis alteration is only possible through accessing older basalts that are often beneath thick marine sediment sequences. Although the nature of individual hydrothermal fluid-rock reactions is generally understood, the magnitude and distribution of chemical exchange remain poorly quantified, as does the partitioning between high- and low-temperature exchange with crustal age. Consequently, the role of the production, hydrothermal alteration, and subsequent subduction of ocean crust in key global geochemical cycles remains uncertain. Drilled sections of hydrothermally altered crust from the Reykjanes Ridge flank provide time-integrated records of geochemical exchange between crust and seawater along an age transect from 2.8 to 32.4 Ma (Figure **F6**). The recovered cores, fluid samples, and wireline logging data will enable us to quantify the timing and extent of hydrothermal fluid–rock exchange across the Reykjanes Ridge flank and assess the hydrothermal contributions of a rapidly sedimented slow-spreading ridge flank to global geochemical budgets.

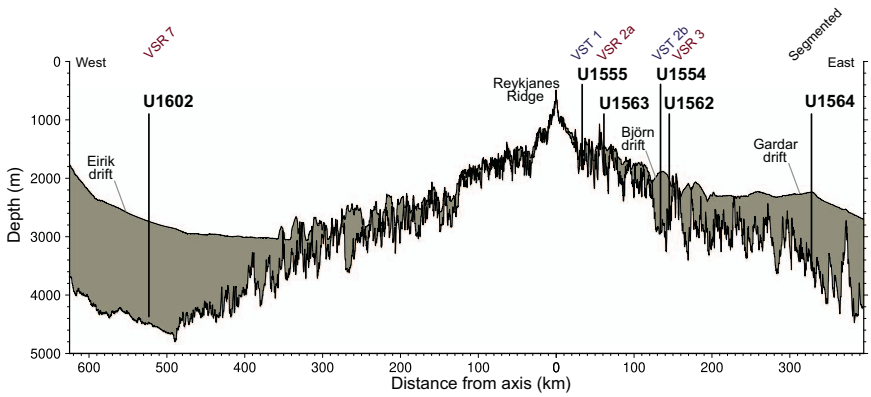

Figure F6. Depth transect showing seafloor depth, sediment/basement interface depth, sedimentary thickness (shading), and Expedition 395 sites. Figure based on Seismic Profile JC50-1 and velocity model from Parnell-Turner et al. (2017).

The ocean basin–wide transect drilled during Expeditions 395 spans crust from 2.8 to 32 Ma in age, which has experienced a spectrum of different sedimentation, geochemical, and hydrogeologic processes. Expedition 395 Sites U1555, U1563, U1554, U1562, and U1564 comprise a west-to-east crustal flow-line transect across the eastern flank of Reykjanes Ridge. The recovered cores sample the uppermost ~130–200 m of lavas produced 2.8, 5.2, 12.4, 14.2, and 32.4 My ago at the Reykjanes Ridge, which provide a unique opportunity to quantify the timing and extent of hydrothermal fluid–rock exchange in a slow-spreading ridge flank that experienced rapid sedimentation and variations in tectonic architecture. These sites address 2050 Science Framework Strategic Objective 2: Oceanic Life Cycle of Tectonic Plates.

Expedition 395 sites provide an exceptionally large variety of subseafloor environments in which to study microbial communities, aiding in the understanding of the habitability of life on Earth, 2050 Science Framework Strategic Objective 1. The comprehensive set of samples collected for microbiological analyses in cores from shallow to deep sedimentary sequences, sediment/basement interface, and from deep within the basement will provide insights into the factors controlling the development of life. These analyses will benefit from the comprehensive record of the corresponding geochemical environment provided by the interstitial fluid, sediment, basement rocks and their alteration products collected at all sites.

4. Site summaries

4.1. Site U1554

4.1.1. Background and objectives

Expedition 395 Site U1554 is located in the North Atlantic Ocean along Reykjanes Ridge south of Iceland and on Björn drift (Figure **F1**) (see the **Site U1554** chapter [Parnell-Turner et al., 2025b]). Site U1554 is located on Seismic Line JC50-1 (Common Midpoint [CMP] 41740), near the intersection with line JC50-C3 (CMP 1005), both obtained in 2010 during RRS *James Cook* Cruise JC50. Site U1554 is located in VST 2b with an estimated basement age of 12.7 Ma. Another target for Site U1554 was to obtain a continuous sedimentary record of Björn drift, which is expected to offer millennial-scale climate records. The sedimentation rate of this drift can serve as a proxy for deep water current strength and provide information for testing proposed vertical oceanic gateway motions and their potential ties to the possible pulsing behavior of the Iceland mantle plume.

Cores and data from this site will address all three of the primary science objectives of Expedition 395: (1) crustal accretion and mantle behavior; (2) ocean circulation, gateways, and sedimentation; and (3) time-dependent hydrothermal alteration of oceanic crust.

4.1.2. Operations

Site U1554 (60°07.5060′N, 26°42.0960′W) consists of eight holes drilled during Expeditions 384, 395C, and 395 (Table **T1**). Holes U1554A–U1554D were cored during Expedition 384 in July 2020. These holes reach 23.5–76.0 m drilling depth below seafloor (DSF). The recovered cores were used to create a stratigraphic splice of the section. Holes U1554E and U1554F were cored and logged during Expedition 395C in 2021. These holes extend to 647.7 and 779.9 m DSF, respectively. Finally, Holes U1554G and U1554H were each cored to ~355 m DSF during Expedition 395.

The sediments and basalts recovered during Expeditions 384 and 395C were sampled for select shipboard measurements during the cruises. Cores from these two expeditions were described postcruise at a core description party held at the Gulf Coast Repository (GCR) in College Station, TX (USA), in May 2022.

A total of 194 cores were recovered for Site U1554. Over a 1683.9 m cored interval, these cores collected 1611.82 m of sediment and basalt (96%). The total time spent on Holes U1554A–U1554H was 22.48 days: 2.09 days during Expedition 384, 16.89 days during Expedition 395C, and 3.5 days during Expedition 395.

4.1.3. Principal results

4.1.3.1. Lithostratigraphy

The Holocene to middle Miocene sediments cored at Site U1554 are relatively homogeneous, primarily composed of silty clay with varying but minor amounts of siliceous and carbonate microfossils, as well as minor proportions of sand (Figure F7). Near the sediment/basement interface, the sediments transition to nannofossil chalk. Core recovery through the sedimentary sequence is near-continuous in the upper 475 m. Based on the observations of sediment composition along with the attenuation pattern of natural gamma radiation (NGR), magnetic susceptibility (MS), and calcium carbonate ($CaCO_3$) weight percent, Site U1554 is divided into four lithostratigraphic units (I–IV). Units I, II, and IV each include two subunits. The measured $CaCO_3$ varies from 0.26 to 84.76 wt%. Features of note include glass layers, bands of variable color at unit or subunit boundaries, basaltic and metamorphic clasts, shell fragments, and halo/pyritized and silt-filled burrows.

Table T1. Hole summary, Expeditions 384, 395C, and 395. (Continued on next page.) **Download table in CSV format.**

Hole	Latitude	Longitude	Water depth (mbsl)	Total penetration (CSF-A [m])	Drilled (m)	Cored (m)	Recovered (m)	Recovery (%)	Cores (*N*)	APC cores (*N*)	HLAPC cores (*N*)	XCB cores (*N*)	RCB cores (*N*)
384-													
U1554A	60°07.5038′N	26°42.0955′W	1,869.8	72.2	0.0	72.2	74.71	103	8	8	0	0	0
U1554B	60°07.5058′N	26°42.0748′W	1,871.0	76.0	0.0	76.0	76.75	101	8	8	0	0	0
U1554C	60°07.4950′N	26°42.0747′W	1,869.0	75.0	0.0	75.0	77.03	103	8	8	0	0	0
U1554D	60°07.4941′N	26°42.0968′W	1,869.0	23.5	14.0	9.5	9.72	102	1	1	0	0	0
395C-													
U1554E	60°07.5235′N	26°42.1324′W	1,869.8	647.7	66.3	581.4	541.07	93	61	16	0	45	0
U1554F	60°07.5136′N	26°42.1140′W	1,869.7	779.9	620.0	159.9	100.15	63	30	0	0	0	30
U1554F	60°07.5136′N	26°42.1140′W	1,869.7										
395-													
U1554G	60°07.5037′N	26°42.1129′W	1,868.7	355.0	0.0	355.0	362.29	102	40	31	3	6	0
U1554H	60°07.4952′N	26°42.1188′W	1,866.7	354.9	0.0	354.9	370.10	104	38	30	0	8	0
		Site U1554 totals:		2,384.2	700.3	1,683.9	1,611.82	96	194	102	3	59	30
384-													
U1555F	60°13.6861′N	28°30.0207′W	1,523.5	184.3	173.7	10.6	8.34	79	8	0	0	0	8
U1555G	60°13.6849′N	28°29.9997′W	1,523.5	309.5	168.6	140.9	60.30	43	26	0	0	0	26
395C-													
U1555H	60°13.6924′N	28°30.0240′W	1,523.7	177.5	0.0	177.5	180.06	101	20	18	0	2	0
U1555I	60°13.6897′N	28°29.9984′W	1,523.6	376.5	159.3	217.2	104.19	48	40	0	0	0	40
		Site U1555 totals:		1,047.8	501.6	546.2	352.90	65	94	18	0	2	74
395C-													
U1562A	60° 06.3030′N	26° 30.1245′W	2,003.4	429.8	0.0	429.8	411.04	96	65	21	36	8	0
U1562B	60° 06.2993′N	26° 30.1026′W	2,003.4	561.5	408.1	153.4	73.08	48	31	0	0	0	31
395-													
U1562C	60°06.3015′N	26°30.0754′W	2,002.8	300.4	7.0	293.4	308.45	105	48	15	33	0	0
		Site U1562 totals:		1,291.7	415.1	876.6	792.57	90	144	36	69	8	31
395C-													
U1563A	60°11.9985′N	28° 00.0209′W	1,417.8	327.6	0.0	327.6	334.98	102	49	21	26	2	0
U1563B	60°11.9946′N	27° 59.9996′W	1,417.8	456.6	301.4	155.2	44.38	29	31	0	0	0	31
		Site U1563 totals:		784.2	301.4	482.8	379.40	79	80	21	26	2	31
395C-													
U1564A	59°51.0377′N	23°16.0071′W	2,208.1	9.5	0.0	9.5	9.89	104	1	1	0	0	0
U1564B	59°51.0371′N	23°15.9868′W	2,207.9	26.2	0.0	26.2	26.81	102	3	3	0	0	0
U1564C	59°51.0374′N	23°16.0087′W	2,208.1	628.9	0.0	628.9	618.71	98	75	17	18	40	0
395-													
U1564D	59°51.0483′N	23°16.0080′W	2,208.1	657.3	2.0	655.3	632.42	97	73	22	6	45	0
U1564E	59°51.0485′N	23°15.9876′W	2,207.3	263.5	0.0	263.5	273.70	104	28	22	0	6	0
U1564F	59°51.0363′N	23°15.9840′W	2,208.1	1,169.7	598.0	571.7	434.15	76	75	0	0	0	75
		Site U1564 totals:		2,755.1	600.0	2,155.1	1,995.70	93	255	65	24	91	75
395-													
U1602A	61°11.7138′N	38°10.8186′W	2,708.6	8.8	0.0	8.8	8.81	100	1	1	0	0	0
U1602B	61°11.7144′N	38°10.8184′W	2,709.2	251.1	0.0	251.1	262.37	104	38	16	22	0	0
U1602C	61°11.7253′N	38°10.8193′W	2,710.0	269.3	2.0	267.3	272.63	102	38	19	19	0	0
U1602D	61°11.7259′N	38°10.7967′W	2,709.1	540.7	0.0	540.7	450.45	83	66	19	18	29	0
U1602E	61°11.7150′N	38°10.7961′W	2,709.2	1,365.2	529.3	835.9	450.39	54	87	0	0	0	87
		Site U1602 totals:		2,435.1	531.3	1,903.8	1,444.70	76	230	55	59	29	87
		Expedition 384/395C/395 totals:		10,698.1	3,049.7	7,648.4	6,577.00	86	997	297	181	191	328

4.1.3.2. Igneous petrology

The cores from Hole 395C-U1554F are mostly slightly to moderately altered basalt (Figure F7). An additional meter of basalt was also recovered in Hole 395C-U1554E. The contact between the basalt and overlying sedimentary strata was partly recovered across Cores 395C-U1554F-4R through 6R. In Hole U1554F, detailed core observations reveal a series of sheet flows and pillow lavas (Figure F8). The sheet flows consist of hypocrystalline aphyric olivine basalt. Flow boundaries and fractures generally show brown alteration halos, especially in the upper third of the hole, and vesicles are often filled. The pillow lavas are highly fragmented with glass rinds, chilled margins, and vesicle bands. In the upper 40 m of the basement, thin sedimentary and volcaniclastic horizons are common, consisting of calcareous mudstone conglomerate layers and peperites. The

Table T1 (continued).

Hole	Start date	Start time UTC (h)	End date	End time UTC (h)	Time on hole (days)	Time on site (days)	Comment
384-							
U1554A	27 Jul 2020	0630	28 Jul 2020	0630	1.00		
U1554B	28 Jul 2020	0630	28 Jul 2020	1500	0.35		
U1554C	28 Jul 2020	1500	28 Jul 2020	2345	0.36		
U1554D	28 Jul 2020	2345	29 Jul 2020	0845	0.38		Core donated to ship for testing the track systems
395C-							
U1554E	24 Jun 2021	0145	29 Jun 2021	0245	5.04		
U1554F	29 Jun 2021	0245	10 Jul 2021	0800	11.22		Reentry system installed
U1554F	21 Jul 2021	0730	21 Jul 2021	2230	0.63		Attempted VSI run
395-							
U1554G	27 Jun 2023	1845	29 Jun 2023	1745	1.96		
U1554H	29 Jun 2023	1745	01 Jul 2023	0645	1.54		
					Site U1554 totals:	22.48	
384-							
U1555F	09 Aug 2020	0915	11 Aug 2020	0830	1.97		Tested PDC RCB bit
U1555G	11 Aug 2020	0830	16 Aug 2020	2200	5.56		
395C-							
U1555H	12 Jun 2021	1300	14 Jun 2021	2000	2.29		
U1555I	14 Jun 2021	2000	23 Jun 2021	2030	9.01		Free fall funnel
					Site U1555 totals:	18.83	
395C-							
U1562A	10 Jul 2021	1306	13 Jul 2021	1930	3.27		
U1562B	13 Jul 2021	1930	21 Jul 2021	0000	7.18		Free fall funnel
395-							
U1562C	01 Jul 2023	1215	03 Jul 2023	0900	1.86		
					Site U1562 totals:	12.31	
395C-							
U1563A	22 Jul 2021	0230	24 Jul 2021	0715	2.20		
U1563B	24 Jul 2021	0715	30 Jul 2021	0518	5.92		
					Site U1563 totals:	8.12	
395C-							
U1564A	30 Jul 2021	1757	31 Jul 2021	0315	0.39		
U1564B	31 Jul 2021	0315	31 Jul 2021	0630	0.13		
U1564C	31 Jul 2021	0630	05 Aug 2021	0100	4.77		
395-							
U1564D	21 Jun 2023	1500	25 Jun 2023	2015	4.22		
U1564E	25 Jun 2023	0000	27 Jun 2023	0640	1.43		
U1564F	25 Jul 2023	2100	10 Aug 2023	2200	16.04		Reentry system installed
					Site U1564 totals:	26.98	
395-							
U1602A	04 Jul 2023	1718	05 Jul 2023	0500	0.49		
U1602B	05 Jul 2023	0500	06 Jul 2023	1600	1.46		
U1602C	06 Jul 2023	1600	08 Jul 2023	0530	1.56		
U1602D	08 Jul 2023	0530	11 Jul 2023	1645	3.47		
U1602E	11 Jul 2023	1645	24 Jul 2023	0409	12.48		
					Site U1602 totals:	19.46	
					Expedition 384/395C/395 totals:	108.18	

peperites become increasingly baked and crystalline downhole. Thin section examination reveals fine-grained aphyric or sparsely olivine phyric basalts with low to moderate alteration. They contain abundant olivine microphenocrysts, as well as some large olivine phenocrysts with occasional spinel inclusions. The groundmass contains acicular and skeletal swallowtail plagioclase laths, rare clinopyroxene microcrystals, opaque oxides, and altered glass. The inferred volcanic stratigraphy consists of a sequence of interbedded extrusive sheet flows and pillow lavas with minor evidence of sediment deposition.

4.1.3.3. Alteration petrology and structural geology

Basalt recovered at Site U1554 (Holes 395C-U1554E and 395C-U1554F) predominantly contains background-type alteration, although localized alteration in the form of halos around fractures is present to a lesser degree. The alteration assemblage is predominantly carbonate with Fe-oxide/oxyhydroxides + phyllosilicate and minor celadonite. In thin section, saponite and celadonite dominate the alteration assemblage and disseminated magnetite is observed. Vesicles are com-

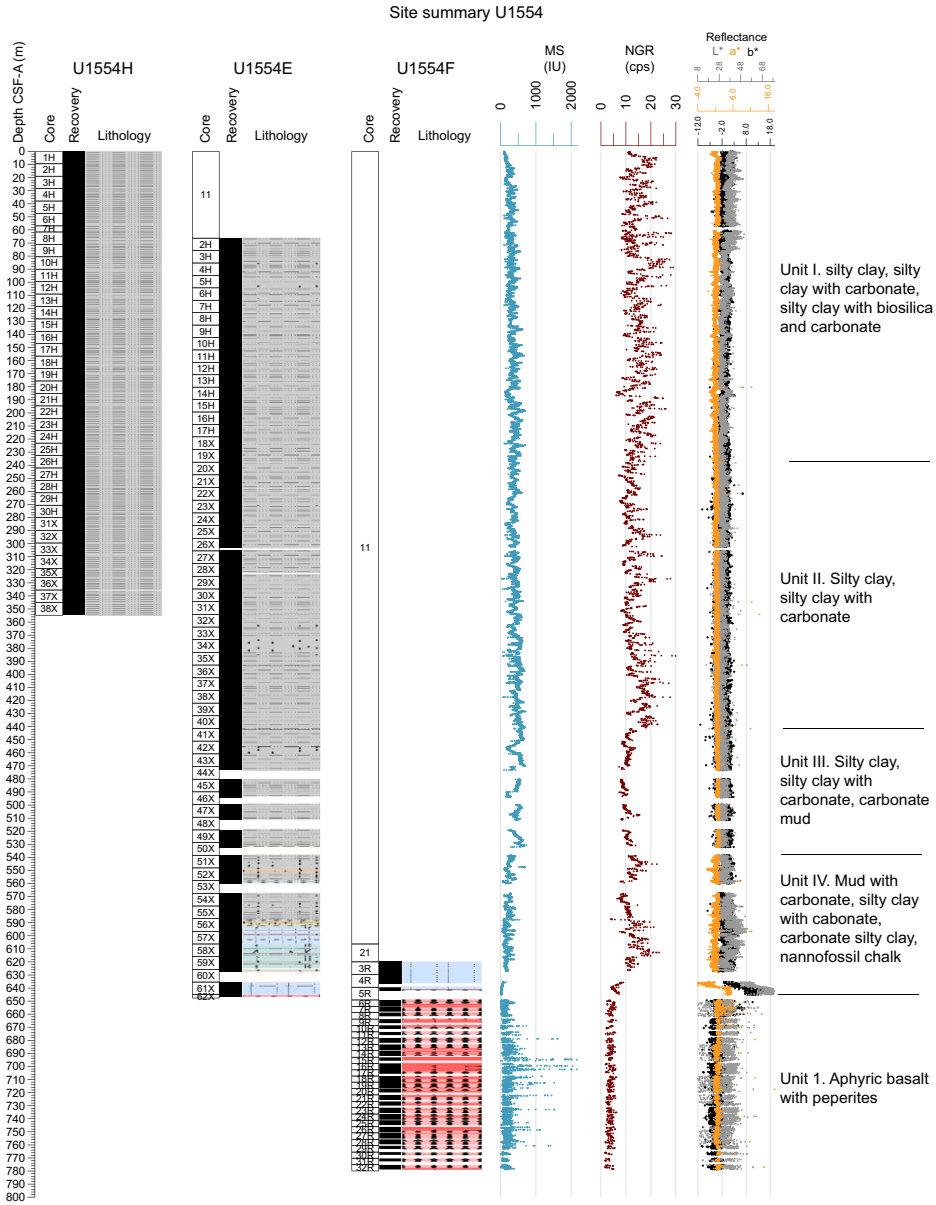

Figure F7. Lithostratigraphic summary, Site U1554. cps = counts per second, Roman numerals = sedimentary units, Arabic numerals = igneous units. For lithology legend, see Figures F9 and F11 in the Expedition 395 methods chapter (Parnell-Turner et al., 2025a).

monly filled with celadonite, and to a lesser extent chlorite, Fe-oxide/oxyhydroxides, carbonate, zeolite, and rare sulfides. Basalt fragments in peperite intervals are variably altered to palagonite material.

Fracture density at Site U1554 is ~17 fractures per meter of recovered core and is uniform with depth. Fracture mineral fill is often Fe-oxide/oxyhydroxide + carbonate ± phyllosilicate with occasional celadonite. Fractures are typically 0.5 mm wide and are described as partially open or veins with an anastomosed or planar shape. Minerals appear as cryptocrystalline or amorphous around basaltic glass. Some fractures are filled with carbonate sediment in intervals where interlayered sediment and peperites are common. Alteration halos are observed around some fractures with colors including gray, brown, and brown with a gray border.

4.1.3.4. Micropaleontology

At Site U1554, a 647 m interval of upper Miocene to upper Pleistocene silty clay and nannofossil chalk was recovered in multiple holes. Micropaleontological analyses were undertaken on sediment samples to 647.7 m core depth below seafloor, Method A (CSF-A), in Hole 395C-U1554E and to 354.97 m CSF-A in Hole 395-U1554G. Biohorizons used in the age model are based on calcareous nannoplankton, planktonic foraminifers, and bolboforms. Calcareous nannofossils and planktonic foraminifers are present with varying abundances, from barren or nearly barren samples to those with very high abundances. Bolboforms, when present, are always rare or few.

A total of eleven calcareous nannofossil Pleistocene biohorizons are identified in the upper 234.96 m of Hole U1554G, representing ages of 0.09 to 1.71 Ma. Four nannofossil biohorizons are identified through the upper Miocene to Pliocene, including the biohorizon top *Coccolithus miopelagicus*, which constrains the bottom of the hole to be older than 11.04 Ma. A total of five Pleistocene, two Pliocene, and three Miocene planktonic foraminifer biohorizons are recognized, with an estimated age of the base of the sediment section to be between 10.54 and 11.76 Ma. Four upper Miocene bolboform biohorizons are recognized with calibrated ages between 5.60 and 10.20 Ma. In the interval ~530–630 m CSF-A, glauconite is abundant in foraminifer sample residues and corresponds to a marked change in sedimentation rate of between 13 and 17 cm/ky in the Pleistocene–upper Pliocene succession to 1 cm/ky in the Pliocene and upper Miocene sequence.

4.1.3.5. Physical properties

At Site U1554, bulk density shows an increase from 1.4 to ~1.8 g/cm^3 from the seafloor to 450 m CSF-A, with noticeable increases and decreases superimposed on this trend. Both MS and NGR

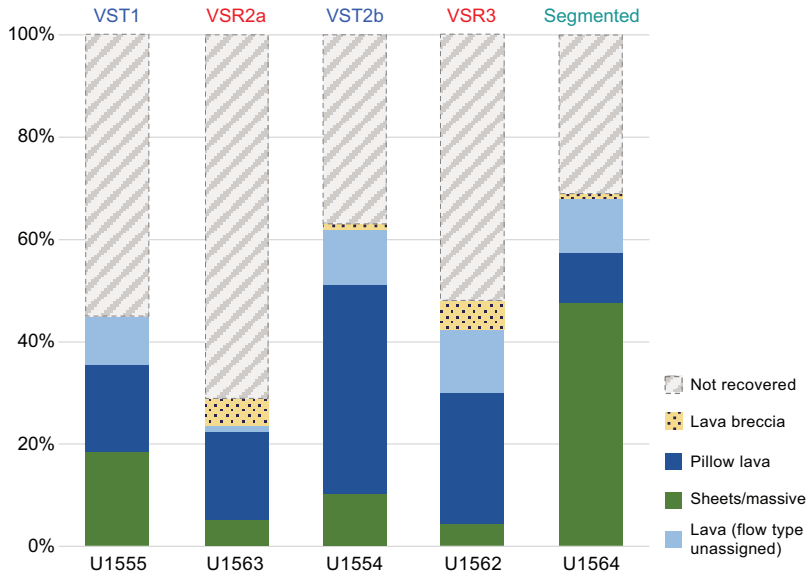

Figure F8. Summary of observed flow morphologies at the five sites that recovered oceanic crust, Expedition 395. The cumulative percentages include intervals without recovery. Sites U1554 and U1555 cored through VSTs, Sites U1562 and U1563 cored through VSRs, and Site U1564 serves as the control site because it cored through segmented crust.

suggest similar oscillatory behavior to that observed in the bulk density (Figure **F7**). These variations become more pronounced below ~450 m CSF-A. Poor core recovery in Hole 395C-U1554E between 470 and 570 m CSF-A makes more detailed interpretations for physical properties challenging in this interval. The bottom ~80 m of Hole U1554E (570–647 m CSF-A) is characterized by large variations in bulk density, a trend also expressed by the MS, color records, and the more variable lithology. The limestone in the bottom two cores (395C-U1554E-61X and 62X) shows higher bulk densities (>1.8 g/cm^3), lower MS, lower NGR, and lighter colors compared to the overlying sediments.

4.1.3.6. Stratigraphic correlation

A ~70 m splice for Holes U1554A–U1554C was constructed during Expedition 384. In the final full splice, the upper 80 m core composite depth below seafloor (CCSF) interval is very similar to that produced during Expedition 384, and it includes only Holes U1554A–U1554C. From Core 395C-U1554E-2H, tied to Core 384-U1554A-7H from the initial splice, through Core 395-U1554H-23H, a continuous splice was constructed using only Holes 395C-U1554E and 395-U1554H. Between 225 and 345 m CCSF, several gaps are unavoidable.

4.1.3.7. Paleomagnetism

Natural remanent magnetization (NRM) was measured for sedimentary cores recovered from Expedition 384 Holes U1554A–U1554C, Expedition 395C Holes U1554E and U1554F, and Expedition 395 Holes U1554G and U1554H. The cores were demagnetized with a stepwise alternating field (AF) cleaning protocol, with the exception of Hole U1554G and Cores 395-U1554H-1H through 7H. The resolution of these measurements varies from 1 to 5 cm. The demagnetization step at 20 mT from Hole U1554E was used to establish an age-depth model for the upper 400 m in Site U1554. Between 400 m CSF-A and the bottom of Core 395C-U1554E-61X at 645 m CSF-A, apparent gaps in sediment deposition hampered interpretation of the magnetostratigraphy.

NRM was measured for basalt cores recovered in Hole U1554F. The basalts in Hole U1554F do not fully demagnetize at 25 mT but the drilling overprint is removed. Demagnetization reveals mostly normal polarities and one of two behaviors: (1) 80% magnetization loss before 25 mT or (2) no significant loss of magnetization by 25 mT. The variations in MS coincide with those in NRM intensity before and after demagnetization at 25 mT.

4.1.3.8. Geochemistry

Cores taken during Expeditions 384 (Hole U1554A), 395C (Holes U1554E and U1554F), and 395 (Holes U1554G and U1554H) were analyzed for headspace gas, interstitial water (IW) chemistry, and bulk sediment geochemistry. Headspace gas analyses were conducted for Holes U1554A and U1554E; methane concentrations are variable and range ~0–12,000 ppmv (Figure **F9**). Ethane was absent in all holes. Holes U1554E and U1554G were analyzed for IW chemistry and bulk sediment

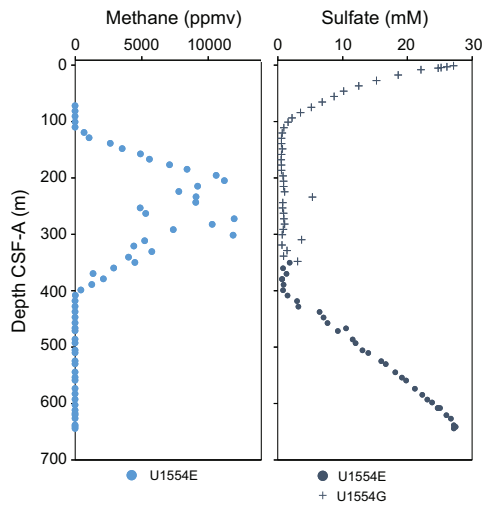

Figure F9. Composite gas analyses of methane concentrations and sulfate concentrations, Site U1554.

geochemistry. Calcium ion (Ca^{2+}) and magnesium ion (Mg^{2+}) concentrations display similar trends with depth. Sulfate ion (SO_4^{2-}) concentrations display a bimodal distribution with seawater-like values at the top and bottom of the sediment column. $CaCO_3$ ranges 0.3–84.8 wt%, with the highest $CaCO_3$ content between 554.01 m CSF-A and the sediment/basement interface. Bulk sediment generally has low total organic carbon (TOC), total nitrogen (TN), and total sulfur (TS) content. Dissolved oxygen measurements were conducted on whole-round cores from Hole U1554G to ~347 m CSF-A (Core 40X).

4.1.3.9. Downhole measurements

Logging operations were undertaken in Holes 395C-U1554E (~0–640 m wireline log matched depth below seafloor [WMSF]) and 395C-U1554F (~604–770 m WMSF). Hole U1554E was logged with the triple combination (triple combo) and Formation MicroScanner (FMS)-sonic tool strings, and Hole U1554F was logged with the triple combo, FMS-sonic, and Ultrasonic Borehole Imager (UBI) tool strings. Logging responses at Site U1554 define five logging units, with subunits in Logging Units L1, L2, and L4. Subunit L1a (0–75 m WMSF) is defined by gamma log measurements collected through drill pipe, and Subunit L1b (75–108 m WMSF) is characterized by low density and low gamma log. Unit L2 (108–440 m WMSF) is characterized by cyclic, 1 to 10 m long fluctuations in gamma log, the peaks of which are dominated by high thorium counts. MS data show a similar cyclic pattern in this logging unit. The cyclic gamma and MS logging responses occur at shorter wavelengths in Subunit L2a (108–375 m WMSF) than in Subunit L2b (375–440 m WMSF). Unit L3 (440–495 m WMSF) is marked by relatively lower gamma log and longer wavelength fluctuations in MS, and the density (~1.8 g/cm^3) and porosity (~0.6) in this unit are remarkably invariant. Unit L4 (495–647 m WMSF) is marked by relatively high gamma log and can be divided into three subunits: Subunit L4a (495–535 m WMSF) shows invariant *P*-wave velocity (V_P) and shear wave velocity (V_S) values, and Subunit L4b (535–635 m WMSF) shows relatively high V_P and V_S (up to ≤ 2615 m/s and 850 m/s, respectively). Subunit L4c (635–647 m WMSF) contains the lowermost sediment and the top of the sediment–basement transition zone, the top of which is marked by an abrupt decrease in density and increase in porosity. FMS borehole images for the sedimentary section of Site U1554 show decimeter-scale, shallow dipping, alternating conductive and resistive layers. Unit L5 denotes the basaltic basement of Site U1554, with an increase in resistivity and density. The FMS and UBI borehole images show clear layering in the basalt basement, some of which contain numerous features that may represent fractures and basaltic pillow margins.

4.1.3.10. Age model

Age model tie points at Site U1554 are based upon paleomagnetic and paleontologic constraints. From the seafloor to the base of Matuyama Chron at 402.34 m CSF-A, the age model is based on magnetostratigraphic reversals complemented by calcareous nannofossil and planktonic foraminifer biostratigraphy. Below this depth, a succession of magnetic polarity reversals is recorded, but their magnetostratigraphic interpretation is highly uncertain because of gaps in core recovery, so the age model relies on biostratigraphy alone, which is based on calcareous nannofossils, planktonic foraminifers, and bolboforms. The age at sediment/basement interface is extrapolated at ~12.16 Ma. Sedimentation rates are high through the uppermost 535 m of the section, ranging 13–17 cm/ky. Below this depth, sedimentation rates are considerably lower (average = 0.9 cm/ky).

4.2. Site U1555

4.2.1. Background and objectives

Site U1555 is located in the North Atlantic Ocean east of Reykjanes Ridge and south of Iceland (see the **Site U1555** chapter [Briais et al., 2025a]). Site U1555 (60°13.6908′N, 28°30.0240′W) is located at the intersection of Seismic Lines JC50-1 (CMP 57881) and JC50-C7 (CMP 3720), obtained in 2010 aboard RRS *James Cook* Cruise JC50. Site U1555 is located in VST 1, with an estimated basement age of 2.8 Ma. Cores and data from this site will address two of the primary science objectives of Expedition 395: (1) crustal accretion and mantle behavior and (2) time-dependent hydrothermal alteration of oceanic crust.

4.2.2. Operations

Operations at Site U1555 first occurred in August 2020 during Expedition 384. Holes U1555A–U1555E were drilled through the sedimentary section and into the underlying basement to test different hard rock drill bits (Blum et al., 2020). Holes U1555F and U1555G were cored during Expedition 384 and recovered 68.64 m of basalt basement cores. In addition to coring, Hole U1555G was logged with downhole tools. Expedition 395C cored Holes U1555H and U1555I, followed by downhole logging in Hole U1555I. The sediments and basalts recovered during Expeditions 384 and 395C were sampled for shipboard measurements during the cruises. All of the cores were described postcruise at a core description party held at the GCR in College Station in May 2022.

Holes U1555F–U1555I were cored in support of Expedition 395 science objectives. The hole depths range 177.5–376.5 m DSF. Overall, 94 cores were recovered for the site, with 352.89 m of core over a 546.2 m interval (65% recovery). Downhole wireline logging operations were undertaken in Holes U1555G and U1555I.

4.2.3. Principal results

IODP technical staff processed all cores and samples from Expeditions 384 and 395C in the shipboard laboratories following the measurement and sampling plan constructed by the shore-based Expedition 395 Co-Chief Scientists and science party. Data interpretation, core description, and biostratigraphic analyses took place postcruise.

4.2.3.1. Lithostratigraphy

Sediments were only recovered from Hole 395C-U1555H and in two cores from Hole 395C-U1555I. The sediments at this site are primarily composed of (1) silty clay or clayey silt and (2) silty clay or clayey silt with biogenics (Figure **F10**). Thin (<1 m) carbonate-rich layers (carbonate silty clay or clayey silt; nannofossil silty clay or clayey silt) are present in some intervals. Both biosilica and carbonate are commonly observed. One lithostratigraphic unit is observed at this site (Unit I), which is divided into two subunits (IA and IB) at 62.0 m CSF-A. The division is based primarily on

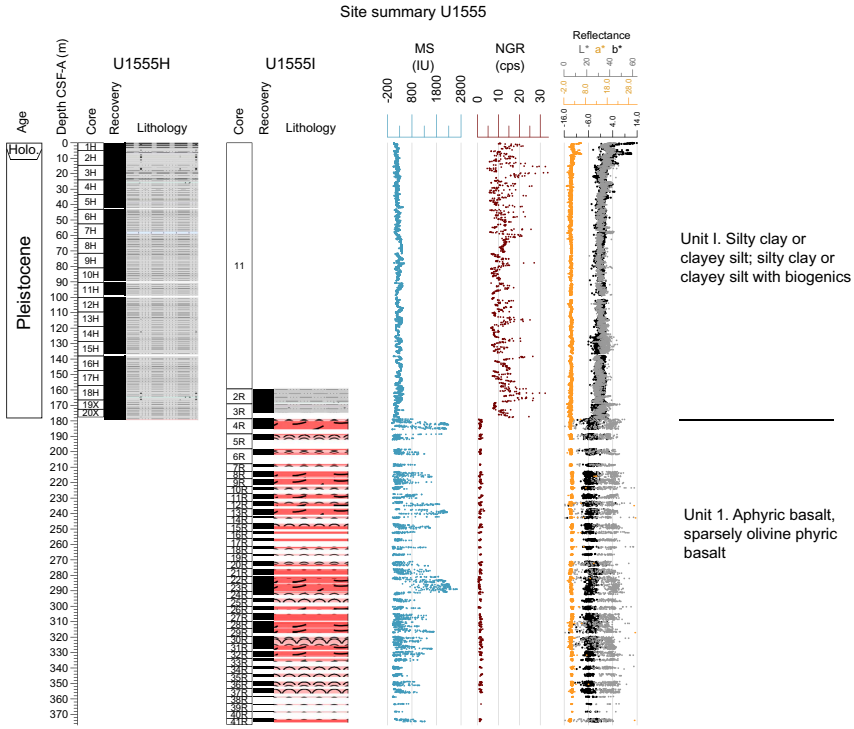

Figure F10. Lithostratigraphic summary, Site U1555. cps = counts per second, Roman numerals = sedimentary units, Arabic numerals = igneous units. For lithology legend, see Figures F9 and F11 in the Expedition 395 methods chapter (Parnell-Turner et al., 2025a).

changes in amplitude and wavelength of NGR and MS. Hole U1555H contains several clasts greater than 2 cm; these are composed of a variety of volcanic and crystalline igneous lithologies, including pumice, basalt, and one of granitic composition. Although the sediments at this site are relatively homogeneous, there are a few graded beds and one sharp contact of note in this hole. Weight percentage $CaCO_3$ and other biogenic content is generally low at this site, although biogenic content is slightly higher in Subunit IB compared to Subunit IA.

4.2.3.2. Igneous petrology

Significant quantities of basalt with minor alteration were recovered from Holes 384-U1555G and 395C-U1555I. Detailed core and thin section descriptions reveal a sequence of intercalated sheet flows and pillow lavas, each of which have thicknesses of up to tens of meters. The sheet flows consist of hypocrystalline aphyric olivine basalt with localized evidence for coarsening and flow banding. Pillow lava fragments have curved glass rinds, chilled margins, and vesicle bands. There are occasional calcareous mudstone layers. Thin section examination reveals fine-grained aphyric or sparsely olivine phyric basalts with slight to moderate alteration. Phenocrysts are largely absent, although there are sparse numbers of small olivines. Plagioclase is the most abundant groundmass crystal phase, often occurring as swallowtail laths. There are occasional clinopyroxene microcrystals, opaque oxides, and altered glass. The inferred volcanic stratigraphy consists of a repeated series of extruded sheet flows and pillow lavas with little evidence for significant sediment deposition.

4.2.3.3. Alteration petrology and structural geology

Basalt at Site U1555 is mostly slightly altered, and alteration is disseminated rather than localized in patches or fracture halos. The alteration assemblage is phyllosilicate + Fe-oxide/oxyhydroxides with minor zeolite and celadonite. Vesicles are commonly filled with celadonite and to a lesser extent saponite, Fe-oxide/oxyhydroxides, carbonate, zeolite, and rare sulfides. Vesicle fills are commonly mineralogically zoned with multiple minerals in each. Celadonite often shows color zonation in vesicle fills.

Fracture density in Holes 384-U1555F, 384-U1555G, and 395C-U1555I is ~14 fractures per meter of recovered core, with notable increases in fracture density at 217–222 m CSF-A in Hole U1555G and 285–292 m CSF-A in Hole U1555I. Fractures are typically <0.5 mm wide, and most fractures are classified as partially open and planar and occur either as isolated, nonconnected fractures or as crosscutting fractures. There is no prevailing fracture orientation with respect to the core axis. Fracture mineral fills are either mainly phyllosilicate + Fe-oxide/oxyhydroxides or celadonite + zeolite, the occurrence of which appears to be depth related in Holes U1555G and U1555I. Alteration halos are observed around some fractures and show color change up to 2.7 cm from the fracture (usually greenish or pale gray), the boundaries of which are defined by brown-colored mineralization that is likely to be due to elevated Fe-oxide/oxyhydroxide concentrations.

4.2.3.4. Micropaleontology

A 177.5 m thick sedimentary succession of latest Pliocene and Pleistocene-age silty clay was recovered in Hole 395C-U1555H. Some sediments were also recovered in Cores 395C-U1555I-2R and 3R. Calcareous nannofossils and planktonic foraminifers are present with moderate to high abundances in most samples studied, although there are some barren intervals. Calcareous nannofossil abundance ranges from few to abundant in most samples, although there are three barren intervals in Samples 395C-U1555H-6H-CC (52.04 m CSF-A), 16H-CC (147.85 m CSF-A), and 18H-CC (166.83 m CSF-A). The preservation of nannofossils is mostly moderate to good, with a few intervals of poor preservation. *Gephyrocapsa* species dominate the upper portion of the record (above ~110 m CSF-A) with common *Coccolithus pelagicus*, *Calcidiscus leptoporus*, *Pseudoemiliania* spp., *Helicosphaera* spp. and *Pontosphaera* spp. Three Pleistocene biozones were identified (NN19, NN20, and NN21), and the base of the hole is constrained to be older than 1.93 Ma (Zone NN18 or older).

Planktonic foraminifers are dominant or abundant in most samples, except where quartz and rock fragments dominate, which are interpreted to be glacial horizons. Preservation is mostly excellent or very good. Above Sample 395C-U1555H-9H-CC (81.51 m CSF-A), samples contain encrusted sinistral *N. pachyderma* and are assigned to the *N. pachyderma* partial range zone (PRZ). Samples

10H-CC (89.35 m CSF-A) to 12H-CC (109.92 m CSF-A) contain *Globoconella inflata* and occasional *Globoconella blowi* and are thus assigned to the *G. inflata* lowest occurrence zone (LOZ). A major change in assemblage occurs between Samples 15H-CC (136.44 m CSF-A) and 17H-CC (157.08 m CSF-A), with the latter containing dominant sinistral *Neogloboquadrina atlantica* in the absence of *G. inflata* and assigned to the *Globoconella puncticulata*/*N. atlantica* concurrent range zone (CRZ). A assemblage similar to that in Sample 17H-CC (157.08 m CSF-A) is found in Samples 395C-U1555I-2R-CC (168.23 m CSF-A) and 3R-CC (174.85 m CSF-A). Sample 3R-CC contains frequent quartz grains that are interpreted as IRD.

4.2.3.5. Physical properties

Gamma ray attenuation (GRA) bulk density values of sediment at Site U1555 typically vary around 1.5 g/cm^3, and basalt values range 2.0–2.5 g/cm^3. Some low values for GRA bulk density and MS in the basalts are likely due to significant voids in the sections. The MS values are also about an order of magnitude higher for the basalts (200 IU) compared to the sediments. The sedimentary MS values often show meter-scale variability with an amplitude of a few 10 IU.

Whole-round V_P was measured on the sediment cores and varies around typical values of 1500 m/s with some point outliers. NGR values are about an order of magnitude lower for the basalts compared to the sediments. NGR shows some cyclicity in the sediments. Notable observations of the Hole 395C-U1555H sedimentary color record is the trend to increasing values (brightening toward lighter colors) in the upper 40 m of the section and a sharp double peak around 60 m CSF-A. This double peak falls close to the inferred boundary between Lithostratigraphic Subunits IA and IB, which is defined using geophysical properties and corresponds to a distinct change in accumulation rate. In the basalt sequences the a* variable appears to covary with MS, and high MS values correspond to lower a* values. The a* variations approximately correspond to described occurrence of sheet flow units and pillow basalt intervals.

4.2.3.6. Paleomagnetism

The sedimentary rocks from Holes 395C-U1555H and 395C-U1555I and basement rocks from Holes 384-U1555F and 384-U1555G were demagnetized with a stepwise AF cleaning protocol. For Hole U1555H, the characteristic remanent magnetization (ChRM) was successfully isolated by 25 mT demagnetization and used to reconstruct the magnetostratigraphy based on polarity reversals. NRM and MS values both show a variable cyclicity between 80 and 170 m CSF-A. For basalts in Holes U1555G and U1555I, demagnetization revealed one of two behaviors: (1) 80% magnetization loss before 25 mT or (2) no significant loss of magnetization by 25 mT.

4.2.3.7. Geochemistry

Cores collected from Holes 395C-U1555H and 395C-U1555I were analyzed for headspace gas, IW chemistry, sediment geochemistry, and bulk sediment and basalt geochemistry. No geochemical analyses were conducted during Expedition 384 at Site U1555 (Holes U1555F and U1555G). Methane and ethane concentrations are low (≤3 ppmv) and below the detection limit, respectively. Downhole trends in IW chemistry include increasing calcium ion (Ca^{2+}) and decreasing magnesium ion (Mg^{2+}) concentrations with depth. Sulfate (SO_4^{2-}) concentrations have a small range of variability (SO_4^{2-} = 28.6 ± 1.5 mM) and exhibit a decreasing trend with depth. As IW samples approach the sediment/basalt interface, ion concentrations support the hypothesis that fluid-rock interactions are influencing IW composition. Bulk sediment TOC and $CaCO_3$ contents are generally low (maximums = 0.3 wt% and 11%, respectively).

4.2.3.8. Downhole measurements

Downhole logging operations at Site U1555 were conducted in Hole 384-U1555G using the triple combo, FMS-sonic, and Versatile Seismic Imager (VSI) tool strings and in Hole 395C-U1555I using the triple combo tool string. Four downhole formation temperatures were recorded with the advanced piston corer temperature (APCT-3) tool while taking Cores 395C-U1555H-4H, 7H, 10H, and 13H. At Site U1555, Logging Unit L1 comprises the sedimentary section, which we divided into Subunit L1a (Hole U1555G = 0–145 m WMSF; Hole U1555I = 0–75 m WMSF) and Subunit L1b (Hole U1555G = 145–180 m WMSF; Hole U1555I = 75–178 m WMSF), the boundary between which is defined by changes in logged gamma ray spectra. Logging data were collected in Subunit L1a through the casing and drill pipe in Hole U1555G and through the drill pipe in Hole

U1555I. Below the drill pipe, gamma ray spectra in Subunit L1b show multiple distinct peaks related to increased Th content. A clear sediment/basement interface is observed at ~180 and ~178 m WMSF in Holes U1555G and U1555I, respectively. This interface is defined by a decrease in gamma radiation, an increase in resistivity, and a change in the MS from relatively stable in Unit L1 to highly variable in the basaltic basement, which is defined as Unit L2. This unit consists of two subunits based on an increase in gamma log response at ~214 and ~274 m WMSF in Holes U1555G and U1555I, respectively. Subunit L2a shows a relatively lower gamma log response and distinct depth intervals with increased resistivity (with separation of deep and shallow resistivity), which correlate to increases in MS, V_P, V_S, and density; decreases in porosity; and uniform caliper measurements in both holes. These intervals are interpreted to represent basaltic sheet flows, which we tentatively correlated between the two holes. Subunit L2b shows an increase in gamma log response and continues to show similar sheet basalt flow signals in other logs. We estimate a heat flow of 0.116 W/m^2 for the sedimentary sequence of Hole 395C-U1555H based on in situ formation temperature measurements and thermal conductivity measured in the laboratory.

4.2.3.9. Age model

Site survey seismic reflection profiles for Site U1555 show acoustically continuous reflections for most of the sedimentary succession, although some uneven reflections could indicate possible stratigraphic discontinuities. Magnetostratigraphic and biostratigraphic age constraints for the sedimentary succession in Hole 395C-U1555H show good consistency between the different data sets. The age constraints indicate that the upper ~60 m of the succession has a lower average apparent sedimentation rate (~3.6 cm/ky) than the rest of the hole (~10 cm/ky). Apart from the sedimentation rate change at ~60 m CSF-A, there are no major changes in lithology or other clear sedimentologic evidence for stratigraphic gaps in any part of the succession.

4.3. Site U1562

4.3.1. Background and objectives

Site U1562 is located in the North Atlantic Ocean, east of Reykjanes Ridge and on Björn drift south of Iceland (Figure **F1**) (see the **Site U1562** chapter [Briais et al., 2025b]). Site U1562 is located on Seismic Line JC50-1 (CMP 39920), near the intersection with Seismic Line JC50-C2 (CMP 685), both obtained in 2010 during RRS *James Cook* Cruise JC50.

Site U1562 is located on VSR 3, and has an estimated basement age of 13.86 Ma. The sediment section at Site U1562 is marked by the Björn drift deposit, a thicker section of which was cored at Site U1554.

Cores and data from this site will address all three primary science objectives: (1) crustal accretion and mantle behavior; (2) ocean circulation, gateways, and sedimentation; and (3) time-dependent hydrothermal alteration of oceanic crust.

4.3.2. Operations

Site U1562 (60°06.3006′N, 26°30.1044′W) consists of three holes, 395C-U1562A, 395C-U1562B, and 395-U1562C, which reach 300.4–561.5 m DSF (Table **T1**). A total of 144 cores were recovered for Site U1562. These cores collected 792.57 m of sediment and basalt over a cored interval of 876.6 m (90% recovery). Downhole wireline logging operations using four logging tool strings took place in Hole U1562B. The total time spent at Site U1562 was 12.3 days.

4.3.3. Principal results

4.3.3.1. Lithostratigraphy

The sediments at Site U1562 include silty clay with variable amounts of carbonate (Lithostratigraphic Units I–III) and nannofossil ooze to chalk (Unit IV) (Figure **F11**). Based on smear slide observations, carbonate microfossils are present in amounts ranging from a few to over 30%. Siliceous microfossils are present throughout but in minor amounts (<10%). The terrigenous component is dominated by quartz and feldspar, although glauconite and glass are also present. Glass abundance increases from Unit I to Unit II. Immediately below the lithologic boundary between Units I and II there are several sharp contacts. Unit III is defined by the abundance of features consistent with soft-sediment deformation, likely caused by a series of slumps. There is a sharp

contact between Units III and IV. Weight percent $CaCO_3$ is variable, but average values increase downhole to the chalk in Unit IV. Small clasts of volcaniclastic material (pumice and scoria) and larger clasts of variable lithology are found throughout the sequence at Site U1562.

4.3.3.2. Igneous petrology

Hole 395C-U1562B was drilled 133 m into basement with a recovery of 48%. In addition, glassy lava fragments and the top of a weathered sheet flow were recovered from the base of Hole 395C-U1562A. The sediment/basement contact is poorly defined. Cores from this site consist of sparsely to moderately olivine phyric pillow lavas with a few massive sheet flow intervals up to 10 m thick (Figure **F11**). Fragmented cryptocrystalline pillow lavas are characterized by curved chilled margins, glassy rinds, and abundant vesicles. The sheet flows have occasional chilled flow margins and medium grained, nonvesicular interiors. Intercalated peperites and mudstone are common. The peperitic intervals display abundant evidence for lava-sediment interaction, including fragmented basalt clasts with quenched rims and fluidal margins. Thin sections from pillow lavas have abundant groundmass olivines, sometimes with dendritic forms suggestive of rapid cooling during the eruptive process. The abundance of sediment-rich material intercalated in the basalts at this site suggests that significant amounts of sediment accumulated between eruptions, with preliminary estimates of eruption hiatuses on the order of ~10^5 y.

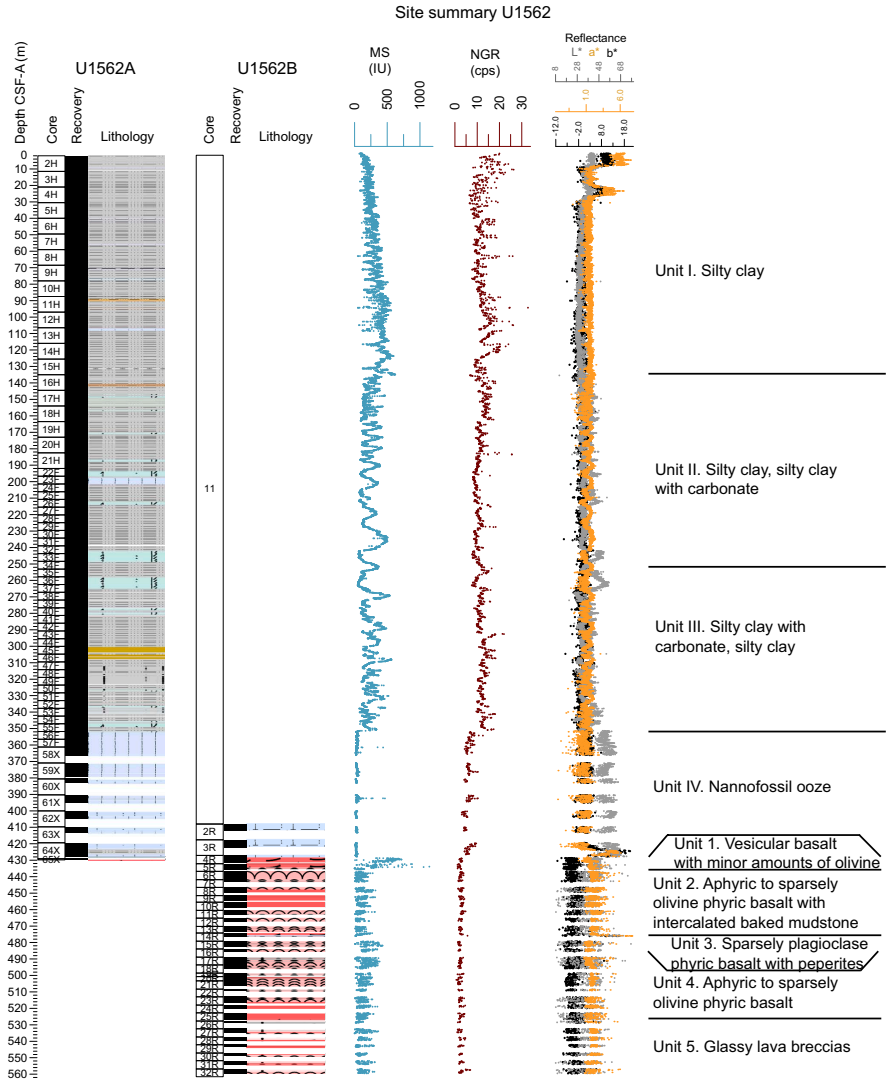

Figure F11. Lithostratigraphic summary, Site U1562. cps = counts per second, Roman numerals = sedimentary units, Arabic numerals = igneous units. For lithology legend, see Figures F9 and F11 in the Expedition 395 methods chapter (Parnell-Turner et al., 2025a).

4.3.3.3. Alteration petrology and structural geology

The majority of basalt core recovered from Site U1562 is slightly to moderately altered. Intervals of the basalt basement intermixed with carbonate sediment and peperite intervals are highly to completely altered. Alteration is mostly pervasive, although localized alteration, mainly in the form of fracture halos, is also observed. The alteration assemblage is phyllosilicate + Fe-oxide/oxyhydroxides with minor celadonite. Basalt clasts in peperite intervals are mostly altered to palagonite material. Vesicles are mainly filled with celadonite, Fe-oxide/oxyhydroxides, and calcite with some saponite and minor zeolite. Vesicle fills are commonly mineralogically zoned with multiple minerals in each. Fracture density in Hole 395C-U1562B is ~21 fractures per meter of recovered core and is near constant with depth. Fractures are predominantly ≤0.5 mm wide and occur either as isolated, nonconnected fractures or within anastomosing networks. Fracture mineral fills are mostly carbonate ± Fe-oxide/oxyhydroxide with minor phyllosilicate and celadonite. Peperite and altered carbonate sediment intervals contain complex carbonate filled fracture networks. Fracture alteration halos are up to 2 cm wide from the fracture wall, and are either pale gray, brown, green-gray, or green-brown in color.

4.3.3.4. Micropaleontology

At Site U1562, micropaleontological analyses were undertaken on samples from all three holes. Calcareous nannofossils and planktonic foraminifers are generally present in moderate to high abundances, with occasional barren or nearly barren samples. Bolboforms, when present, are generally rare or few. Calcareous microfossil preservation is mostly excellent to very good, with occasional intervals of moderate preservation. The Pleistocene succession is well constrained by biostratigraphy, with eight calcareous nannofossil biohorizons identified in Hole 395-U1562C and five planktonic foraminifer biohorizons identified in both Holes 395C-U1562A and U1562C. No upper Pliocene biohorizons were identified, but one calcareous nannofossil and two planktonic foraminifer biohorizons constrain the lower Pliocene succession. The upper Miocene sedimentary succession is constrained by two calcareous nannofossil biohorizons, four planktonic foraminifer biohorizons, and three bolboform biohorizons. Based on calcareous microfossil biostratigraphy, the bottom of the sedimentary succession is between 11.04 and 11.76 Ma. During the rotary drilling of Hole 395C-U1562B into basement, a substantial interval of sediment (~0.65 m thick) was encountered 45 m into basalt and yielded a well-preserved foraminifer assemblage that is significantly older than the lowermost sample examined from the sedimentary succession.

4.3.3.5. Physical properties

Holes 395C-U1562A and 395-U1562C recovered overlapping stratigraphic sections and thus display similar physical properties. GRA bulk density, MS, and NGR increase gradually downhole to 130 m CSF-A with meter-scale oscillations superimposed on this trend (Figure **F12**). MS and NGR sharply drop at 130 m CSF-A. Below this depth, bulk density displays small variations around an average of 1.6 g/cm^3, and MS and NGR show a more variable pattern: large amplitude variations to ~350 m CSF-A, below which core recovery is lower and both measures show lower values. The changes in color properties in the sediments of Holes U1562A and U1562C define stratigraphic intervals similar to those defined from the other physical properties profiles.

In Hole 395C-U1562B, voids and gaps between the core and liners in the basalt sections make the interpretation of the whole-round physical properties profile less straightforward. The sedimentary and peperite units in Hole U1562B are apparent in color records, with higher red-green-blue (RGB), a*, and b* values.

Caliper measurements of V_P for sediments from Hole U1562B are about 1700 m/s, and they vary between 4725 and 6053 m/s for the basalt section. Sedimentary V_P values for Hole U1562C average around 1500 m/s. Bulk density values in Hole U1562A range 1.370–1.673 g/cm^3. Porosity is around 80 vol% and ranges to 65 vol% (average = 70 vol%). Grain density decreases downhole from 2.85 to 2.60 g/cm^3 (average = 2.74 g/cm^3). Thermal conductivity, K, is typically 0.75–1.20 W/(m·K) for the sediments in Holes U1562A and U1562C and 1.40–1.80 W/(m·K) for the basalt in Hole U1562B.

4.3.3.6. Stratigraphic correlation

Correlation was achieved without gaps from the seafloor through Cores 395C-U1562A-16H and 395-U1562C-17F (155.125 m core composite depth below seafloor, Method A [CCSF-A]). Small coring gaps are present below this depth to ~280 m CCSF-A, but cores can still be tied with some confidence based on the broad cyclic patterns and the comparison with wireline logging MS data from Hole 395C-U1562B. Below Core 395C-U1562A-35F, correlation between holes becomes difficult, probably due to the presence of disrupted sequences (e.g., soft-sediment deformation).

4.3.3.7. Paleomagnetism

The sedimentary rocks of Site U1562 were demagnetized with a stepwise AF cleaning protocol (Figure **F13**). For sediments, an overprint to the NRM was removed by application of an AF of 10 mT. The primary ChRM was successfully isolated by 25 mT and used to create an age-depth plot for the hole. NRM and MS values both show a variable cyclicity between 160 and 350 m CSF-A. For basalts in Hole 395C-U1562B, demagnetization revealed one of two behaviors: (1) 80% magnetization loss before 25 mT or (2) no significant loss of magnetization by 25 mT. The variations in MS coincide with those in NRM intensity and intensity after 25 mT of demagnetization.

4.3.3.8. Geochemistry

Holes 395C-U1562A and 395C-U1562B were analyzed for headspace gas, IW chemistry, and bulk sediment geochemistry. Cores collected from Hole 395-U1562C were analyzed for bulk sediment geochemistry. Methane concentrations are low and range ~0–3 ppmv (Figure **F14**). Ethane is absent in all samples. IW calcium ion (Ca^{2+}) concentrations are highest near the sediment/water and sediment/basement interfaces. Magnesium ion (Mg^{2+}) concentrations display a generally decreasing trend with depth, with a small increase at the sediment/basement interface. Sulfate ion (SO_4^{2-}) concentrations have seawater-like values at the top and bottom of the sediment column. $CaCO_3$ weight percent generally increases downcore, trending from ~0 to 33 wt% in the top 100 m

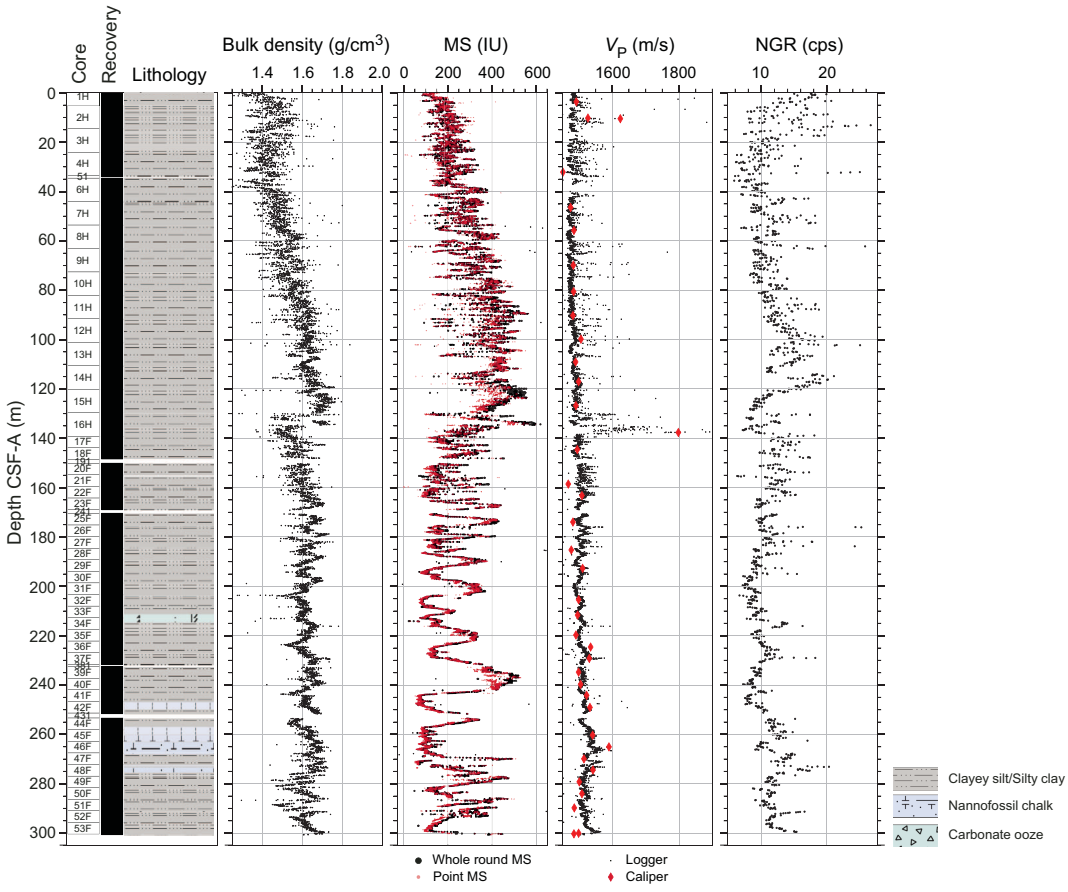

Figure F12. Physical properties measurements, Hole U1562C. cps = counts per second.

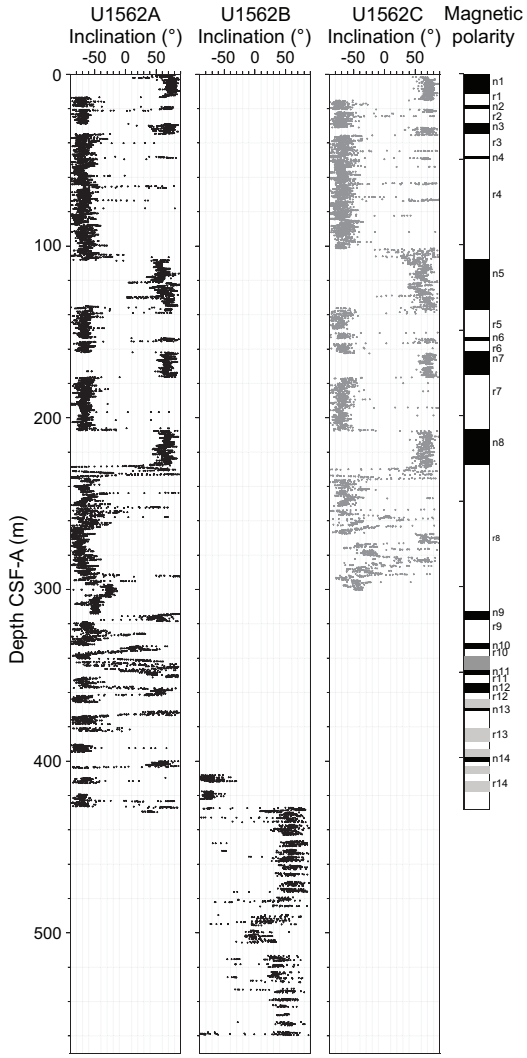

Figure F13. Inclinations and interpreted polarity chrons, Holes U1562A–U1562C. Magnetic polarity: n = normal, r = reverse, gray = depth for which a polarity interpretation was not unequivocal.

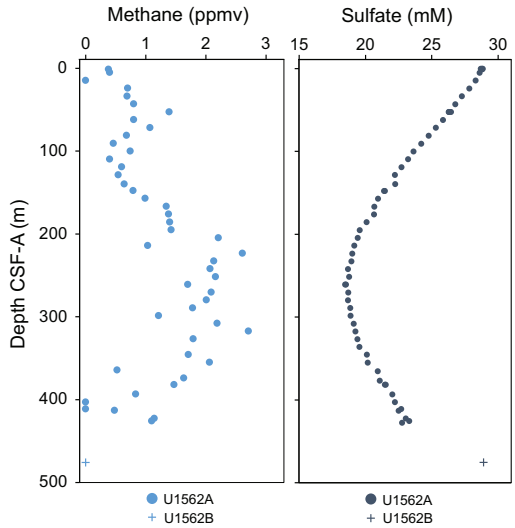

Figure F14. Composite gas analyses of methane concentrations and sulfate concentrations, Site U1562.

to ~83 wt% near the sediment/basement interface. Bulk sediment generally exhibits low TOC, TN, and TS content.

4.3.3.9. Downhole measurements

Logging operations were carried out in Hole 395C-U1562B. A full suite of downhole logs was collected with the triple combo, FMS-sonic, and VSI tool strings for the sediment and basement sections. In the basement section, the UBI was also deployed. Formation temperature measurements were acquired in Hole 395C-U1562A.

The sedimentary section shows three distinct logging units with multiple subunits. Logging Subunit L1a (0–85 m WMSF) was collected through the drill pipe and only collected gamma log and spectral gamma ray. Subunit L1b (85–136 m WMSF) shows an increase in the gamma log to peaks up to ~25 gAPI, which are dominated by Th counts. The density increases in this interval from ~1.2 to ~1.6 g/cm^3. Unit L2 (136–350 m WMSF) is characterized by an overall higher cyclic gamma signal (average = 20.5 ± 2.8 gAPI). This cyclic logging response is also observed in the MS, V_S, and porosity measurements of this logging unit. Subunits L2a (136–305 m WMSF) and L2b (305–350 m WMSF) are differentiated from each other based on the thickness of these logging response cycles. Unit L3 (350–426 m WMSF) shows clearly different logging responses with a sharp drop in gamma log and an increase in density with depth from 1.58 to 1.72 g/cm^3. MS is very low (average = 7.9 SI). The image logs of the sedimentary section show layering as well as mottling patterns; however, the frequent ledges and borehole breakouts influence the data quality.

Logging Unit L4 encompasses the entire basement section of the hole (426–560 m WMSF). The top of Unit L4 is defined by marked changes in resistivity, density, porosity, V_P, V_S, and MS, rather than the gamma log. All logging responses show variability throughout the basement sequence, with increases in MS correlating to increases in V_P, density, and resistivity and decreases in porosity and vice versa. The image logs and wireline data indicate the potential presence of sedimentary layers intercalated with the basaltic basement. Overall, both image logs are of excellent quality in the basement section of the hole.

4.3.3.10. Age model

Magnetostratigraphic and biostratigraphic age constraints for the sedimentary succession in Holes 395C-U1562A and 395-U1562C are combined to create a site age model. Thirteen age datums were chosen to anchor the age-depth model. The succession appears relatively continuous to ~22 m CSF-A. From ~22 to 28.83 m CSF-A, the succession is evidently condensed and/or subject to hiatuses. From 28.83 to 135 m CSF-A there is a sequence of magnetic reversals in Chron 2, together indicating a relatively rapid sedimentation rate over this interval. The age model for the lower part of the succession in Hole U1562A is based on a series of foraminifer, bolboform, and nannofossil biohorizons. These constraints are considered to have a low reliability for various reasons relating to taxonomic uncertainty, low or variable abundances, and/or age calibration issues. Linear extrapolation of the age model suggests an approximate age of 13.0 Ma for the oldest part of the sedimentary succession overlying basalt.

Sedimentation rates are low (1.8 cm/ky) in the uppermost Pleistocene interval above ~22 m CSF-A, before increasing to 10 cm/ky from ~28 to 135 m CSF-A and then returning to relatively normal sedimentation rates for a pelagic ooze of ~2.4 to 3.5 cm/ky to the base of the sedimentary succession.

4.4. Site U1563

4.4.1. Background and objectives

Site U1563 (60°11.9964′N, 28°00.0000′W) is located in the North Atlantic Ocean east of Reykjanes Ridge, south of Iceland (see the **Site U1563** chapter [Briais et al., 2025c]). Site U1563 is positioned on the intersection of Seismic Lines JC50-1 (CMP 53393) and JC50-C6 (CMP 888), both obtained during 2010 aboard RRS *James Cook* Cruise JC50. Site U1563 is located on VSR 2a with an estimated basement age of 5.2 Ma. Cores and data from this site will address two of the primary science objectives: (1) crustal accretion and mantle behavior and (2) time-dependent hydrothermal alteration of oceanic crust.

The operational objectives for this site were to core the sedimentary section using the advanced piston corer (APC), half-length APC (HLAPC), and extended core barrel (XCB) systems to the sediment/basement interface; use the rotary core barrel (RCB) system to core ~130 m into the basement; and use downhole wireline tools to log the borehole. All of the operations took place during Expedition 395C in 2021.

4.4.2. Operations

Site U1563 consists of two holes, Holes U1563A and U1563B, reaching 327.6 and 456.6 m DSF, respectively. A total of 80 cores were recovered at Site U1563. These cores collected 397.36 m of sediment and basalt over a 482.8 m cored interval (79% recovery). Downhole wireline logging operations using three logging tool strings took place in Hole U1563B. The total time spent at Site U1563 was 8.12 days.

4.4.3. Principal results

4.4.3.1. Lithostratigraphy

The sediments at Site U1563 are mostly silty clay and nannofossil chalk (Figure **F15**). The upper lithostratigraphic units (Units I–III) are primarily silty clay or clayey silt, with variable amounts of silty clay or clayey silt with carbonate or carbonate silty clay or clayey silt. Carbonate microfossils are present in amounts ranging from a few to over 30%. Siliceous microfossils are present throughout but in minor amounts (<10%). The terrigenous component is mostly quartz and feldspar, although glauconite and glass are also present, particularly in the lower section of Unit I and throughout Unit II. Unit I includes some layers with dispersed gravel (floating in matrix). Unit II includes four beds with coral fragments: one with large, centimeter-scale pieces and three graded gravel-sand layers with sharp erosive bases that also include sand- and gravel-sized fragments of

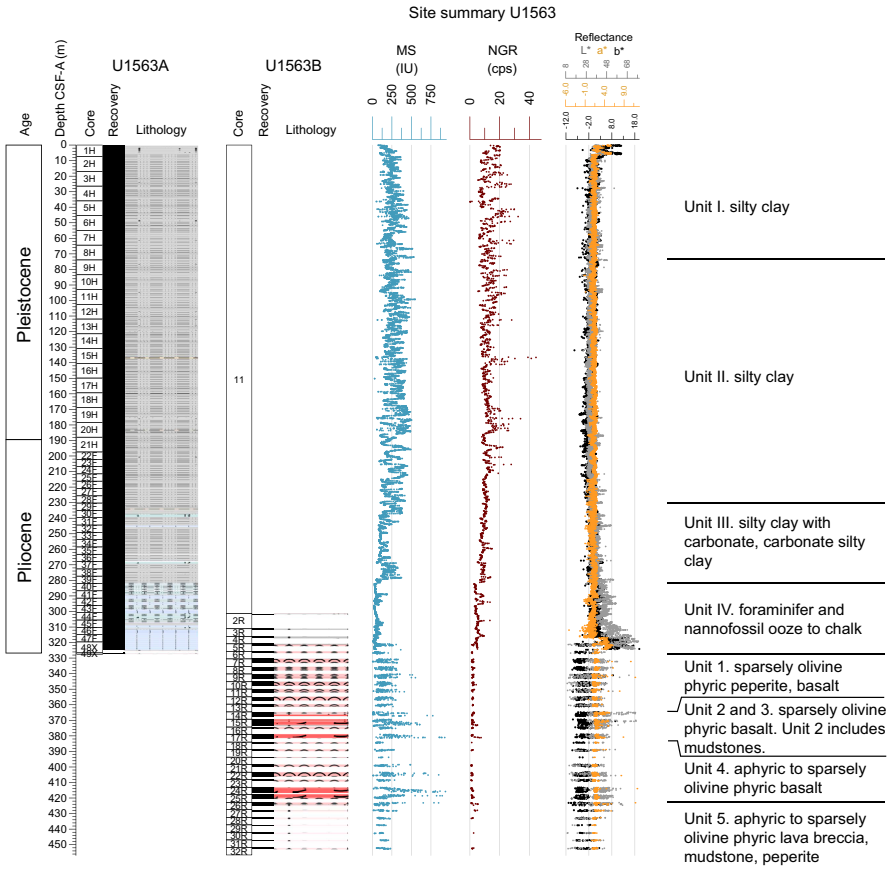

Figure F15. Lithostratigraphic summary, Site U1563. cps = counts per second, Roman numerals = sedimentary units, Arabic numerals = igneous units. For lithology legend, see Figures F9 and F11 in the Expedition 395 methods chapter (Parnell-Turner et al., 2025a).

coral. Clasts are present but rare in Units I and II. The lower unit (Unit IV) is mainly foraminifer or nannofossil ooze transitioning to chalk with depth. Unit IV also contains clasts, several of which are composed of basalt or scoria.

4.4.3.2. Igneous petrology

Hole 395C-U1563B cored ~154 m into basement with a recovery of ~29%. Additional basalt fragments (<1 m) were recovered from the base of Hole 395C-U1563A. The sediment/basement interface is poorly defined, consisting of basalt clasts embedded in calcareous ooze. This site is dominated by sparsely to moderately olivine phyric pillow basalts, which make up >50% of the recovered material. Intercalated sediments and peperitic layers are also common in Hole U1563B (~15% of the recovered material). Peperite intervals show abundant evidence for lava-sediment interaction with quenched rims on basalt clasts, baked carbonate, and fluidal margins and morphologies. There are several sheet flows up to 6 m thick, whose interiors are medium grained and mostly nonvesicular. Their mostly crystalline groundmass contrasts with the cryptocrystalline to glassy groundmass observed in pillow lavas. Thin sections from pillow basalts reveal abundant groundmass olivines, often with dendritic forms that suggest rapid cooling and high degrees of undercooling during eruption and emplacement. The abundance of sediment-rich material between basaltic layers at this site indicates significant amounts of sediment accumulation between eruptions, suggesting this hole may be sampling lavas that either erupted off-axis or flowed into the site after it spread beyond the sediment-poor neovolcanic zone.

4.4.3.3. Alteration petrology and structural geology

Basalt at Site U1563 is moderately to slightly altered, whereas the intermixed carbonate sediments and peperite intervals are completely altered. Alteration is mostly pervasive, although localized alteration in the form of fracture halos also occurs throughout the basalts, more commonly within intervals that contain sediment and peperite material. The alteration assemblage is phyllosilicate + Fe-oxide/oxyhydroxides. Thin sections suggest clay alteration varies in composition from clay mix to celadonite, saponite replacement of olivine, disseminated magnetite/titanomagnetite, and some calcite replacement of plagioclase. Basalt clasts within peperites are mostly altered to palagonite, although some relic, less altered basalt is observed to remain in places. Vesicles are typically filled with celadonite and Fe-oxide/oxyhydroxides, with moderate carbonate, amorphous silica, and saponite, and minor zeolite. Vesicle fills are commonly mineralogically zoned, with multiple minerals in each. Celadonite often shows color zonation in vesicle fills.

Fractures in Hole 395C-U1563B occur at a density of ~18 fractures per meter of recovered core, although this varies with depth. Fractures are typically ≤0.5 mm wide and occur either as isolated, nonconnected fractures or within anastomosing networks. There is no dominant fracture orientation with respect to the core long axis. Fracture mineral fills are either carbonate ± Fe-oxide/oxyhydroxide or Fe-oxide/oxyhydroxide + phyllosilicate, with minor zeolite, celadonite, and epidote in some fractures. Peperite and altered carbonate sediment intervals contain complex carbonate vein networks in places. Fracture alteration halos are up to 1.8 cm wide from the fracture wall and are either pale green or brown.

4.4.3.4. Micropaleontology

In Hole 395C-U1563A, a 327.6 m interval of early Pliocene- and Pleistocene-age silty clay was recovered. Calcareous nannofossils and planktonic foraminifers are present in moderate to high abundances in most samples studied, although there are some barren intervals.

Calcareous nannofossils are present in most samples, ranging in abundance from common to dominant and with moderate to good preservation. The preservation of calcareous nannofossils is best in the upper part of the succession, above ~75 m CSF-A. Three samples are barren or contain very few nannofossils (Samples 395C-U1563A-15H-CC [140.85 m CSF-A]; 16H-CC [150.28 m CSF-A]; and 24F-CC [211.66 m CSF-A]). In the Pleistocene succession above ~112 m CSF-A, *Gephyrocapsa* species are consistently present, becoming dominant in some intervals, and cooccur with frequent *Calcidiscus* spp., *Pseudoemiliania* spp., *Helicosphaera* spp., and *Pontosphaera* spp. *C. pelagicus* is consistently present to abundant except in the interval between Samples 5H-CC (45.83 m CSF-A) and 9H-CC (83.86 m CSF-A). Below the barren (or very low abundance) interval from Sample 15H-CC (140.85 m CSF-A) to 16H-CC (150.28 m CSF-A), species of the

genus *Reticulofenestra* are common to abundant to the base of the hole. The succession is assigned to Pliocene–Pleistocene Biozones NN21, NN20, and undifferentiated NN16-19. The top *Reticulofenestra pseudoumbilicus* between Samples 42F-CC (295.86 m CSF-A) and 44F-CC (305.39 m CSF-A) constrains the base of the hole to be older than 3.82 Ma.

Planktonic foraminifers are a dominant or abundant component of most samples examined except where quartz grains accompanied by frequent rock fragments dominate, which are interpreted as glacigenic deposits. Preservation is excellent in the interval from the core top to Sample 395C-U1563A-5H-CC (45.83 m CSF-A), mostly very good to Sample 36F-CC (267.18 m CSF-A), and finally good to the lowermost sample examined, Sample 48X-CC (324.43 m CSF-A). Sinistral encrusted *N. pachyderma* is common to dominant in Samples 1H-CC to 13H-CC, which are therefore assigned to the *N. pachyderma* PRZ. The lowest occurrence of *G. inflata*, marking the base of the *G. inflata* LOZ, was found between Samples 14H-CC and 16H-CC. The top occurrence of *N. atlantica*, which marks the base of the *Globigerina bulloides* PRZ, is placed between Samples 17H-CC and 18H-CC. The base of *G. puncticulata*, which marks the base of the *G. puncticulata*/*N. atlantica* CRZ, occurs between Samples 44F-CC and 46F-CC, suggesting that the oldest sediments at the site are older than 4.54 Ma.

4.4.3.5. Physical properties

At Site U1563, the full suite of physical properties measurements was acquired for the sediment section (Hole 395C-U1563A) and the basement section (Hole 395C-U1563B). Density, MS, and V_P measurements were acquired using the Whole-Round Multisensor Logger (WRMSL) successfully on sediment core from Hole U1563A; however, for Hole U1563B, WRMSL V_P measurements were not possible because the smaller diameter RCB cores did not fill the liner completely. Density increases with depth within the sediment sequence (mean = ~1.5 g/cm^3), and a notable increase in density occurs below ~300 m CSF-A, with values ranging 2–2.5 g/cm^3 in the basement sequence. MS in the sediment sequence shows meter-scale cyclic behavior (mostly ranging 200–400 IU) from the top of the section to ~280 m CSF-A, where it decreases and becomes less variable (<100 IU). Basement core mostly shows similar or lower MS (<250 IU) than the sediments, although specific intervals show very high MS peaks (up to 1000 IU). Sediments display higher NGR than the basement rocks. Color reflectance, colorimetry, and MS measured on half-round core follows the cyclical trends recorded by WRMSL data. Discrete measurements of V_P were recorded only on basement cores and range 5178–5874 m/s. Moisture and density (MAD) measurements were made on discrete samples of the sediment core and show that bulk density measurements match density measurements collected using the WRMSL. Porosity measurements from MAD average around 70%, and grain density ranges 2.693–2.995 g/cm^3 for sediment core.

4.4.3.6. Paleomagnetism

NRM was measured for sedimentary cores recovered from Hole 395C-U1563A and basement cores recovered in Hole 395C-U1563B. The cores were demagnetized with a stepwise AF cleaning protocol. The resolution of these measurements varied from 2 to 2.5 cm. The demagnetization step at 25 mT for cores from Hole U1563A was used to establish the magnetostratigraphy for the upper 240 m. Between about 240 m CSF-A and the bottom of the hole, both NRM intensity and MS decrease and the paleomagnetic inclinations are not suitable for an unambiguous magnetostratigraphic interpretation.

The transition from sedimentary to basement rocks is at about 300 m CSF-A in Hole U1563B. The basalts usually do not fully demagnetize at 25 mT, although this step allowed for the removal of a drilling overprint and the recognition of a predominantly normal polarity.

4.4.3.7. Geochemistry

Hole 395C-U1563A was analyzed for headspace gas, IW chemistry, and bulk sediment geochemistry. Methane concentrations are low (<2 ppmv), and ethane is below the detection limit. Calcium (Ca^{2+}), magnesium (Mg^{2+}), and sulfate (SO_4^{2-}) generally covary with depth, with higher seawater-like values at the top and bottom of the sediment column. IW strontium, lithium, and silicon concentrations are generally more variable, with concentrations of the dissolved ions reflecting changes in sediment lithology. The average TOC content is 0.3 ± 0.2 wt%. $CaCO_3$ displays a trend similar to that of TOC over the same intervals, with low but variable values in the upper portion of

Hole U1563A (average = 33.5 ± 30.8 wt%); however, from ~285 m CSF-A (Section 395C-U1563A-40F-2) to the sediment/basement interface, the average $CaCO_3$ content is 80.4 ± 4.2 wt%.

4.4.3.8. Downhole measurements

After coring operations concluded, hole conditions in Hole 395C-U1563B deteriorated quickly and a decision was made to only log the sedimentary section of the hole. Hole U1563B was logged with the triple combo, FMS-Sonic, and VSI tool strings. The sedimentary section can be divided into two logging units, each containing logging subunits. Logging Unit L1 (0–136 m WMSF) is divided into Subunit L1a (0–85 m WMSF), which acquired log data through the drill pipe, and Subunit L1b, which shows a variable gamma signal and fluctuating resistivity. The base of Unit L1 is defined by an increase in gamma radiation, and Unit L2 (136–310 m WMSF) shows cyclical behavior in the gamma log and MS for Subunits L2a and L2b (136–239 m WMSF). Subunits L2a and L2b are distinguished by a change in the length scale of the fluctuations in the MS log (at 216 m WMSF). Subunit L2c (239–281 m WMSF) is marked by a decrease in the MS and fewer and shorter length scale fluctuations. Resistivity increases slightly compared to previous units. Subunit L2d (281–308 m WMSF) is marked by increases in resistivity, V_S, and MS. Resistivity image logs from Hole U1563B are of poor quality; however, some alternating conductive and resistive layers can be seen at the meter to decimeter scale. Thermal conductivity measurements were made on sediment core, and four downhole temperature measurements were acquired during APC coring in Hole 395C-U1563A, yielding a vertical heat flow estimate of 32.6 mW/m^2.

4.4.3.9. Age model

Biostratigraphic and magnetostratigraphic age constraints for Hole 395C-U1563A were combined to create an age model, although we note that the magnetostratigraphic interpretation below 250 m CSF-A is uncertain. In general, there is good agreement between the results from the various data sets. The sedimentary succession appears fairly continuous through the Pleistocene and upper Pliocene succession to ~300 m CSF-A, with sedimentation rates between ~6.3 and 10.5 cm/ky. Below ~300 m CSF-A, the age model is constrained by biostratigraphic horizons only and is more uncertain but clearly shows lower sedimentation rates of ~1.5 cm/ky. By extrapolation, the age of the sediment at the bottom of Hole U1563A is estimated at 5.22 Ma, which is consistent with the basement age of 5.2 Ma estimated from satellite and regional shipboard magnetic data.

4.5. Site U1564

4.5.1. Background and objectives

Site U1564 is located in the North Atlantic Ocean on the eastern flank of Reykjanes Ridge, south of Iceland (Figure **F1**) (see the **Site U1564** chapter [Parnell-Turner et al., 2025c]). Expedition 395 sites comprise a crustal flow line transect across the eastern flank of Reykjanes Ridge. Four sites, U1554, U1555, U1562, and U1563, sampled two pairs of VSRs and VSTs that straddle the flanks of Reykjanes Ridge. Site U1564 is located on the same flow line on crust with a segmented pattern that does not show evidence for VSRs or VSTs. The estimated basement age at Site U1564 is 32.4 Ma based on magnetic anomalies and plate reconstructions. Basalt samples from this site will provide a record with which to compare samples from VST/VSR pairs, which will provide constraints on the formation of these crustal structures and on hydrothermal alteration of the crust with time.

Site U1564 is also located on Gardar drift, one of the major contourite drifts in the North Atlantic Ocean, which has the potential to provide high-resolution, millennial-scale records for paleoceanographic research. The sedimentation rate of this drift can serve as a proxy for deep water current strength, providing information on oceanic gateways and their potential ties to mantle plume pulses. ODP Site 983 was cored on Gardar drift, obtaining a sedimentary sequence back to ~2 Ma (early Pleistocene). Cores at Site U1564 extend this record back to the Oligocene epoch.

One main target for Site U1564 was to obtain basalt core from crust that does not exhibit VST/VSR structures. Another main target was to obtain a continuous sedimentary record of Gardar drift. Cores and data from this site will address all three of the primary science objectives: (1) crustal accretion and mantle behavior; (2) ocean circulation, gateways, and sedimentation; and (3) time-dependent hydrothermal alteration of oceanic crust.

4.5.2. Operations

Site U1564 (59°51.0366′N, 23°15.9858′W) consists of six holes drilled during Expeditions 395C and 395. These holes reach 9.5–1169.7 m DSF (Table **T1**). A total of 255 cores were recovered at Site U1564. These cores collected 1881.5 m of sediment and 114.2 m of basalt over a 2155.1 m cored interval (93% recovery). Downhole wireline logging operations using the triple combo tool string, FMS-sonic, and UBI took place in Holes 395C-U1564C and 395-U1564F. The total time spent at Site U1564 was 27 days during Expeditions 395C and 395.

4.5.3. Principal results

4.5.3.1. Lithostratigraphy

The Holocene to lower Oligocene sediments cored at Site U1564 are primarily composed of silty clay, silty clay/claystone with nannofossils, nannofossil silty clay/claystone, and nannofossil chalk with silty clay (Figure **F16**). Based primarily on lithologic observations and sediment composition,

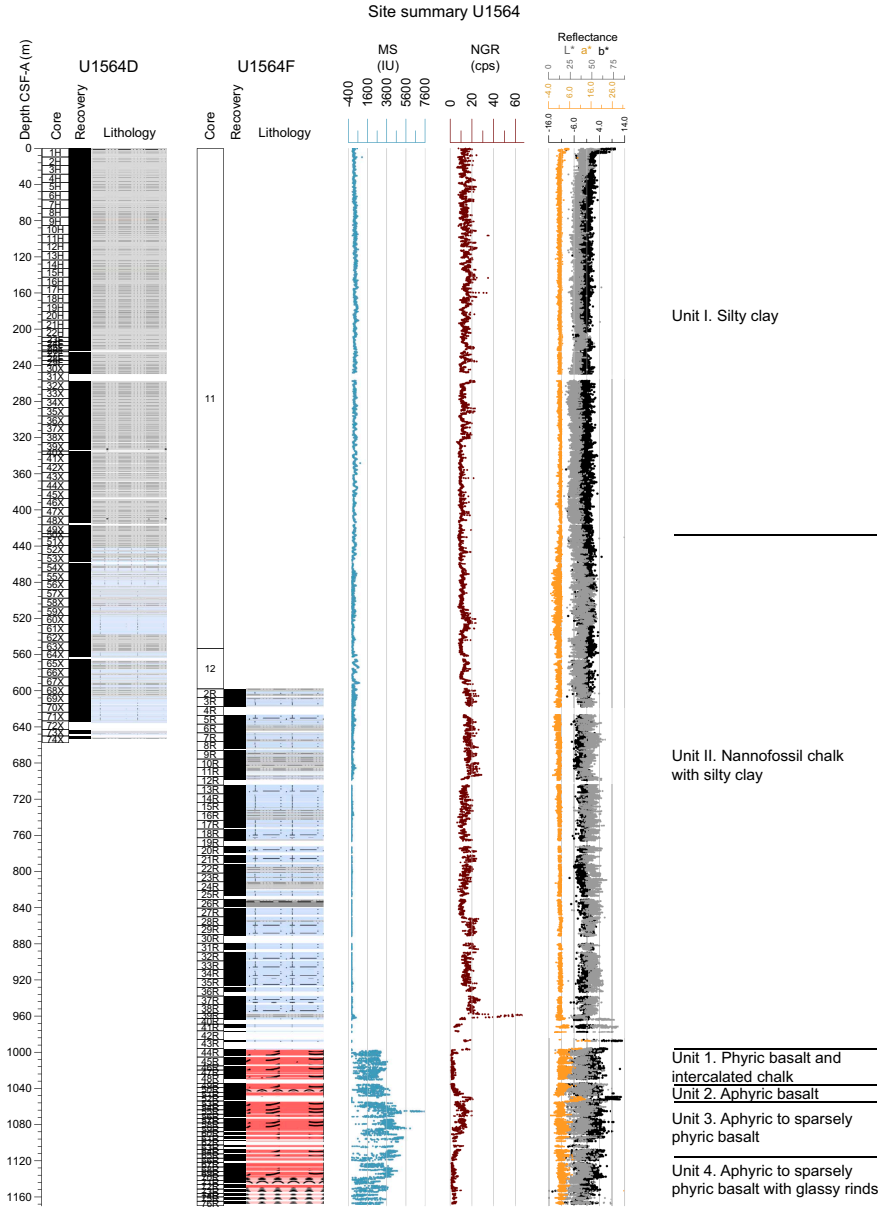

Figure F16. Lithostratigraphic summary, Site U1564. cps = counts per second, Roman numerals = sedimentary units, Arabic numerals = igneous units. For lithology legend, see Figures F9 and F11 in the Expedition 395 methods chapter (Parnell-Turner et al., 2025a).

alongside NGR and $CaCO_3$ measurements, Site U1564 is divided into two major lithostratigraphic Units, I and II. Each unit is divided into three subunits.

In Unit I, Subunit IA is dominated by gray silty clay with a variable but generally minor biogenic component. The biogenic component is dominated by nannofossils; foraminifers and siliceous microfossils are also observed. $CaCO_3$ weight percent is variable in this subunit. Several prominent glass layers are present, dark green banding is observed throughout, and some sharp contacts are observed intermittently. Subunit IB is similarly dominated by gray silty clay and silty clay with biogenics. In addition to thin glass layers and intermittent sharp contacts, pyritization of burrows and halos around burrows are observed. Subunit IC is dominated by dark gray silty clay; this subunit contains the least biogenic carbonate of all units in Site U1564 (supported by smear slide analysis and $CaCO_3$ weight percent).

Unit II is marked by an increase in both carbonate content and lithification. In this unit, glass layers, sharp contacts, and dark banding continue to be present. Fractures with slickensides and/or calcite veins and soft-sediment deformation features are also observed (Figure **F17**). Subunit IIA is

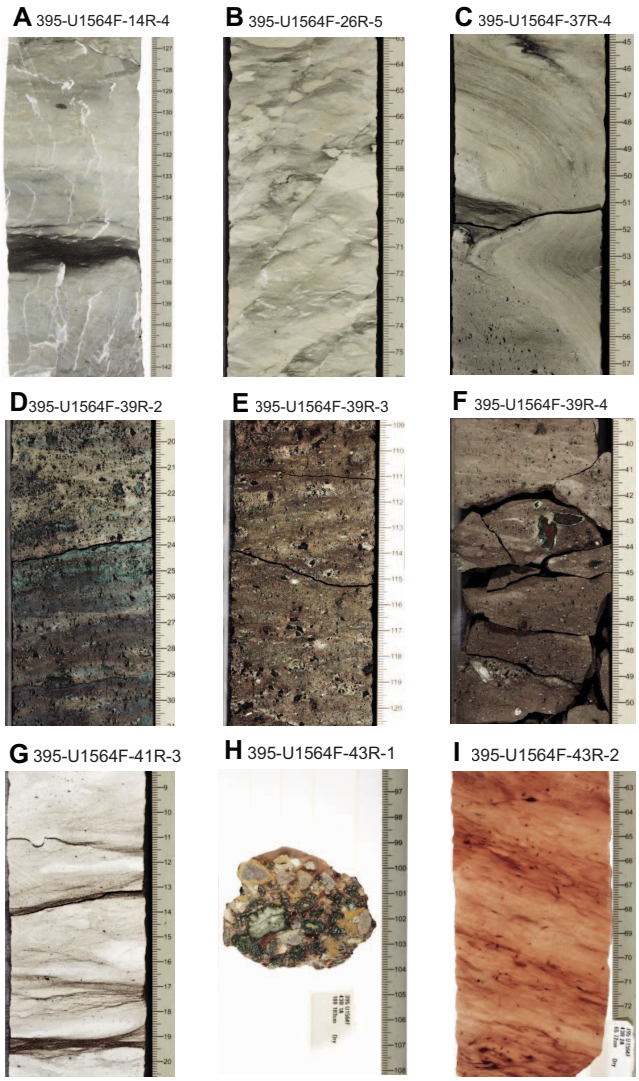

Figure F17. Fracturing, soft-sediment deformation, glauconite-rich interval, stylolites, malachite-bearing breccia, and pink chalk, Hole U1564F. A. Network of thin, calcite-infilled fractures. B. Parallel fractures. C. Well-defined soft-sediment fold. D–F. Brightly colored sediment with abundant glauconite pellets. This layer coincides with a strong peak in NGR values. G. Stylolites (thin dark brown bands) within nannofossil chalk. H. Breccia with clasts of malachite and malachite-rimmed calcite, along with other minerals associated with hydrothermal alteration such as jarosite. The matrix of this breccia is pinkish nannofossil chalk, as seen in I.

dominated by dark gray silty clay with nannofossils interbedded with nannofossil chalk. There is a significant increase in the variability of both biogenic carbonate and $CaCO_3$ weight percent coinciding with cyclical color grading of sediment beds. Subunit IIB is dominated by greenish gray nannofossil chalk and dark gray silty nannofossil chalk. Subunit IIC is dominated by gray nannofossil chalk with silty clay, with some intervals of silty nannofossil chalk. Near the base of the sedimentary sequence, red and pink nannofossil chalks become interbedded. Evidence for hydrothermal mineralization is observed.

4.5.3.2. Igneous petrology

Site U1564 recovered the oldest oceanic crust drilled during this expedition (~32.4 Ma). Site U1564 is located in faulted abyssal hill topography that formed when the ridge axis was segmented by a series of transform offsets. The sediment/basement interface was encountered at 997 m CSF-A. Basement was drilled to 1170 m CSF-A in Hole 395-U1564F, penetrating 172.4 m of basalt, of which 114.2 m of core was recovered (66%). The bulk of this core consists of continuous sheet flows that are highly to completely altered, with sparsely plagioclase phyric basalt and occasional clinopyroxene microphenocrysts. The fine- to medium-grained groundmass consists of plagioclase, clinopyroxene, and opaque minerals. A 4 m thick reddish brown sediment layer was encountered at ~1050 m CSF-A. In the bottom ~40 m of the cored section, pillow lavas are more abundant, with chilled margins and occasional glassy rinds. Filled fractures and complex anastomosing veins are common throughout the hole.

4.5.3.3. Alteration petrology and structural geology

The majority of basalt core recovered from Site U1564 is completely or highly altered. Alteration is mainly pervasive, although localized alteration mainly in the form of fracture halos occurs throughout the basalts. Alteration intensity is observed to be slightly higher in sheet flows than in pillow lavas. The basalt alteration assemblage is Fe-oxide/oxyhydroxides + celadonite + clay with minor, localized chlorite (Figure **F18**). Vesicles are mostly filled with celadonite, calcite, Fe-oxide/oxyhydroxides, some saponite, and minor zeolite. Vesicle fills are commonly mineralogically zoned with multiple minerals in each. Fracture density in Hole 395-U1564F is ~23 fractures per meter of recovered core and increases gradually with depth. Fractures are typically <1 mm wide and occur mostly within complex crosscutting networks. Fractures up to 3.4 cm wide are more

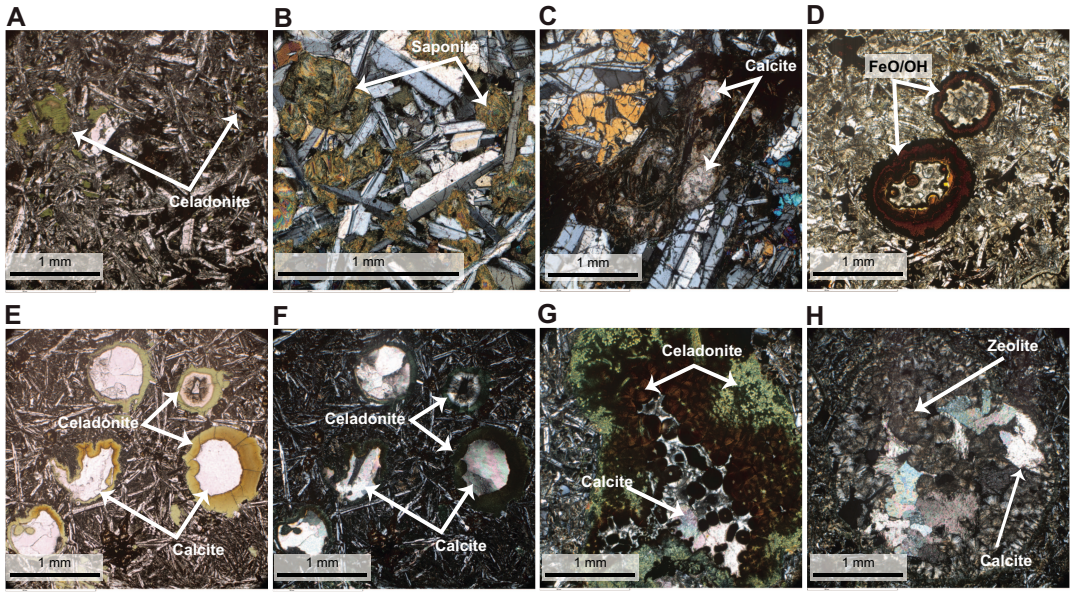

Figure F18. Alteration, calcite replacement, and vesicles, Hole U1564F. A. Celadonite alteration in groundmass (49R-1, 145–147 cm; plane-polarized light [PPL]). B. Saponite alteration (45R-2, 60–62 cm; cross-polarized light [XPL]). C. Calcite replacement in crystals (61R-2, 86–89 cm; XPL). D. FeO/OH-rimmed vesicles (63R-1, 40–43 cm; PPL). E. Yellow and green celadonite-rimmed vesicles filled with calcite (73R-1, 21–23 cm). F, G. Zoned vesicle containing, from the rim to the center, green celadonite, brown celadonite spherules and calcite in (F) XPL and (G) PPL (53R-2, 114–116 cm). Vesicle filled with zeolite and calcite (63R-1, 99–102 cm; XPL).

common in the upper intervals of basalt. Fracture mineral fills are mostly carbonate ± Fe-oxide/oxyhydroxide ± celadonite with minor clay. Chlorite fracture fill occurs in specific intervals and quartz is sporadically observed as a late fill in some mineralogically layered fractures. Fracture alteration halos can be >15 cm wide, and are red, brown, green-gray, to green-brown in color.

4.5.3.4. Micropaleontology

At Site U1564, a 997.23 m long interval of lower Oligocene to upper Pleistocene sediments was recovered across multiple holes. Planktonic foraminifers are common to dominant in most samples examined except where quartz grains and rock fragments predominate and their preservation is very good to excellent to ~530 m CSF-A (Figure **F19**). Below this depth, the sediment becomes

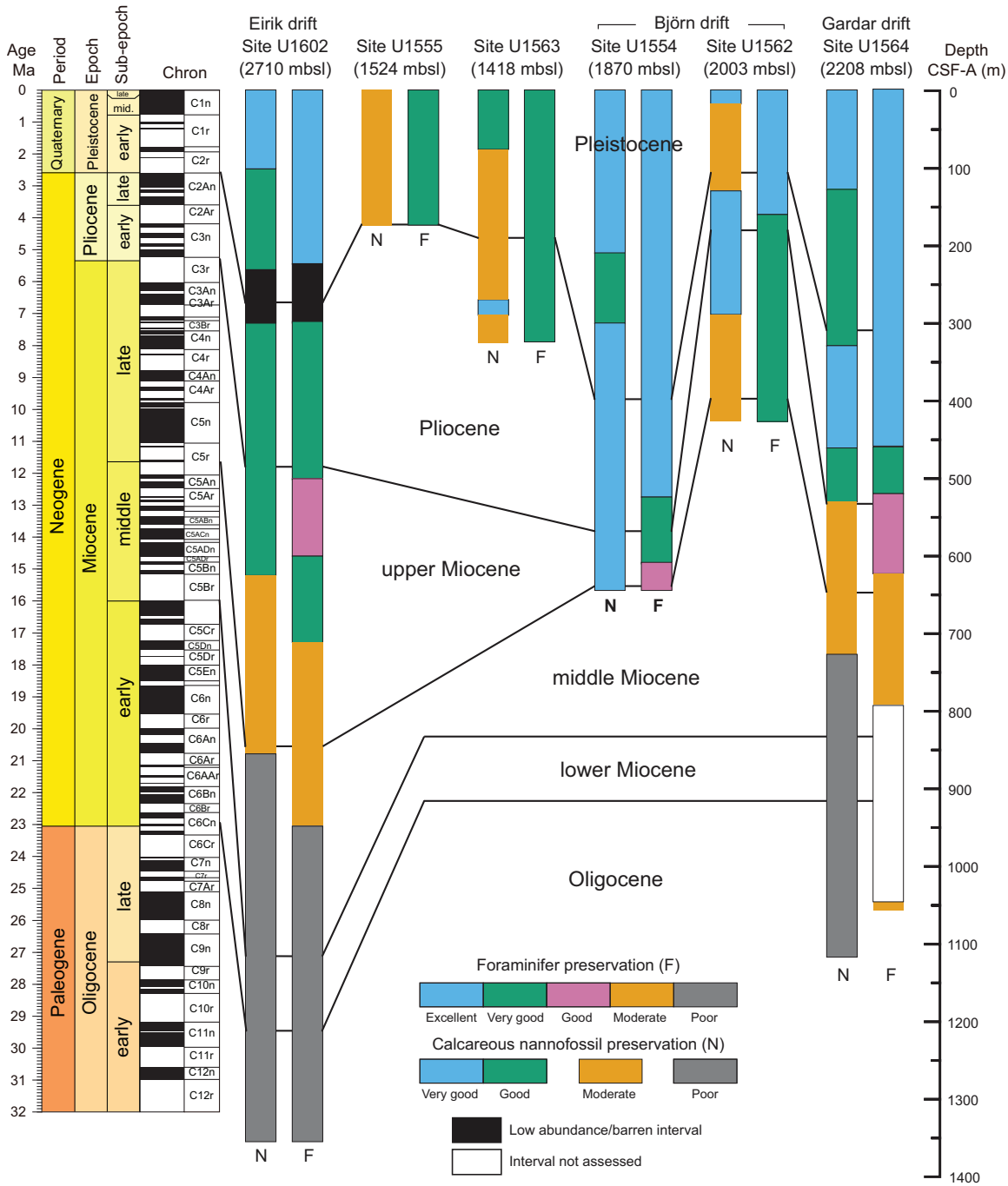

Figure F19. Calcareous microfossil preservation summary, Expedition 395. Foraminifer preservation below 800 m CSF-A at Site U1564 is not well documented because the sediments are lithified. Paleomagnetic chrons and geologic timescale are from Ogg (2020).

progressively more lithified and the foraminifers are mostly infilled by calcite, although they continue having moderate to good preservation to ~800 m CSF-A. Seven early Pliocene to Pleistocene biohorizons, three Miocene biohorizons, and two Oligocene biohorizons were recorded. The last sample of the regular succession above the basement has an assemblage that indicates an early Oligocene age (32.2–27.29 Ma), and the assemblage in the sedimentary layer recovered between the basement succession (~1050 m CSF-A) points to an age between 33.8 and 32.2 Ma.

Similar to the planktonic foraminifers, calcareous nannofossils are present in almost all samples observed, ranging from few to dominant in abundance and with very good to poor preservation. Preservation worsens with depth in the succession (Figure **F19**). Nine Pleistocene biohorizons, one Pliocene biohorizon, and eleven Miocene biohorizons spanning the interval between 5.53 and 17.65 Ma were identified. Oligocene assemblages are present below ~920 m CSF-A, characterized by the presence of *Cyclicargolithus abisectus*, with the lower Oligocene biohorizon top *Reticulofenestra umbilicus* at ~987 m CSF-A constraining the base of the sedimentary succession to be older than 32.02 Ma.

4.5.3.5. Physical properties

Physical properties measurements for Site U1564 consist of whole-round and half-round measurements on cores from Holes 395C-U1564B through 395-U1564F. Discrete physical properties were measured for Holes 395-U1564D, 395-U1564E, and U1564F. Whole-round density measurements show an increase with depth, with marked increases at ~550, ~700, and ~1000 m CSF-A (the sediment/basement interface). Density measured on discrete samples is consistently higher than those measured on whole-round sections below ~700 m CSF-A. Whole-round and point MS measurements covary, showing meter- to decameter-scale fluctuations throughout the sedimentary section. Below 700 m CSF-A, MS drops dramatically to values below 10 IU. V_P from whole-round measurements increases between 450 and 650 m CSF-A, below which the measurements were constrained to caliper measurements due to the diameter of the RCB core not filling the core liner. Below 650 m CSF-A in the sediment interval, velocities increase from 2200 to 3000 m/s. Caliper-derived velocities in the basalts were measured in the orthogonal direction using the paleomagnetic cubes; these velocities vary between 3600 and 6000 m/s. NGR measurements show an increase between 600 and 700 m CSF-A and then fluctuate between 700 and ~1000 m CSF-A. NGR is generally lower in the basaltic record. RGB, L*, and a* show meter- to decameter-scale variations with depth. Amplitudes between 0 and 450 m CSF-A are relatively low, and below 450 m CSF-A the data display higher amplitude variability. RGB measurements have lower values in the basaltic intervals, averaging around 50. L* shows lower values in the basalts, averaging around 40, and L* and b* display a similar range of values to the sediment intervals.

4.5.3.6. Stratigraphic correlation

The stratigraphic splice for Site U1564 contains two long uninterrupted intervals that are complete, with a ~200 m long interval in between that has several gaps. A continuous splice was constructed using only Holes 395-U1564D and 395-U1564E to 239 m CCSF-A. The lowermost, continuous part of the Site U1564 shipboard splice was constructed using material from Holes 395C-U1564C and U1564D to 674.71 m CCSF-A. Between these intervals, several gaps are unavoidable, and cores from Holes U1564C–U1564E were positioned based on our best judgment, with additional guidance from the downhole wireline MS logging profile from Hole U1564C.

4.5.3.7. Paleomagnetism

NRM was measured for sedimentary cores recovered from Site U1564. The cores from Holes 395C-U1564B, 395C-U1564C, and 395-U1564E were then demagnetized with a stepwise AF cleaning protocol at a resolution of 5 cm, and a resolution of 2.5 cm was used for cores from Holes 395C-U1564A, 395-U1564D, and 395-U1564F. A set of about 150 discrete samples were collected to confirm the semicontinuous measurements. The inclinations measured at the demagnetization step of 20 mT from Holes U1564D and U1564F were used to interpret a sequence of normal and reversed polarities. The change in lithology below about 750 m CSF-A corresponds to a decrease in NRM intensity and MS, together with the deterioration quality of the paleomagnetic signal. Below 997 m CSF-A, the depth of the sediment/rock interface between Sections 395-U1564F-44R-1 and 44R-2 marks a three-fold increase in the intensity of MS, but the alteration of the basement rocks causes a deterioration of the paleomagnetic signal. Therefore, between about 760 m CSF-A

and the bottom of the hole the paleomagnetic inclinations are not suitable for a univocal magnetostratigraphic interpretation. Magnetic polarities from Holes U1564D and U1564F were correlated with the geomagnetic polarity timescale (GPTS) chrons to establish an age-depth trend for Site U1564.

4.5.3.8. Geochemistry

Cores collected from Site U1564 were analyzed for headspace gas, IW chemistry, and bulk sediment geochemistry. Headspace gas analyses were conducted for Holes 395C-U1564A, 395C-U1564B, 395C-U1564C, 395-U1564D, and 395-U1564F; methane concentrations are variable and range ~0–1260 ppmv. Ethane, at concentrations lower than 94.6 ppmv, was present in Holes U1564C, U1564D, and U1564F below 510.31 m CSF-A.

Material from Holes U1564D, 395-U1564E, and U1564F was analyzed for IW chemistry and bulk sediment geochemistry. IW calcium ion (Ca^{2+}) concentrations generally increase, and magnesium ion (Mg^{2+}) concentrations decrease with depth. Sulfate ion (SO_4^{2-}) concentrations decrease from seawater-like values at the top of the sediment column <1 mM at 173.87 m CSF-A, with a small increase in concentration below 607.12 m CSF-A. $CaCO_3$ weight percent generally increases downcore, trending from an average of 13.3 ± 9.6 wt% through Sample 395-U1564D-52X-2, 141–151 cm (442.31 m CSF-A), to an average of 35.4 ± 20.6 wt% for the remaining sediment samples to the sediment/basement interface. Bulk sediment generally has low TOC, TN, and TS content.

4.5.3.9. Downhole measurements

After coring operations concluded in Holes 395C-U1564C and 395-U1564F, the holes were cleaned with a mud sweep and the drilling mud was displaced with seawater before logging operations started. Hole U1564C was logged with the triple combo and the FMS-sonic tool strings from the seafloor to ~630 m WMSF. Hole U1564F was logged from ~550 to 1160 m WMSF to allow for some data overlap with Hole U1564C. For Site U1564, six logging units are identified from first-order variations in the wireline measurements, predominantly using observable changes in the gamma ray log, and in places using other logs such as resistivity, MS, and density. Logging Subunit L1a encompasses data collected through the drill pipe, and Subunit L1b records the open hole logging responses of Unit L1. Unit L1 is defined by gamma log measurements of 19 ± 3 gAPI and densities ranging 1.2–1.6 g/cm^3. Unit L2 (108–318 m WMSF) is defined by an increase in gamma log to an average value around 21 ± 3 gAPI, spectral gamma ray that shows several large distinct peaks in thorium counts, and an increase in MS (average = 117 ± 45 SI), the latter of which increasingly fluctuates with depth. Unit L3 is marked by a decrease in gamma radiation, and gradually increasing V_P and V_S. This unit is divided into two subunits based on changes in the frequency of fluctuations observed in the MS. A large distinct peak in uranium radiation at ~529 m WMSF is observed in Subunit L3b. Unit L4 (560–957 m WMSF) is marked by an increase in gamma radiation, resistivity, MS, and density. This logging unit contains three subunits defined by variations in gamma radiation. Unit L5 is marked by a large spike in gamma log as well as an increase in resistivity and density. Unit L6 marks the transition from sediment to basaltic basement, which sees a decrease in gamma log and thorium counts in the spectral gamma ray log and large increases in resistivity and density. FMS image logging of Hole U1564C is of good quality, and alternating conductive and resistive bedding features are observed. FMS and UBI image logging in the sediment and basement lithologies of Hole U1564F is good quality and shows multiple sedimentary and structural geology features.

4.5.3.10. Age model

The age model is based mainly on a combination of paleomagnetic and biostratigraphic age determinations from Holes U1564D and U1564F, with additional biostratigraphic constraints from Hole U1564C. Fourteen tie points were selected that divide the stratigraphy into a series of intervals characterized by significantly different estimated sedimentation rates, ranging ~1.4–15.3 cm/ky. The age of the sediment in the lowermost part of the regular succession above igneous basement is early Oligocene (between 32.02 and 32.20 Ma). This finding is in good agreement with the age of basement anticipated from regional magnetic surveys at 32.4 Ma.

4.6. Site U1602

4.6.1. Background and objectives

Site U1602 is located on the eastern margin of Greenland in the North Atlantic Ocean, coinciding with the elongate sedimentary body, Eirik drift (Figure **F1**) (see the **Site U1602** chapter [Parnell-Turner et al., 2025d]). Site U1602 is located on a VSR, tentatively identified in free-air gravity anomaly data, that is one of the V-shaped structures that straddle the Reykjanes Ridge flanks and whose origin in relation to the Iceland hotspot is debated. The site sits on ocean crust with an age of 49.8 Ma, estimated from magnetic anomalies and plate reconstruction models.

The Reykjanes Ridge flanks are the site of major contourite drift deposits, with Björn and Gardar drifts on the eastern flank of the ridge. In contrast, Eirik drift consists of an elongate, mounded contourite deposit that is plastered along the East Greenland margin. The sedimentary section at Site U1602 on Eirik drift has the potential to preserve detailed records of the evolution of the Greenland and Iceland Ice Sheets and of variations in the Western Boundary Undercurrent. Site U1602 complements the drift sites on the eastern side of Reykjanes Ridge and, paired with the predrift record of Site U1564, will recover older sediment, providing insights into the North Atlantic ocean circulation and sedimentation deep into the Cenozoic. Site U1602 is located on Seismic Line JC50-1, obtained in 2010 during RRS *James Cook* Cruise JC50. Sediment thickness at Site U1602 is ~1376 m based on seismic imagery.

The main target for Site U1602 was to obtain a continuous sedimentary record of Eirik drift. Another target was to obtain a sedimentary record throughout the middle Miocene warm period. A final target, time permitting, was to core into the basement. This final objective was not achieved because of time constraints. Cores and data from this site will address the primary science Objectives 1 and 2 related to mantle behavior, ocean circulation, gateways, and sedimentation.

4.6.2. Operations

Site U1602 (61°11.7138′N, 38°10.8186′W) consists of five holes, which reach 8.8–1365.2 m DSF (Table **T1**). A total of 230 cores were recovered for Site U1602. These cores collected 1444.65 m of sediment over a 1903.8 m cored interval (76% recovery). Two drilled intervals were recorded over a 531.3 m interval. Downhole wireline logging operations were attempted in Hole 395-U1602E and were partially successful. The total time spent at Site U1602 was 19.5 days.

4.6.3. Principal results

4.6.3.1. Lithostratigraphy

The Holocene to upper Eocene/lower Oligocene sediments cored at Site U1602 are primarily composed of silty clay, silty clay/claystone with nannofossils, nannofossil silty clay/claystone, nannofossil chalk, and sandstone (Figure **F20**). Based on the observations of sediment composition along with attenuation patterns of NGR, MS, and $CaCO_3$ content, Site U1602 is divided into three major lithostratigraphic units (I–III). Unit III consists of two subunits (IIIA and IIIB). The site is dominated by terrigenous components, mainly quartz, feldspar, glass, opaque grains, pyrite, and glauconite with smaller amounts of chlorite and Fe/Mn oxides (Figure **F21**). Biogenic components are dominated by nannofossils, which generally increase downhole. Foraminifers and biosilica are common to rare in Unit I and trace to absent in Units II and III. Thin beds (a few to ~10 cm thick) of silt and sand, often laminated or graded, are pervasively interbedded with both the drift-type and pelagic-type sediments, particularly in Units I and II. More generally, sediments at Site U1602 contain a wide variety of sedimentary structures such as laminations, graded bedding, alternating grading, cross-bedding, flaser bedding, mud drapes, and sand injections; mud drapes and sand injections are particularly pervasive in Unit III. Fractures with slickensides are also present in Units II and III. Bioturbation is generally sparse to moderate in Units I and II. In Unit III, however, bioturbation is generally abundant in the chalk, but absent to sparse in the sandstone intervals.

4.6.3.2. Micropaleontology

At Site U1602, a 1357.99 m interval of upper Eocene/lower Oligocene to upper Pleistocene material was recovered across multiple holes. Micropaleontological analyses were undertaken on

sediment samples from Holes 395-U1602B (0–251.43 m CSF-A), 395-U1602C (255.43–264.9 m CSF-A), 395-U1602D (250.31–532.36 m CSF-A), and 395-U1602E (537.07–1357.99 m CSF-A). Biohorizons used in the age model are based on calcareous nannofossils, planktonic foraminifers, and one bolboform species.

Calcareous nannofossils are present in most samples and have variable preservation, which generally worsens with depth below seafloor (Figure **F19**). A distinct interval where barren samples are more frequent occurs in the Pliocene to early Pleistocene. Seven biohorizons spanning the Pleistocene are identified in Hole U1602B, covering an interval between 0.09 and 1.71 Ma. The top of *R. pseudoumbilicus*, found in Hole U1602D, is the only recorded Pliocene biohorizon. The Miocene is well resolved in Hole U1602E, with fourteen biohorizons covering the interval between 5.53 and 22.9 Ma. Finally, the top of *R. umbilicus*, found in the deepest recovered core catcher sample from Hole U1602E, indicates an early Oligocene (>32 Ma) age for the base of this hole.

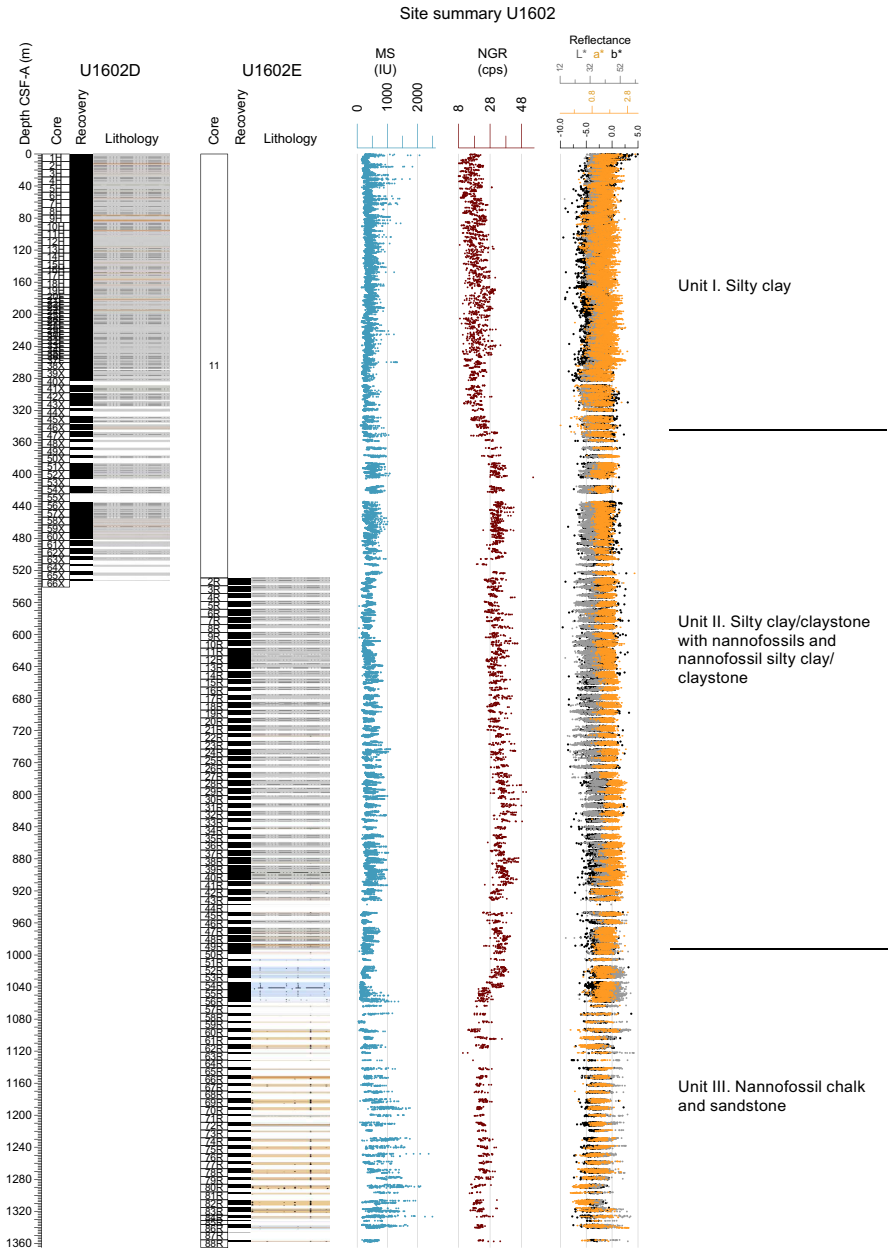

Figure F20. Lithostratigraphic summary, Site U1602. cps = counts per second. Lithostratigraphic units: sedimentary units are shown. For lithology legend, see Figures F9 and F11 in the Expedition 395 methods chapter (Parnell-Turner et al., 2025a).

Planktonic foraminifers also demonstrate variable preservation (Figures **F19**, **F22**) that worsens with depth and highly variable abundance. Sample processing became more difficult as sediments progressively lithified with depth (below ~100 m CSF-A). Despite the difficulties in sample preparation, relatively good biostratigraphic control was achieved across the studied interval. A total of three Pleistocene, four Miocene, and one late Eocene planktonic foraminifer biohorizons are identified across the studied holes. Finally, bolboforms are rare and mostly moderately to poorly preserved. Despite that shortcoming, one Miocene biohorizon was recorded in Hole U1602E, using the top occurrence of *Bolboforma metzmacheri*.

4.6.3.3. Physical properties

Physical properties measurements for Site U1602 consist of whole-round and half-round measurements on cores from Holes U1602A–U1602E, including X-Ray Linescan Logger (XSCAN) images of section halves (Figure **F23**). Discrete physical properties measurements were measured

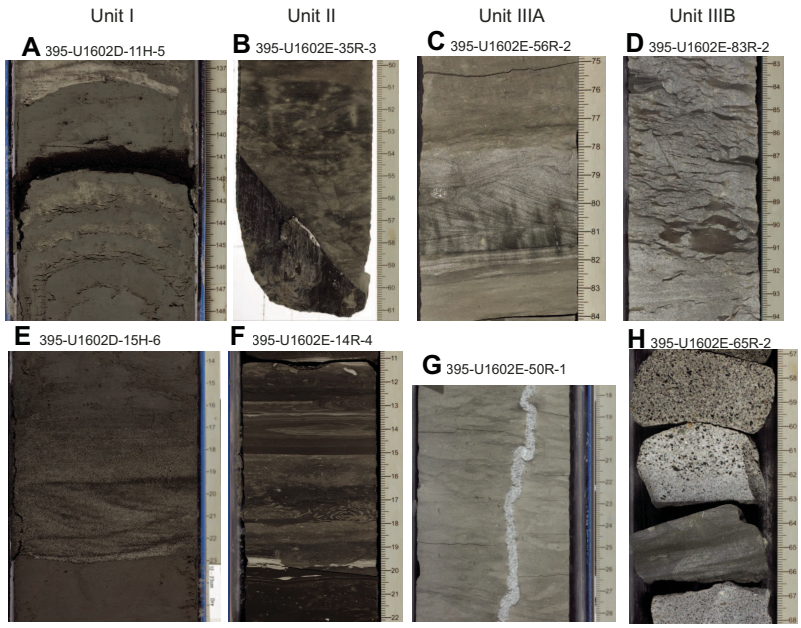

Figure F21. Sedimentary textures and features, Site U1602. A. Silty clay layer with thin bands of silt layers and a dark thick band of glass (ash) layer in the middle. B. Nannofossil silty claystone interval including a fracture with slickensides at the base. C. Nannofossil chalk with an interval of cross bedded siltstone. D. Sandstone containing complex bedform showing rip-up clast or possible flaser bedding features. E. Silty clay with a silt interval displaying cross bedding, graded bedding, and fining-upwards sequence. F. Highly bioturbated silty clay interval with laminations and burrows crosscutting the laminations. G. Nannofossil chalk with sand injection in the middle. H. Laminated siltstone contained within fine- and coarse-grained sandstone.

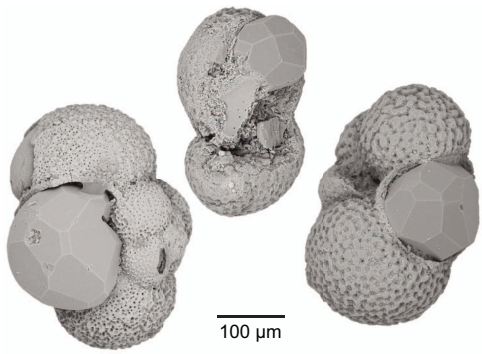

Figure F22. Deformed and broken planktonic foraminifer shells with equant crystal infillings identified as analcime (395-U1602E-25R-CC; 757.61 m CSF-A).

for Holes U1602B, U1602D, and U1602E. Density increases with depth and has marked increases downhole at ~350 and ~1050 m CSF-A. Density values measured on discrete samples are consistently higher than whole-round density values below ~500 m CSF-A, a discrepancy due to the diameter of the core being smaller than that of the liner. Porosity shows the inverse trend of density, with values decreasing with depth and marked decreases occurring at ~350 and ~1050 m CSF-A. Whole- and half-round MS measurements covary, showing meter- to decameter-scale fluctuations from the top of the section to ~1050 m CSF-A where more variability is observed. V_P increases sharply from 350 to 650 m CSF-A and increases at a more gentle rate to 950 m CSF-A, below which the measurements show a wider range of values. NGR measurements show an increase from 300 to 400 m CSF-A and fluctuate downhole to ~950 m CSF-A, followed by an overall decrease and reduced range in values. RGB, L*, and a* show meter- to decameter-scale variations between 0 and 1050 m CSF-A. Thermal conductivity of the measured sediments at Site U1602 increases slightly with depth.

4.6.3.4. Stratigraphic correlation

A continuous stratigraphic splice was created from the seafloor to 169.45 m CCSF-A using cores from Holes 395-U1602B and 395-U1602D. Below this depth to ~270 m CCSF-A, there are three small (<1–2 m) gaps in the stratigraphic record. For these intervals, cores were appended below the overlying core.

4.6.3.5. Paleomagnetism

NRM was measured for all sedimentary cores recovered from Site U1602 at a resolution of 2.5 cm. The cores were then demagnetized with a stepwise AF cleaning protocol. A set of ~260 discrete samples were collected to confirm the semicontinuous measurements. The inclination measured at the maximum demagnetization step (20, 25, and 30 mT for Holes 395-U1602B, 395-U1602D,

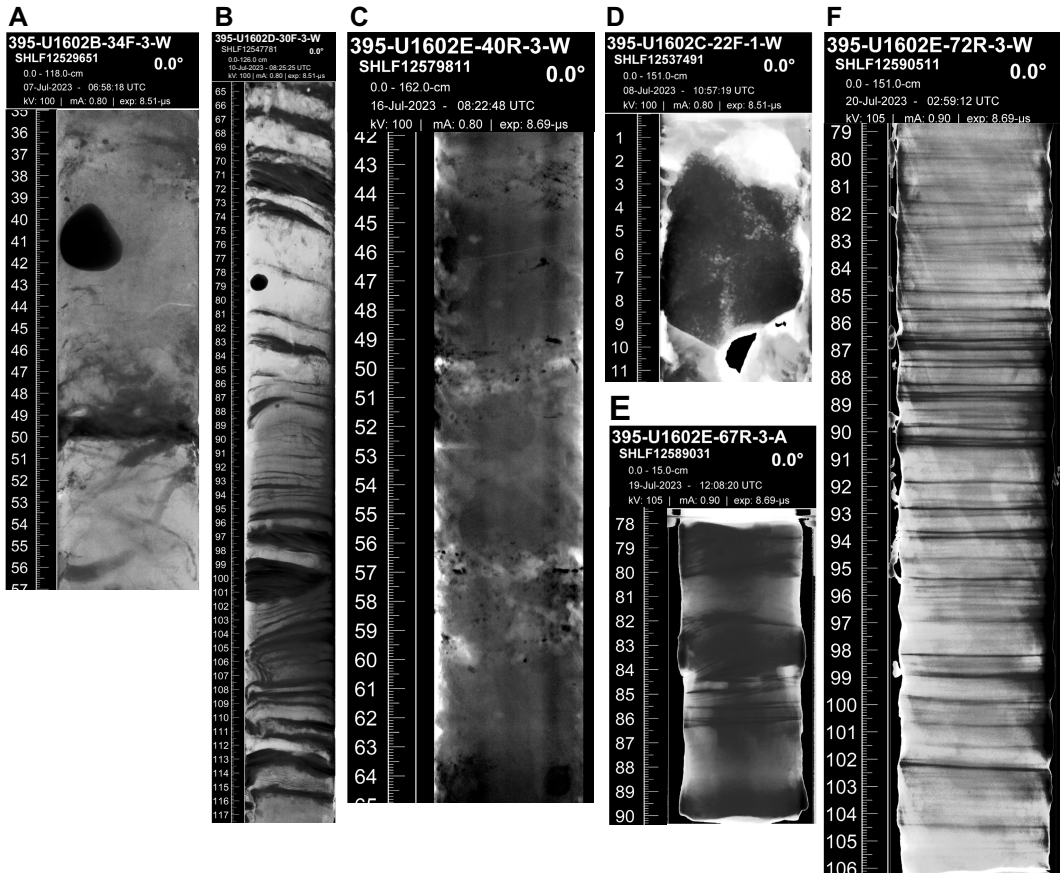

Figure F23. Archive-half XSCAN images showing typical characteristics, Site U1602. A. Dropstone. B. Laminated sequences. C. IRD deposits. D. A large clast that is most likely not in situ. E. Cross-bedding. F. Laminated interval.

and 395-U1602E, respectively) was used to interpret a downcore sequence of normal and reversed polarities. Magnetic polarities from Holes U1602D and U1602E were correlated with the GPTS chrons to establish an age-depth trend for Site U1602. Between about 1060 m CSF-A and the bottom of the hole, the NRM intensity and MS decrease, and the paleomagnetic inclinations were not suitable for a univocal magnetostratigraphic interpretation.

4.6.3.6. Geochemistry

Cores collected from Site U1602 were analyzed for headspace gas, IW chemistry, and bulk sediment geochemistry. Headspace methane concentrations range 0–328 ppmv (n = 143), and low ethane concentrations (<4.6 ppmv) were detected in a subset of the headspace samples (n = 21). The pH and alkalinity of IW display an inverse relationship with depth. Alkalinity is near seawater values (3.68 mM) in the uppermost IW sample and increases to 6.1 mM at ~103 m CSF-A before decreasing to low values (<1.0 mM) below ~320 m. pH is generally constant in the upper ~340 m (7.9 ± 0.1) and increases downhole to 8.9 at ~786 m CSF-A, below which limited IW extracted from the sediment prevented additional pH measurements. IW calcium ion (Ca^{2+}) concentrations display an increasing trend with depth; the highest Ca^{2+} concentrations occur at ~871 m CSF-A. Magnesium ion (Mg^{2+}) concentrations display a general decreasing trend with depth. The highest Mg^{2+} concentrations (51.6 mM) occur at the top of the sediment column (1.4 m CSF-A). Sulfate ion (SO_4^{2-}) concentrations display a decreasing trend downhole and reach the minimum value ~240 m CSF-A. SO_4^{2-} concentrations increase below ~600 m CSF-A to between 5 and 9 mM. Downhole trends in other dissolved elements including barium (Ba), lithium (Li), potassium (K), and silicon (Si) indicate a change in concentrations at around 388 m CSF-A. $CaCO_3$ weight percent generally increases downhole, from ~0 to 30 wt% in the uppermost 100 m to as high as ~80 wt% near the bottom of Hole 395-U1602E. Bulk sediment generally exhibits low TOC (<0.7 wt%), TN (<0.2 wt%), and TS (≤1.0 wt%). Bulk sediment major and minor element concentrations were also analyzed using inductively coupled plasma–atomic emission spectroscopy (ICP-AES) on select samples. Downhole variations in major oxides (e.g., SiO_2, Al_2O_3, TiO_2 K_2O, MgO, and CaO) and trace elements (e.g., S and Sr) show variable concentrations that likely reflect changing lithologies.

4.6.3.7. Downhole measurements

After coring operations in Hole 395-U1602E concluded, the hole was prepared for logging operations. The triple combo tool string became stuck during its first descent downhole and operations to recover the tool were successful, but all further logging operations at Site U1602 were canceled. Therefore, downhole logging data from Hole U1602E consist of a single downhole logging pass that includes measurements of gamma log and spectral gamma ray, formation resistivity, and MS.

Seven logging units are defined for Hole U1602E, the boundaries of which are primarily defined by notable changes in the gamma log and in some instances from other logging responses. Logging Unit L1 (32–162 m WMSF) is characterized by gamma log measurements of ~27.7 gAPI, which fluctuate with depth. Increases in gamma radiation positively correlate with increases in thorium and negatively correlate with uranium spectral gamma counts. Unit L2 (162–340 m WMSF) is defined by a step increase in gamma log to ~35 gAPI. MS in Unit L2 has an average value of 259 SI and contains meter-scale fluctuations. The bottom of Unit L2 and top of Unit L3 is defined by an increase in formation resistivity. Unit L3 (340–588 m WMSF) displays an average gamma log of ~47 gAPI and shows meter- to decameter-scale fluctuations throughout. Several distinct intervals present very low gamma radiation measurements, which correspond to increases in MS. Unit L4 (588–630 m WMSF) is defined by a large ~42 m long fluctuation in gamma log and MS measurements. Unit L5 (630–1039 m WMSF) is defined by an initial decrease in gamma log and an increase in MS and shows fluctuations in gamma log at meter, decameter, and hectometer scales. Unit L6 (1039–1162 m WMSF) is characterized by variable logging responses separated into five subunits. Unit L7 (1162–1280 m WMSF) shows meter-scale, fluctuating, cyclical gamma log and MS responses. Below ~1250 m WMSF, values of MS increase; however, this could be a measurement artifact caused by deteriorating hole conditions and not a response to geologic variation.

Four downhole temperature measurements were acquired in Hole 395-U1602B (between 33.7 and 116 m DSF). Formation temperature increases from 3.22°C to 10.43°C across this interval. These measurements, along with thermal conductivity, were used to calculate heat flow for the site.

4.6.3.8. Age model

The age model for Site U1602 is based on a combination of paleomagnetic and biostratigraphic age determinations. Some of the biostratigraphic data are only upper or lower depth constraints because rarity and/or variable preservation makes them difficult to locate precisely. There is good agreement between the paleomagnetic and biostratigraphic data sources to the base of Gilbert Chron C3r. Below that level, the paleomagnetic record continues to follow the expected reversal sequence to the interpreted base of Subchron C5n.2n (11.06 Ma). However, some of the biostratigraphic data appear to depart from this trend, most likely due to the poor calibration of these events in the high latitudes. The combined biostratigraphic and paleomagnetic record of Site U1602 in this interval will be critical in improving these calibrations in future. The age model is based largely on calcareous nannofossils below Subchron C5n.2n and assumes that Oligocene–Miocene global age calibrations are accurate at this location. Planktonic foraminifers suggest that Hole 395-U1602E terminated in the upper Eocene (>34.5 Ma), but that is based on a very poorly preserved assemblage from just one sample near the bottom of the hole.

5. Preliminary scientific assessment

The broad objective of Expedition 395 was to deliver the samples and data required to test a range of interdisciplinary scientific hypotheses about topics that include mantle convection and crustal accretion, paleoclimates, ocean circulation, and the deep limits of life. The expedition focused on a unique part of the North Atlantic Ocean where the Mid-Atlantic Ridge is strongly influenced by the Iceland mantle plume and where rapidly accumulated drift sediments record changes in bottom currents associated with deepwater circulation and contain proxy records of climate with millennial timescale resolution. Considered together, Expeditions 384, 395C, and 395 targeted six primary sites that were chosen to build on scientific breakthroughs from previous scientific drilling in the region, notably during DSDP Leg 49 and ODP Legs 105, 152, and 162.

The Expedition 395 project comprises three expeditions: Expedition 384 in 2020 (Blum et al., 2020), Expedition 395C in 2021 (Parnell-Turner et al., 2022), and Expedition 395 in 2023. Expedition 395 had three initial operational goals. First, to recover basement rocks from two pairs of crustal VSRs and VSTs (Sites U1555 and U1563 and Sites U1554 and U1562) and from segmented crust with no V-shaped structure (Site U1564) by coring ~130 m into basement. Second, to recover complete sedimentary sequences through Björn and Gardar drifts. Third, time permitting, Expedition 395 aimed to recover a significant portion of the sedimentary section of Eirik drift on the eastern margin of Greenland (Site U1602), with a tentative objective of reaching late Miocene sediments near 7.8 Ma. As detailed below, all of these objectives were attained during the Expedition 395 project, with the additional achievement of sampling an extensive Neogene and Paleogene predrift sedimentary succession at Eirik drift (Site U1602) (Figure **F24**).

5.1. Operational achievements

Each of the initial operational objectives of Expedition 395 was met, and in many cases they were exceeded. Although the expedition initially planned to recover ~3,500 m of core, the three expeditions combined achieved a total penetration of 10,698 m and recovered 6,577 m of core with an overall recovery rate of 86% (Figure **F25**; Table **T1**). This total includes an overall recovery rate of 49% in the basaltic basement. The ephemeral properties measurements and microbiological sampling programs were remarkably successful during Expeditions 395 and 395C, collecting a total of 385 interstitial fluid samples to 1050 m CSF-A (achieved in Hole 395-U1564F). The 33 microbiological samples collected from the basement section of Site U1564 at a spacing of ~5 m represent one of the most complete records of their kind to date. In total, over 400 samples were collected for shore-based microbiologic studies from all six sites, comprising sediment and basalt. Downhole wireline logging was undertaken at each site with mixed results.

5.1.1. Objective 1: crustal accretion and V-shaped ridge origins

Basalt was drilled across the full target interval at five sites during Expeditions 384, 395C, and 395, fully satisfying the needs for crustal sampling of Objective 1. Material from segmented crust at Site U1564, potentially representing North Atlantic end-member crust not influenced by the Iceland

plume, was cored during Expedition 395, and the other four sites, representing VSRs and VSTs, were drilled during Expeditions 384 and 395C. Measurements of the chemical composition of these basalts and analyses of their eruption characteristics will enable testing of VSR formation hypotheses and potentially improve understanding of Iceland mantle plume dynamics. The large amount of basement material recovered from the five sites reveals variability in lava morphology (e.g., pillows versus sheet flows) between the sites (Figure **F8**), and preliminary shipboard geochemical analyses indicate differences in degrees of melting and variability in source composition. Postcruise geochemical measurements, lithologic analysis, and modeling will provide the foundations for evaluating existing hypotheses, in addition to furthering the exploration of crustal accretion processes along the plate spreading transect.

The high basement recovery rate helped meet the objective to sample a representative number of flow units from each site, minimizing possible sampling biases. Favorable weather and timing enabled deeper basalt penetration than originally planned at Sites U1555 and U1564. This additional recovery was particularly valuable at Site U1564, where a significant amount of glassy material was recovered near the end of coring operations, deeper than the initially planned 130 m basement penetration target. In the otherwise highly altered basaltic section at Site U1564, this glass will be invaluable for future geochemical analyses and will play a critical role in constraining mantle source composition and melting processes at Reykjanes Ridge 32 My ago. The paired basement sections recovered in Holes 384-U1555G and 395C-U1555I represent a petrological splice through the basaltic basement, which leads to a rare opportunity to study both the spatial- and depth-dependent properties of the oceanic crust. The core recovery is paired with extensive downhole logging data sets, including FMS-sonic logs and UBI data, which provide a 360° view of the borehole. These images are of exceptional quality, providing insight into the eruptive units, structural features, and alteration character of the basalt sequence.

5.1.2. Objective 2: paleoclimate and deepwater circulation

To satisfy the paleoclimate and ocean circulation objectives, the first-order operational aim of Expedition 395 was to collect near-complete splices through key sedimentary intervals of Gardar, Björn, and Eirik drifts. Enabled by the excellent work of the shipboard drilling and technical staff, near-complete splices throughout the APC-cored sections of each of these drifts were achieved. These splices include key climatic intervals, such as the intensification of Northern Hemisphere Glaciation at 2.7 Ma and the onset of rapid contourite drift sedimentation. The shipboard data

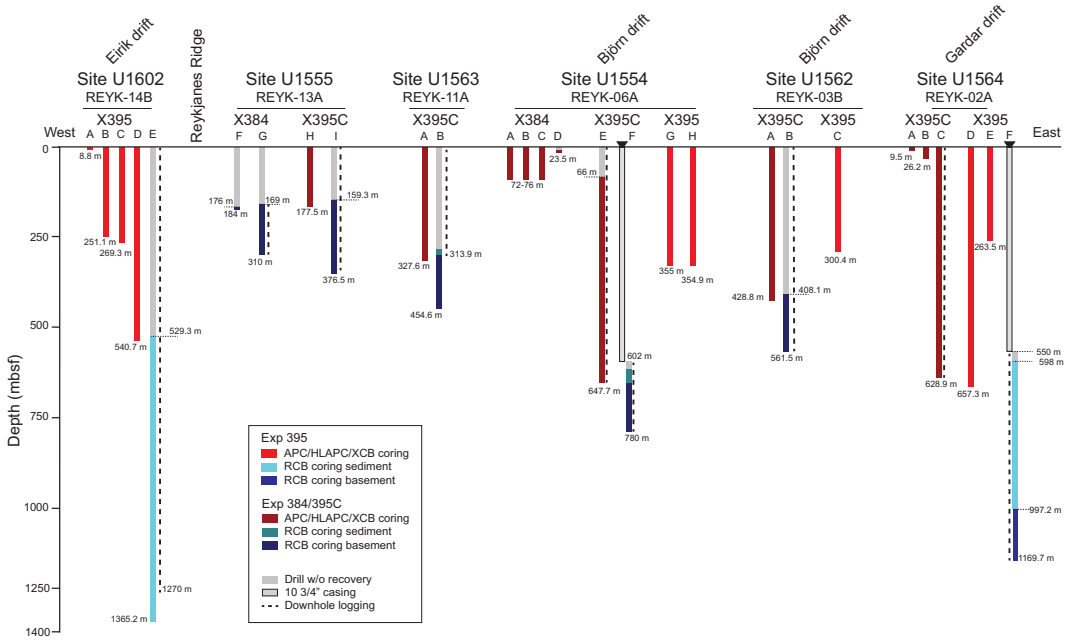

Figure F24. Summary of completed operations, Expeditions 384, 395C, and 395.

already reveal new insights into changes in sedimentation, climate, and ocean circulation through these important intervals. Enabled by the high accumulation rates of sediments recovered, post-cruise analysis of Expedition 395 cores and data will enable addressing detailed questions about climatic and oceanographic history of the North Atlantic region.

An important goal of Expedition 395 was to obtain high-resolution records of sediment accumulation rates in contourite drift sediments across a North Atlantic transect at the key 60°N latitude. Expedition 395 sites were chosen to maximize the chance of success for this objective, located in undisturbed, thick deposits of Björn, Gardar, and Eirik drifts. Continuous core recovery with near-continuous splices, well-resolved magnetostratigraphic records, and excellent microfossil preservation (Figure **F19**), leading to the identification of many biohorizons, means that the age models generated by Expedition 395 are exceptional in quality (Figure **F26**). These well-constrained age models considerably extend previous reference models from ODP Sites 982 and 983, reaching from recent to Miocene (Björn drift), Oligocene (Gardar drift), and Eocene (Eirik drift) times, and

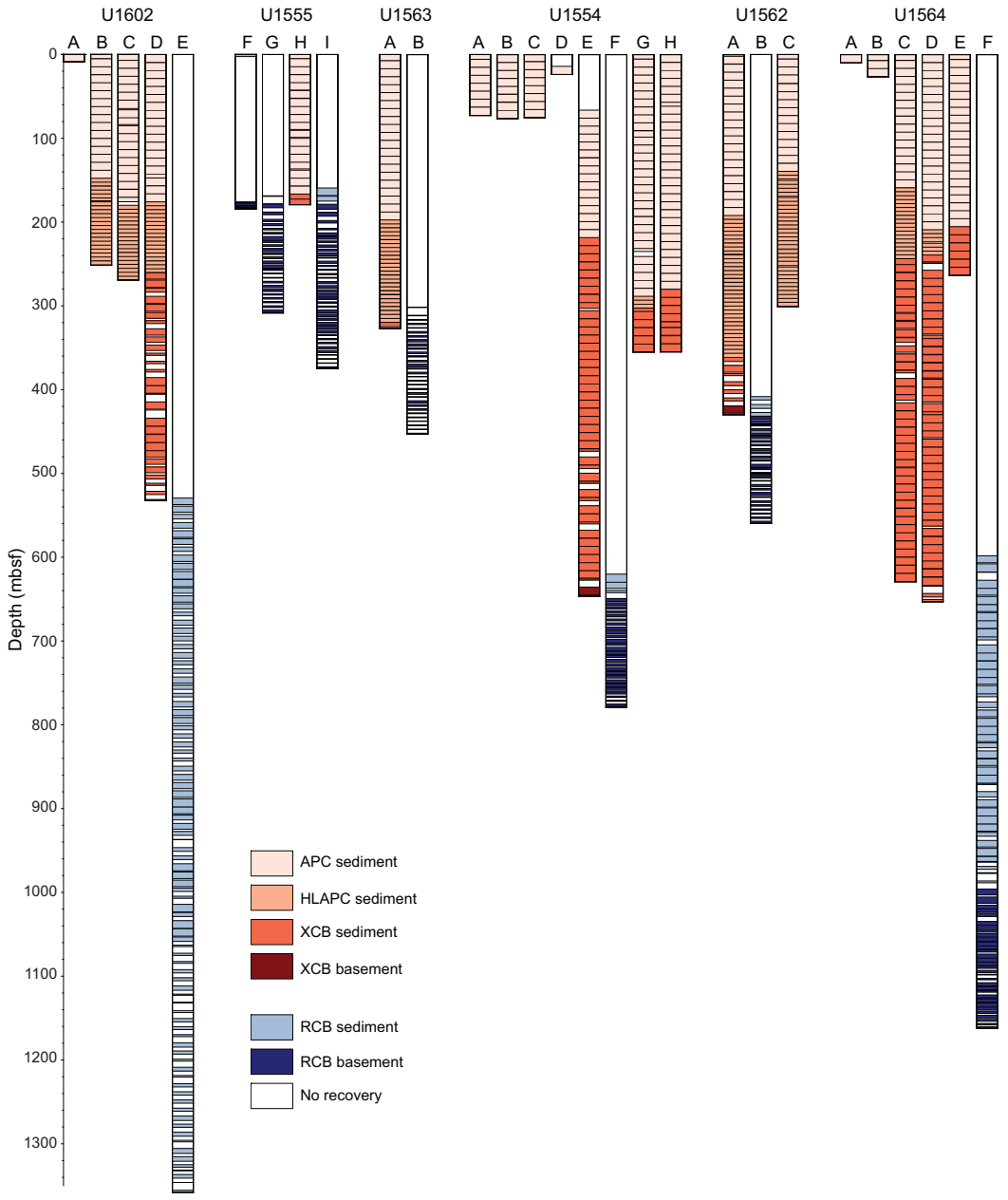

Figure F25. Core recovery summary, Expedition 395.

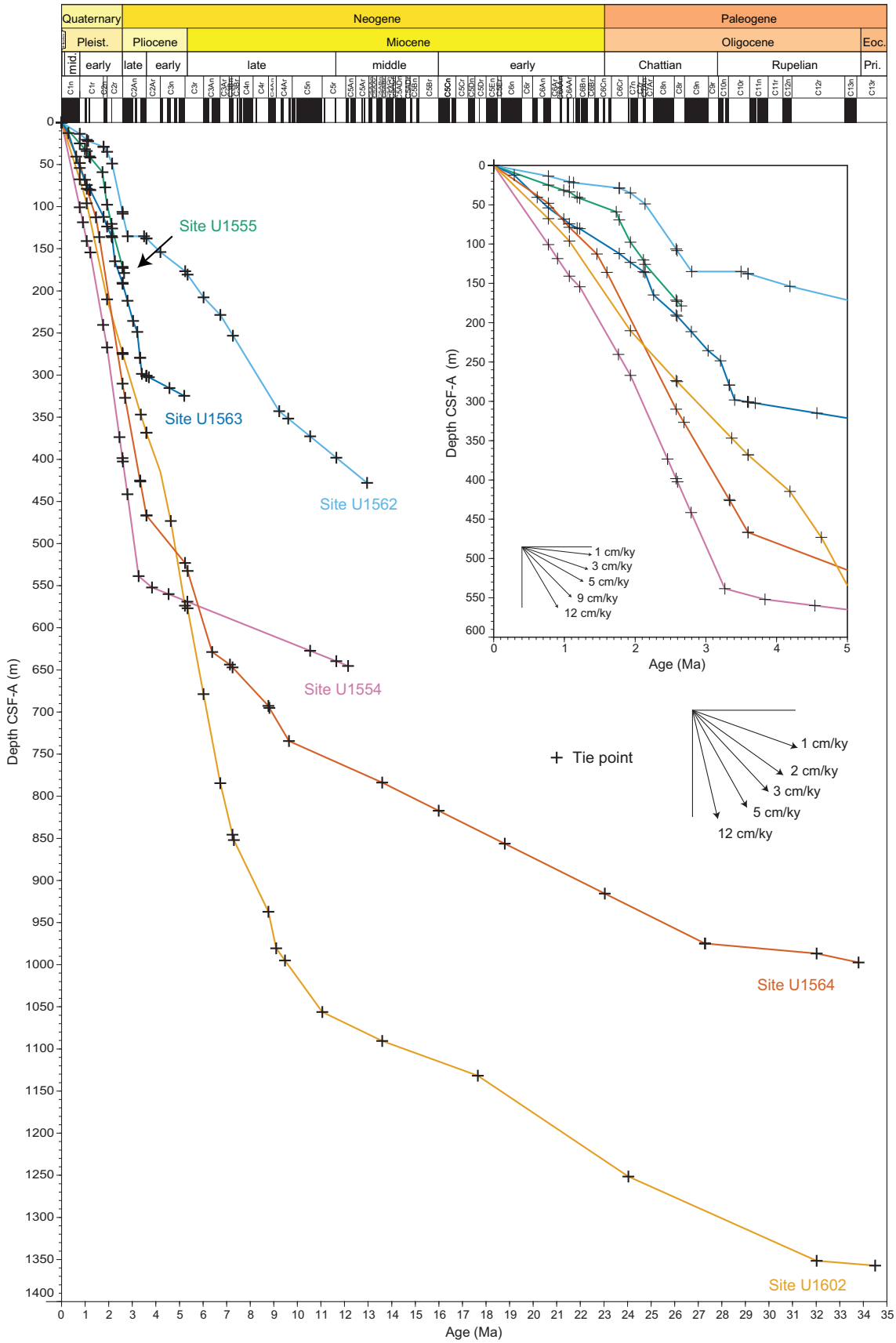

Figure F26. Age-depth plots for all six Expedition 395 sites. The selected datum points can be found in Age model in each site chapter. Inset: enlarged age-depth plot from 0 to 5 Ma. An increase in sedimentation rates at three sites occurs ~3.6 Ma. Geologic stages to periods and magnetochrons are from Ogg (2020). Eoc. = Eocene, Pri. = Priabonian.

will be important reference sections for the geologic history of the North Atlantic region. Importantly, Expedition 395 sites cored through the onset and Pliocene intensification of sedimentation at major drifts in the North Atlantic Ocean, demonstrating the value of drilling sites with multiple holes across a transect.

Favorable weather and operational efficiencies meant that additional, initially unplanned APC coring was possible in Hole U1562C during Expedition 395. This site, located on the eastern fringe of Björn drift, contains a late Miocene record with remarkably well preserved calcareous microfossils, which is invaluable for the deployment of carbonate-based geochemical proxies, owing to its relatively shallow burial depth. The additional APC hole enabled a continuous splice to be obtained through this key interval and is likely to yield important insights into North Atlantic oceanography during this warm climate state.

Operations during Expeditions 384 and 395C allowed the addition of Site U1602 to Expedition 395 (Parnell-Turner et al., 2023). Site U1602 recovered a unique record of sedimentation of Eirik drift back to the late Eocene, with implications for reconstructions of the development and stability of Greenland ice sheet and the evolution of the early subpolar North Atlantic Ocean by providing sedimentary records with standard pelagic microplankton groups preserved through large intervals, as well as the potential for biomarker proxy data generation. This record from Eirik drift is particularly valuable given that Eirik drift Site 646 only recovered a partial record of the drift, and end of the IODP program and retirement of *JOIDES Resolution* in 2024 means that further drilling at Eirik drift likely will not be realized for decades to come.

Considered together, the excellent recovery and magnetic recording potential of sediments across the transect of six sites will lead to a significant contribution to our understanding of Earth's magnetostratigraphic history. Although nearby ODP Sites 982 and 983 are reference sites for the fine-scale geomagnetic intensity timescale (GITS), the new material recovered from Expedition 395 will extend their records well beyond Quaternary times and beyond the Matuyama polarity chron. Comparison between the multiple high-resolution magnetostratigraphic records contained across Expedition 395 sites is likely to address existing uncertainty in the GITS, previously caused by reliance upon single sites.

The transect of Expedition 395 sites, spanning the central subpolar North Atlantic and proximal to the Greenland ice sheet, is also positioned to capture a continuous record of Pleistocene Northern hemisphere ice sheet dynamics. Combining the continuous recovery with novel shipboard X-ray images collected during Expedition 395 means that a detailed analysis of the pacing of IRD episodes older than 1.8 Ma is likely possible. The recovery of laminated silt horizons on the Greenland margin at Site U1602 also opens the unexpected possibility to track ice sheet behavior through the record of meltwater pulses and grain provenance.

5.1.3. Objective 3: crustal aging and hydrothermal alteration

Altered basalt drilled at four sites as old as 12.3 Ma during Expeditions 384 and 395C partially satisfied the needs for crustal sampling of Objective 3. However, the oldest crustal material, at Site U1564, was necessary to complete the 32 My transect as originally planned. The 119 m of basalt recovered during Expedition 395 at Site U1564 contains a rich variety of alteration fabrics, mineralogy, and structural features that will enable the aims of Objective 3 to be satisfied. The successful acquisition of high-resolution 360° borehole images at all five basement sites means that a full evaluation of the structural evolution of the basaltic crust will be feasible postcruise. Finally, the large number of microbiological samples collected across all sites will allow feedbacks between crustal alteration, fluid flow, and microbial life to be investigated in unprecedented detail.

The transect of sites east of Reykjanes Ridge comprehensively samples the different controls at play in determining the extent and timing of crustal alteration. The deep sediment recovery from Site U1602, which comprises lithified sediment containing fractures with various mineral fill, poses new questions about the connectivity between crust, sediment, and ocean to be addressed.

The IW and microbial samples collected in both sediment and basalt during Expedition 395 form one of the most comprehensive collections of their kind ever obtained. Paired with a history of alteration made possible by exceptionally high recovery rates, the combined results of the six site

Expedition 395 transect opens up new opportunities to explore the links between petrology, chemical exchange, alteration mineralogy, and microbial life within and between the basement, sediment, and ocean.

The remarkable success of Expedition 395 was partly enabled by favorable weather conditions. More importantly, however, it was enabled by the well-established drilling and laboratory procedures aboard *JOIDES Resolution*, which have been refined and perfected over decades of operation. Our success also relied upon the dedication and expertise of the shipboard drilling and technical staff, who bring with them decades of experience and knowledge. These technical, operational, and personnel resources will almost certainly be lost once *JOIDES Resolution* ceases to operate, at great cost to future generations of scientists.

References

Bailey, I., Hole, G.M., Foster, G.L., Wilson, P.A., Storey, C.D., Trueman, C.N., and Raymo, M.E., 2013. An alternative suggestion for the Pliocene onset of major Northern Hemisphere glaciation based on the geochemical provenance of North Atlantic Ocean ice-rafted debris. Quaternary Science Reviews, 75:181–194. **https://doi.org/10.1016/j.quascirev.2013.06.004**

Barker, S., Chen, J., Gong, X., Jonkers, L., Knorr, G., and Thornalley, D., 2015. Icebergs not the trigger for North Atlantic cold events. Nature, 520(7547):333–336. **https://doi.org/10.1038/nature14330**

Barker, S., Knorr, G., Conn, S., Lordsmith, S., Newman, D., and Thornalley, D., 2019. Early interglacial legacy of deglacial climate instability. Paleoceanography and Paleoclimatology, 34(8):1455–1475. **https://doi.org/10.1029/2019PA003661**

Barker, S., Starr, A., van der Lubbe, J., Doughty, A., Knorr, G., Conn, S., Lordsmith, S., Owen, L., Nederbragt, A., Hemming, S., Hall, I., Levay, L., Berke, M.A., Brentegani, L., Caley, T., Cartagena-Sierra, A., Charles, C.D., Coenen, J.J., Crespin, J.G., Franzese, A.M., Gruetzner, J., Han, X., Hines, S.K.V., Jimenez Espejo, F.J., Just, J., Koutsodendris, A., Kubota, K., Lathika, N., Norris, R.D., Periera dos Santos, T., Robinson, R., Rolison, J.M., Simon, M.H., Tangunan, D., Yamane, M., and Zhang, H., 2022. Persistent influence of precession on northern ice sheet variability since the early Pleistocene. Science, 376(6596):961–967. **https://doi.org/10.1126/science.abm4033**

Benediktsdóttir, Á., Hey, R., Martinez, F., and Höskuldsson, Á., 2012. Detailed tectonic evolution of the Reykjanes Ridge during the past 15 Ma. Geochemistry, Geophysics, Geosystems, 13(2):Q02008. **https://doi.org/10.1029/2011GC003948**

Blum, P., Rhinehart, B., and Acton, G.D., 2020. International Ocean Discovery Program Expedition 384 Preliminary Report. International Ocean Discovery Program. **https://doi.org/10.14379/iodp.pr.384.2020**

Bodine, J.H., Steckler, M.S., and Watts, A.B., 1981. Observations of flexure and the rheology of the oceanic lithosphere. Journal of Geophysical Research: Solid Earth, 86(B5):3695–3707. **https://doi.org/10.1029/JB086iB05p03695**

Bond, G., Broecker, W., Johnsen, S., McManus, J., Labeyrie, L., Jouzel, J., and Bonani, G., 1993. Correlations between climate records from North Atlantic sediments and Greenland ice. Nature, 365(6442):143–147. **https://doi.org/10.1038/365143a0**

Briais, A., Parnell-Turner, R.E., LeVay, L.J., Cui, Y., Di Chiara, A., Dodd, J.P., Dunkley Jones, T., Dwyer, D., Eason, D.E., Friedman, S.A., Hemming, S.R., Hochmuth, K., Ibrahim, H., Jasper, C., Karatsolis, B.T., Lee, S., LeBlanc, D.E., Lindsay, M.R., McNamara, D.D., Modestou, S.E., Murton, B., OConnell, S., Pasquet, G.T., Pearson, P.N., Qian, S.P., Rosenthal, Y., Satolli, S., Sinnesael, M., Suzuki, T., Thulasi Doss, T., White, N.J., Wu, T., Yang Yang, A., dos Santos Rocha, V., Pearman, C., and Tian, C.Y., 2025a. Site U1555. In Parnell-Turner, R.E., Briais, A., LeVay, L.J., and the Expedition 395 Scientists, Reykjanes Mantle Convection and Climate. Proceedings of the International Ocean Discovery Program, 395: College Station, TX (International Ocean Discovery Program). **https://doi.org/10.14379/iodp.proc.395.104.2025**

Briais, A., Parnell-Turner, R.E., LeVay, L.J., Cui, Y., Di Chiara, A., Dodd, J.P., Dunkley Jones, T., Dwyer, D., Eason, D.E., Friedman, S.A., Hemming, S.R., Hochmuth, K., Ibrahim, H., Jasper, C., Karatsolis, B.T., Lee, S., LeBlanc, D.E., Lindsay, M.R., McNamara, D.D., Modestou, S.E., Murton, B., OConnell, S., Pasquet, G.T., Pearson, P.N., Qian, S.P., Rosenthal, Y., Satolli, S., Sinnesael, M., Suzuki, T., Thulasi Doss, T., White, N.J., Wu, T., Yang Yang, A., dos Santos Rocha, V., Pearman, C., and Tian, C.Y., 2025b. Site U1562. In Parnell-Turner, R.E., Briais, A., LeVay, L.J., and the Expedition 395 Scientists, Reykjanes Mantle Convection and Climate. Proceedings of the International Ocean Discovery Program, 395: College Station, TX (International Ocean Discovery Program). **https://doi.org/10.14379/iodp.proc.395.105.2025**

Briais, A., Parnell-Turner, R.E., LeVay, L.J., Cui, Y., Di Chiara, A., Dodd, J.P., Dunkley Jones, T., Dwyer, D., Eason, D.E., Friedman, S.A., Hemming, S.R., Hochmuth, K., Ibrahim, H., Jasper, C., Karatsolis, B.T., Lee, S., LeBlanc, D.E., Lindsay, M.R., McNamara, D.D., Modestou, S.E., Murton, B., OConnell, S., Pasquet, G.T., Pearson, P.N., Qian, S.P., Rosenthal, Y., Satolli, S., Sinnesael, M., Suzuki, T., Thulasi Doss, T., White, N.J., Wu, T., Yang Yang, A., dos Santos Rocha, V., Pearman, C., and Tian, C.Y., 2025c. Site U1563. In Parnell-Turner, R.E., Briais, A., LeVay, L.J., and the Expedition 395 Scientists, Reykjanes Mantle Convection and Climate. Proceedings of the International Ocean Discovery Program, 395: College Station, TX (International Ocean Discovery Program). **https://doi.org/10.14379/iodp.proc.395.106.2025**

Briais, A., and Rabinowicz, M., 2002. Temporal variations of the segmentation of slow to intermediate spreading mid-ocean ridges, 1. Synoptic observations based on satellite altimetry data. Journal of Geophysical Research: Solid Earth, 107(B5):2098. **https://doi.org/10.1029/2001JB000533**

Channell, J.E.T., Mazaud, A., Sullivan, P., Turner, S., and Raymo, M.E., 2002. Geomagnetic excursions and paleointensities in the Matuyama Chron at Ocean Drilling Program Sites 983 and 984 (Iceland Basin). Journal of Geophysical Research: Solid Earth, 107(B6):2114. **https://doi.org/10.1029/2001JB000491**

Coggon, R.M., and Teagle, D.A.H., 2011. Hydrothermal calcium-carbonate veins reveal past ocean chemistry. TrAC Trends in Analytical Chemistry, 30(8):1252–1268. **https://doi.org/10.1016/j.trac.2011.02.011**

Dupré, B., and Allègre, C.J., 1980. Pb–Sr–Nd isotopic correlation and the chemistry of the North Atlantic mantle. Nature, 286(5768):17–22. **https://doi.org/10.1038/286017a0**

Fitton, J.G., Saunders, A.D., Norry, M.J., Hardarson, B.S., and Taylor, R.N., 1997. Thermal and chemical structure of the Iceland Plume. Earth and Planetary Science Letters, 153(3–4):197–208. **https://doi.org/10.1016/S0012-821X(97)00170-2**

Gillis, K.M., and Coogan, L.A., 2011. Secular variation in carbon uptake into the ocean crust. Earth and Planetary Science Letters, 302(3–4):385–392. **https://doi.org/10.1016/j.epsl.2010.12.030**

Hart, S.R., Schilling, J.G., and Powell, J.L., 1973. Basalts from Iceland and along the Reykjanes Ridge: Sr isotope geochemistry. Nature Physical Science, 246(155):104–107. **https://doi.org/10.1038/physci246104a0**

Hartley, R.A., Roberts, G.G., White, N., and Richardson, C., 2011. Transient convective uplift of an ancient buried landscape. Nature Geoscience, 4(8):562–565. **https://doi.org/10.1038/ngeo1191**

Hey, R., Martinez, F., Höskuldsson, Á., and Benediktsdóttir, Á., 2010. Propagating rift model for the V-shaped ridges south of Iceland. Geochemistry, Geophysics, Geosystems, 11(3):Q03011. **https://doi.org/10.1029/2009GC002865**

Jansen, E., and Raymo, M.E., 1996. Leg 162: new frontiers on past climates. In Jansen, E., Raymo, M.E., Blum, P., et al., Proceedings of the Ocean Drilling Program, Initial Reports. 162: College Station, TX (Ocean Drilling Program), 5–20. **https://doi.org/10.2973/odp.proc.ir.162.101.1996**

Jones, S.M., Murton, B.J., Fitton, J.G., White, N.J., Maclennan, J., and Walters, R.L., 2014. A joint geochemical–geophysical record of time-dependent mantle convection south of Iceland. Earth and Planetary Science Letters, 386:86–97. **https://doi.org/10.1016/j.epsl.2013.09.029**

Jones, S.M., White, N., and Maclennan, J., 2002. V-shaped ridges around Iceland: implications for spatial and temporal patterns of mantle convection. Geochemistry, Geophysics, Geosystems, 3(10):1–23. **https://doi.org/10.1029/2002GC000361**

Kempton, P.D., Fitton, J.G., Saunders, A.D., Nowell, G.M., Taylor, R.N., Hardarson, B.S., and Pearson, G., 2000. The Iceland plume in space and time: a Sr–Nd–Pb–Hf study of the North Atlantic rifted margin. Earth and Planetary Science Letters, 177(3):255–271. **https://doi.org/10.1016/S0012-821X(00)00047-9**

Kleiven, H.F., Hall, I.R., McCave, I.N., Knorr, G., and Jansen, E., 2011. Coupled deep-water flow and climate variability in the middle Pleistocene North Atlantic. Geology, 39(4):343–346. **https://doi.org/10.1130/G31651.1**

Krause, D.C., and Schilling, J.-G., 1969. Dredged basalt from the Reykjanes Ridge, North Atlantic. Nature, 224(5221):791–793. **https://doi.org/10.1038/224791b0**

Le Voyer, M., Kelley, K.A., Cottrell, E., and Hauri, E.H., 2017. Heterogeneity in mantle carbon content from CO_2-undersaturated basalts. Nature Communications, 8(1):14062. **https://doi.org/10.1038/ncomms14062**

Luyendyk, B.P., Cann, J. R., et al., 1979. Initial Reports of the Deep Sea Drilling Project, 49: Washington, DC (US Government Printing Office). **https://doi.org/10.2973/dsdp.proc.49.1979**

Martinez, F., and Hey, R., 2017. Propagating buoyant mantle upwelling on the Reykjanes Ridge. Earth and Planetary Science Letters, 457:10–22. **https://doi.org/10.1016/j.epsl.2016.09.057**

Martinez, F., Hey, R., and Höskuldsson, Á., 2020. Reykjanes Ridge evolution: effects of plate kinematics, small-scale upper mantle convection and a regional mantle gradient. Earth-Science Reviews, 206:102956. **https://doi.org/10.1016/j.earscirev.2019.102956**

McCave, I.N., Thornalley, D.J.R., and Hall, I.R., 2017. Relation of sortable silt grain-size to deep-sea current speeds: calibration of the 'Mud Current Meter'. Deep Sea Research, Part I: Oceanographic Research Papers, 127:1–12. **https://doi.org/10.1016/j.dsr.2017.07.003**

Menviel, L., Timmermann, A., Friedrich, T., and England, M.H., 2014. Hindcasting the continuum of Dansgaard–Oeschger variability: mechanisms, patterns and timing. Climate of the Past, 10(1):63–77. **https://doi.org/10.5194/cp-10-63-2014**

Murton, B.J., Taylor, R.N., and Thirlwall, M.F., 2002. Plume–ridge Interaction: a geochemical perspective from the Reykjanes Ridge. Journal of Petrology, 43(11):1987–2012. **https://doi.org/10.1093/petrology/43.11.1987**

Ogg, J.G., 2020. Geomagnetic Polarity Time Scale. In Gradstein, F.M., Ogg, J.G., Schmitz, M., and Ogg, G. (Eds.), Geologic Time Scale 2020. Amsterdam (Elsevier), 159–192. **https://doi.org/10.1016/B978-0-12-824360-2.00005-X**

Parnell-Turner, R., Briais, A., and LeVay, L.J., 2022. Expedition 395C Preliminary Report: Reykjanes Mantle Convection and Climate: Crustal Objectives. International Ocean Discovery Program. **https://doi.org/10.14379/iodp.pr.395C.2022**

Parnell-Turner, R., Briais, A., and LeVay, L.J., 2023. Expedition 395 Scientific Prospectus Addendum: Reykjanes Mantle Convection and Climate. International Ocean Discovery Program. **https://doi.org/10.14379/iodp.sp.395add.2023**

Parnell-Turner, R.E., Briais, A., LeVay, L.J., Cui, Y., Di Chiara, A., Dodd, J.P., Dunkley Jones, T., Dwyer, D., Eason, D.E., Friedman, S.A., Hemming, S.R., Hochmuth, K., Ibrahim, H., Jasper, C., Karatsolis, B.T., Lee, S., LeBlanc, D.E., Lindsay, M.R., McNamara, D.D., Modestou, S.E., Murton, B., OConnell, S., Pasquet, G.T., Pearson, P.N., Qian, S.P., Rosenthal, Y., Satolli, S., Sinnesael, M., Suzuki, T., Thulasi Doss, T., White, N.J., Wu, T., and Yang Yang, A., 2025a. Expedition 395 methods. In Parnell-Turner, R.E., Briais, A., LeVay, L.J., and the Expedition 395 Scientists, Reyk-

janes Mantle Convection and Climate. Proceedings of the International Ocean Discovery Program, 395: College Station, TX (International Ocean Discovery Program). **https://doi.org/10.14379/iodp.proc.395.102.2025**

Parnell-Turner, R.E., Briais, A., LeVay, L.J., Cui, Y., Di Chiara, A., Dodd, J.P., Dunkley Jones, T., Dwyer, D., Eason, D.E., Friedman, S.A., Hemming, S.R., Hochmuth, K., Ibrahim, H., Jasper, C., Karatsolis, B.T., Lee, S., LeBlanc, D.E., Lindsay, M.R., McNamara, D.D., Modestou, S.E., Murton, B., OConnell, S., Pasquet, G.T., Pearson, P.N., Qian, S.P., Rosenthal, Y., Satolli, S., Sinnesael, M., Suzuki, T., Thulasi Doss, T., White, N.J., Wu, T., Yang Yang, A., dos Santos Rocha, V., Pearman, C., and Tian, C.Y., 2025b. Site U1554. In Parnell-Turner, R.E., Briais, A., LeVay, L.J., and the Expedition 395 Scientists, Reykjanes Mantle Convection and Climate. Proceedings of the International Ocean Discovery Program, 395: College Station, TX (International Ocean Discovery Program). **https://doi.org/10.14379/iodp.proc.395.103.2025**

Parnell-Turner, R.E., Briais, A., LeVay, L.J., Cui, Y., Di Chiara, A., Dodd, J.P., Dunkley Jones, T., Dwyer, D., Eason, D.E., Friedman, S.A., Hemming, S.R., Hochmuth, K., Ibrahim, H., Jasper, C., Karatsolis, B.T., Lee, S., LeBlanc, D.E., Lindsay, M.R., McNamara, D.D., Modestou, S.E., Murton, B., OConnell, S., Pasquet, G.T., Pearson, P.N., Qian, S.P., Rosenthal, Y., Satolli, S., Sinnesael, M., Suzuki, T., Thulasi Doss, T., White, N.J., Wu, T., Yang Yang, A., and dos Santos Rocha, V., 2025c. Site U1564. In Parnell-Turner, R.E., Briais, A., LeVay, L.J., and the Expedition 395 Scientists, Reykjanes Mantle Convection and Climate. Proceedings of the International Ocean Discovery Program, 395: College Station, TX (International Ocean Discovery Program). **https://doi.org/10.14379/iodp.proc.395.107.2025**

Parnell-Turner, R.E., Briais, A., LeVay, L.J., Cui, Y., Di Chiara, A., Dodd, J.P., Dunkley Jones, T., Dwyer, D., Eason, D.E., Friedman, S.A., Hemming, S.R., Hochmuth, K., Ibrahim, H., Jasper, C., Karatsolis, B.T., Lee, S., LeBlanc, D.E., Lindsay, M.R., McNamara, D.D., Modestou, S.E., Murton, B., OConnell, S., Pasquet, G.T., Pearson, P.N., Qian, S.P., Rosenthal, Y., Satolli, S., Sinnesael, M., Suzuki, T., Thulasi Doss, T., White, N.J., Wu, T., and Yang Yang, A., 2025d. Site U1602. In Parnell-Turner, R.E., Briais, A., LeVay, L.J., and the Expedition 395 Scientists, Reykjanes Mantle Convection and Climate. Proceedings of the International Ocean Discovery Program, 395: College Station, TX (International Ocean Discovery Program). **https://doi.org/10.14379/iodp.proc.395.108.2025**

Parnell-Turner, R., White, N., Henstock, T., Murton, B., Maclennan, J., and Jones, S.M., 2014. A continuous 55-million-year record of transient mantle plume activity beneath Iceland. Nature Geoscience, 7(12):914–919. **https://doi.org/10.1038/ngeo2281**

Parnell-Turner, R., White, N., Henstock, T.J., Jones, S.M., Maclennan, J., and Murton, B.J., 2017. Causes and consequences of diachronous v-shaped ridges in the North Atlantic Ocean. Journal of Geophysical Research: Solid Earth, 122(11):8675–8708. **https://doi.org/10.1002/2017JB014225**

Parnell-Turner, R., White, N.J., McCave, I.N., Henstock, T.J., Murton, B., and Jones, S.M., 2015. Architecture of North Atlantic contourite drifts modified by transient circulation of the Icelandic mantle plume. Geochemistry, Geophysics, Geosystems, 16(10):3414–3435. **https://doi.org/10.1002/2015GC005947**

Parnell-Turner, R.E., White, N.J., Maclennan, J., Henstock, T.J., Murton, B.J., and Jones, S.M., 2013. Crustal manifestations of a hot transient pulse at 60°N beneath the Mid-Atlantic Ridge. Earth and Planetary Science Letters, 363:109–120. **https://doi.org/10.1016/j.epsl.2012.12.030**

Poore, H., White, N., and Maclennan, J., 2011. Ocean circulation and mantle melting controlled by radial flow of hot pulses in the Iceland plume. Nature Geoscience, 4(8):558–561. **https://doi.org/10.1038/ngeo1161**

Poore, H.R., Samworth, R., White, N.J., Jones, S.M., and McCave, I.N., 2006. Neogene overflow of northern component water at the Greenland-Scotland Ridge. Geochemistry, Geophysics, Geosystems, 7(6):Q06010. **https://doi.org/10.1029/2005GC001085**

Rabinowicz, M., and Briais, A., 2002. Temporal variations of the segmentation of slow to intermediate spreading mid-ocean ridges, 2. A three-dimensional model in terms of lithosphere accretion and convection within the partially molten mantle beneath the ridge axis. Journal of Geophysical Research: Solid Earth, 107(B6):2110. **https://doi.org/10.1029/2001JB000343**

Raymo, M.E., Ganley, K., Carter, S., Oppo, D.W., and McManus, J., 1998. Millennial-scale climate instability during the early Pleistocene epoch. Nature, 392(6677):699–702. **https://doi.org/10.1038/33658**

Rickers, F., Fichtner, A., and Trampert, J., 2013. The Iceland–Jan Mayen plume system and its impact on mantle dynamics in the North Atlantic region: evidence from full-waveform inversion. Earth and Planetary Science Letters, 367:39–51. **https://doi.org/10.1016/j.epsl.2013.02.022**

Schilling, J.G., 1973. Iceland mantle plume: geochemical study of Reykjanes Ridge. Nature, 242(5400):565–571. **https://doi.org/10.1038/242565a0**

Schoonman, C.M., White, N.J., and Pritchard, D., 2017. Radial viscous fingering of hot asthenosphere within the Icelandic plume beneath the North Atlantic Ocean. Earth and Planetary Science Letters, 468:51–61. **https://doi.org/10.1016/j.epsl.2017.03.036**

Sclater, J.G., Jaupart, C., and Galson, D., 1980. The heat flow through oceanic and continental crust and the heat loss of the Earth. Reviews of Geophysics, 18(1):269-311. **https://doi.org/10.1029/RG018i001p00269**

Shorttle, O., and Maclennan, J., 2011. Compositional trends of Icelandic basalts: implications for short–length scale lithological heterogeneity in mantle plumes. Geochemistry, Geophysics, Geosystems, 12(11):Q11008. **https://doi.org/10.1029/2011GC003748**

Thornalley, D.J.R., Blaschek, M., Davies, F.J., Praetorius, S., Oppo, D.W., McManus, J.F., Hall, I.R., Kleiven, H., Renssen, H., and McCave, I.N., 2013. Long-term variations in Iceland–Scotland overflow strength during the Holocene. Climate of the Past, 9(5):2073–2084. **https://doi.org/10.5194/cp-9-2073-2013**

Vogt, P.R., 1971. Asthenosphere motion recorded by the ocean floor south of Iceland. Earth and Planetary Science Letters, 13(1):153–160. **https://doi.org/10.1016/0012-821X(71)90118-X**

White, R.S., 1997. Rift–plume interaction in the North Atlantic. Philosophical Transactions of the Royal Society, A: Mathematical, Physical and Engineering Sciences, 355(1723):319–339. **https://doi.org/10.1098/rsta.1997.0011**

White, R.S., Bown, J.W., and Smallwood, J.R., 1995. The temperature of the Iceland plume and origin of outward-propagating V-shaped ridges. Journal of the Geological Society (London, UK), 152(6):1039–1045. **https://doi.org/10.1144/GSL.JGS.1995.152.01.26**

Wood, D.A., Tarney, J., Varet, J., Saunders, A.D., Bougault, H., Joron, J.L., Treuil, M., and Cann, J.R., 1979. Geochemistry of basalts drilled in the North Atlantic by IPOD Leg 49: implications for mantle heterogeneity. Earth and Planetary Science Letters, 42(1):77–97. **https://doi.org/10.1016/0012-821X(79)90192-4**

Wright, J.D., and Miller, K.G., 1996. Control of North Atlantic Deep Water circulation by the Greenland-Scotland Ridge. Paleoceanography and Paleoclimatology, 11(2):157–170. **https://doi.org/10.1029/95PA03696**